Tracing water masses and terrestrial inputs with radiogenic neodymium and hafnium isotopes and rare earth elements in the southeastern Atlantic Ocean

Dissertation zur Erlangung des Doktorgrades

Dr. rer. nat.

der Mathematisch-Naturwissenschaftlichen Fakultät

der Christian-Albrechts-Universität zu Kiel

vorgelegt von

Peer Rahlf

Kiel, 2020

GUTACHTER

1. Gutachter und Betreuer: Prof. Dr. Martin Frank

2. Gutachter: Prof. Dr. Tina van de Flierdt

Eingereicht am:	27.08.2020
Tag der Disputation:	28.10.2020
Zum Druck genehmigt:	28.10.2020

Gez. Prof. Dr. Frank Kempken, Dekan

Erklärung

Hiermit erkläre ich an Eides statt, dass ich die vorliegende Abhandlung, abgesehen von der Beratung durch meine Betreuer, nach Inhalt und Form selbstständig erarbeitet habe und keine anderen, als die von mir aufgeführten Quellen und Hilfsmittel, verwendet wurden.

Diese Arbeit ist unter Einhaltung der Regeln guter wissenschaftlicher Praxis der Deutschen Forschungsgemeinschaft entstanden und wurde weder in Auszügen noch in ganzer Form an einer anderen Stelle im Rahmen eines Prüfungsverfahrens eingereicht.

Teile dieser Arbeit sind bereits in einer Fachzeitschrift veröffentlicht, wurden zur Veröffentlichung eingereicht oder sind in Vorbereitung, eingereicht zu werden.

Es wurde kein akademischer Grad entzogen.

Kiel, den 27.08.2020

Peer Rahlf

Peer Rahlf

CONTENTS

ABSTRACT *1*

KURZFASSUNG *3*

1. INTRODUCTION *6*

1.1. The Atlantic Meridional Overturning Circulation and water masses in the southeastern Atlantic Ocean **6**

1.2. Principles of radiogenic neodymium and hafnium isotopes as water mass tracers **8**

1.2.1. Samarium-neodymium isotope evolution 8

1.2.2. Neodymium and hafnium isotopes and continental weathering 10

1.2.3. Dissolved Nd and Hf isotopes as water mass tracers 12

1.2.4. Dissolved rare earth elements in seawater 13

1.3. Previous work, motivation and research questions **14**

1.3.1. Previous work 14

1.3.2. Motivation and research questions 15

1.3.3. Outline of the thesis 16

2. METHODS *18*

2.1. Sampling and pre-concentration **18**

2.2. Chemical procedures including chromatographic purification **19**

2.3. Nd and Hf isotope measurements **21**

2.4. Nd and Hf concentration measurements by isotope dilution **22**

2.4.1. Chemical treatment and spike addition 22

2.4.2. Mass spectrometry 23

2.5. Rare earth element measurements **24**

3. PUBLICATION AND MANUSCRIPTS *25*

CHAPTER I **25**

CHAPTER II **51**

CHAPTER III **80**

4. SUMMARY, CONCLUSIONS AND OUTLOOK *100*

4.1. Summary and Conclusions **100**

4.2. Outlook **103**

DANKSAGUNG *105*

REFERENCES *106*

DATA TABLES *122*

ABSTRACT

The southeastern Atlantic Ocean is a key region to investigate large-scale ocean circulation as the water masses passing this region comprise important parts of the return flow of the Atlantic Meridional Overturning Circulation (AMOC), which controls the distribution and transport of oceanic heat and salt as well as the cycling and storage of trace elements and climate-relevant gases. This doctoral thesis is embedded in the international GEOTRACES program and presents the first detailed investigation of water mass mixing processes and the distribution and fluxes of trace elements in the Angola and Cape Basins based on dissolved radiogenic neodymium (ε_{Nd}) and hafnium (ε_{Hf}) isotopes as well as rare earth element (REE) concentrations.

Near surface water εNd signatures reaching −17 in the uppermost 200 m of the Angola Basin are mainly a consequence of the admixture of an unradiogenic coastal plume originating from the dissolution of Fe-Mn coatings of particles in the oxygen minimum zone. In contrast, εNd signatures of up to -17.6 in the upper water column of the northern Cape Basin are a consequence of advection of shallow waters via the Agulhas current, which originates from the Mozambique Channel. The Nd isotope compositions of the deep water masses in both basins primarily reflect conservative water mass mixing, while Nd isotope signatures of deep and bottom waters of the central Angola Basin are significantly overprinted by terrestrial inputs. Bottom waters of the Cape Basin show excess Nd concentrations likely originating from resuspended bottom sediments and/or dissolution of dust, but without changing the Nd isotopic composition of the bottom waters significantly due to similar εNd values of particles and seawater.

The Congo River is the second largest river by discharge in the world and its plume carries extraordinarily high Nd and Hf concentrations of up to 4000 pmol/kg and 54 pmol/kg into the northern Angola Basin. Its freshwater is characterized by ε_{Nd} and ε_{Hf} values ranging between -15.6 and -16.4 and between 0.35 and -1.4, respectively. Rapid scavenging and removal of light rare earth elements (LREEs) and middle rare earth elements (MREEs) by coagulation processes form typical seawater REE patterns at salinities between 0 and 23. However, particle-seawater interactions in the low salinity zone may also result in Nd release from or exchange with Congo-derived particulate phases, as is indicated by elevated Congo-shelf-zone REE and Hf fluxes. Yet, this

process is not reflected by changes in Nd and Hf isotopic compositions given that the latter are identical in the dissolved and particulate pools of the Congo River. Having passed the estuary, the Nd and Hf concentrations and isotopic signatures in the Congo freshwater plume are mixed conservatively for up to 1000 km northwest of the river mouth. Subsurface waters are marked by riverine REE removal, whereas intermediate and deep waters below the plume and in the open northern Angola Basin are strongly affected by inputs from the Congo River resulting in less radiogenic signatures compared to what is expected from water mass mixing only. REE concentrations of bottom waters of the northern Angola Basin indicate limited REE release from seafloor sediments.

Surface waters of the Angolan coast near the Angola Benguela Front (ABF) are characterized by unradiogenic ε_{Nd} signatures of up to -21 and elevated REE concentrations (~ 35 pmol/kg for Nd), which are likely caused by dissolution of Fe-Mn oxide coatings of coastal sediment particles in the prevailing oxygen minimum zone. Decreasing REE concentrations in intermediate and deep waters suggest removal via scavenging due to high vertical particle fluxes, while ε_{Nd} signatures of about -15 indicate release of unradiogenic Nd. Surface waters off the Namibian coast are more radiogenic (ε_{Nd} ~ -12) and have lower REE concentrations (~ 12 pmol/kg for Nd) suggesting minor terrestrial inputs from the Namib and Kalahari or the Orange River. Waters off the Namibian coast are strongly influenced by upwelling and resuspension of particles from shelf sediments into the oxygen minimum zone, where REEs and distinct Nd isotope signatures are released and advected into the surface waters. Mixing calculations indicate that unradiogenic Nd isotope signatures of surface waters of the open western Angola Basin cannot be entirely explained by admixture of unradiogenic waters of the Agulhas Current (AC) but require contributions from the unradiogenic coastal waters near the ABF.

The investigations support the application of Nd isotopes as a quasi-conservative tracer of present and past deep water mass mixing in the southeastern Atlantic Ocean. Nd isotopes and REE concentrations trace advection of near surface water masses with distinct isotope composition such as the Agulhas current but also serve to monitor non-conservative terrestrial inputs. In coastal areas, Nd isotopes can be used to examine seawater-particle exchange processes and in combination with Hf isotope

compositions and element distributions serve to quantify riverine fluxes of elements to the open ocean, such as across the Congo estuary. Overall, this study demonstrates that combined REE concentrations and Nd and Hf isotopes help to better understand the mixing and advection of the water masses of the AMOC in the SE Atlantic Ocean and the importance of local terrestrial inputs, which has implications for the application of these geochemical tools in other parts of the world ocean and for the reconstruction of past ocean circulation.

KURZFASSUNG

Der südöstliche Atlantik ist eine ideale Region zur Untersuchung der großräumigen Ozeanzirkulation, da die Wassermassen, die diese Region passieren, wichtige Teile des Rückflusses der atlantischen meridionalen Umwälzirkulation (Atlantic Meridional Overturning Circulation, AMOC) bilden. Die AMOC kontrolliert die Verteilung und den Transport von Wärme und Salz sowie den Kreislauf und die Speicherung von Spurenelementen und klimarelevanten Gasen im tiefen Ozean. Dies Untersuchungen dieser Dissertation sind Teil des internationalen GEOTRACES-Programms und stellen die erste systematische und detaillierte Untersuchung von Wassermassenmischungsprozessen basierend auf radiogenen Neodym- (ε_{Nd}) und Hafnium- (ε_{Hf}) Isotopensystemen sowie auf der Verteilung und den Flüssen von Seltenerdelementen (REEs) im Angolabecken und Kapbecken dar. Die ε_{Nd}-Signaturen erreichen in den obersten 200 m des Angolabeckens einen Wert von –17. Diese sind hauptsächlich eine Folge der Zumischung einer unradiogenen Küstensignatur, die von Fe-Mn-Coatings auf Sedimentpartikeln stammt, die in der Sauerstoffminimumzone aufgelöst wurden. Die ε_{Nd}-Signaturen in der oberen Wassersäule des nördlichen Kapbeckens erreichen unradiogene Werte von bis zu -17,6. Diese Signatur wird aber im Gegensatz zum Angolabecken aus dem Kanal von Mosambik über den Agulhas-Strom in den südöstlichen Atlantik eingetragen. Die Nd-Isotopenzusammensetzungen der Tiefenwassermassen in beiden Becken spiegeln hauptsächlich die konservative Mischung der Wassermassen wider, während die Nd-Isotopensignaturen des Tiefen- und Bodenwassers des zentralen Angolabeckens durch terrestrische Einträge signifikant überprägt sind. Das Bodenwasser des

Kapbeckens weist überschüssige Nd-Konzentrationen auf, die wahrscheinlich aus resuspendierten Bodensedimenten bzw. der Auflösung von Wüstenstaub stammen. Jedoch werden aufgrund ähnlicher ε_{Nd}-Werte von Partikeln und Meerwasser die Nd-Isotopenzusammensetzung des Bodenwassers dadurch nicht signifikant verändert.

Der Kongo ist der zweitgrößte Fluss der Erde und sein Süßwasser transportiert außerordentlich hohe Nd-Konzentrationen von bis zu 4000 pmol/kg und Hf-Konzentrationen von bis zu 54 pmol/kg in das nördliche Angolabecken. Die Süßwasserfahne ist durch ε_{Nd}- und ε_{Hf}-Werte zwischen -15,6 und -16,4 bzw. zwischen 0,35 und -1,4 gekennzeichnet. Zwischen Salinitäten von 0 und 23 werden leichte Seltenerdelemente (LREEs) und mittlere Seltenerdelemente (MREEs) aus der Wassersäule durch Koagulationsprozesse effizient entfernt und es bilden sich typische Meerwasser-REE-Muster heraus. Partikel-Meerwasser-Wechselwirkungen im Bereich der niedrigen Salinitäten können jedoch auch zur Freisetzung von Nd, bzw. zum Nd-Austausch mit Partikeln aus dem Kongo führen. Dies wird durch erhöhte REE- und Hf-Flüsse in der Kongo-Schelfzone angezeigt. Dieser Prozess spiegelt sich jedoch nicht in Änderungen der Nd- und Hf-Isotopenzusammensetzungen wider, da letztere in den gelösten und partikulären Phasen identisch sind. Nach dem Passieren der Flussmündung werden die Nd- und Hf-Konzentrationen und Isotopensignaturen in der Kongofahne bei Salinitäten über 23 bis zu 1000 km nordwestlich der Flussmündung konservativ mit dem umgebenden Meerwasser vermischt. Direkt unter dem Oberflächenwasser sind die Wassermassen durch Scavenging-Prozesse an REEs abgereichert von REEs gekennzeichnet. Die intermediären und tiefen Wassermassen unterhalb der Fahne und im offenen nördlichen Angolabecken werden hingegen stark von Einträgen aus der teilweisen Lösung von sinkenden Partikeln aus der r Kongofahne beeinflusst, was zu unradiogeneren Isotopensignaturen führt und das Signal der konservativen Wassermassenmischung überprägt. REE-Konzentrationen des Bodenwassers im nördlichen Angolabecken weisen auf eine begrenzte REE-Freisetzung aus Meeresbodensedimenten hin.

Oberflächenwässer der angolanischen Küste in der Nähe der Angola-Benguela-Front (ABF) sind durch unradiogene ε_{Nd}-Signaturen von bis zu -21 und erhöhte REE-Konzentrationen (~35 pmol/kg für Nd) gekennzeichnet. Diese werden vermutlich durch die Lösung von Fe-Mn-Coatings auf Sedimentpartikeln, die von der Küste

stammen, in der Sauerstoffminimumzone verursacht. REEs in intermediären und tiefen Wassermassen werden aufgrund hoher vertikaler Partikelflüsse entfernt, während ε_{Nd}-Signaturen nahe -15 gleichzeitig auf die Freisetzung von unradiogenem Nd hinweisen. Das Oberflächenwasser vor der namibischen Küste ist deutlich radiogener (εNd ~ -12) und weist niedrigere REE-Konzentrationen (~12 pmol/kg für Nd) auf als das Oberflächenwasser der angolanischen Küste, was auf geringere terrestrische Einträge aus der Namib und Kalahari, bzw. aus dem Orange River hindeutet. Wassermassen vor der namibischen Küste werden stark durch den Auftrieb und die Resuspension von Partikeln aus Schelfsedimenten beeinflusst. Diese setzen in der Sauerstoffminimumzone REEs und Nd-Isotopensignaturen frei, die über den Auftrieb in das Oberflächenwasser transportiert werden. Mischungsberechnungen zeigen, dass unradiogene Nd-Isotopensignaturen des Oberflächenwassers des offenen, westlichen Angolabeckens nicht vollständig durch Zumischung von unradiogenen Signaturen des Agulhas-Stroms (AC) erklärt werden können, sondern auch Beiträge der unradiogenen Küstengewässer in der Nähe der ABF erfordern.

Die Ergebnisse dieser Dissertation unterstützen die Anwendung von Nd-Isotopensignaturen als quasi-konservative Indikatoren für die Mischung der gegenwärtigen und vergangenen tiefen Wassermassen im südöstlichen Atlantik. Nd-Isotope und REE-Konzentrationen spiegeln die Advektion oberflächennaher Wassermassen mit unterschiedlicher Isotopenzusammensetzung, wie dem Agulhas-Strom wider, dienen aber auch zur Erfassung nichtkonservativer, terrestrischer Einträge. In Küstengebieten können Nd-Isotope zur Untersuchung von Austauschprozessen zwischen Meerwasser und Partikeln verwendet werden. In Kombination mit Hf-Isotopenzusammensetzungen und REE-Verteilungen können Einträge der Elemente aus Flüssen in den offenen Ozean, beispielsweise über die Kongo-Mündung, quantifiziert werden. Insgesamt zeigen die Ergebnisse der Dissertation, dass REE-Konzentrationen, kombiniert mit Nd- und Hf-Isotopen dazu beitragen, die Mischung und Advektion der Wassermassen der AMOC im Südostatlantik sowie die Bedeutung lokaler terrestrischer Einträge besser zu verstehen. Dies ist wiederum von Bedeutung für die Rekonstruktion der gegenwärtigen und vergangenen Ozeanzirkulation in anderen Teilen der Weltmeere.

1. INTRODUCTION

1.1. The Atlantic Meridional Overturning Circulation and water masses in the southeastern Atlantic Ocean

The Atlantic meridional overturning circulation (AMOC) plays a key role in the Earth's climate by controlling the distribution of water masses, heat and salt transport as well as the cycling and storage of gases such as O_2 and CO_2. At depth it consists of a southward flowing deep-water mass (North Atlantic Deep water, NADW), which is formed by mixing of source waters in the Labrador and Nordic Seas and of a northward flowing abyssal water mass (Antarctic Bottom Water, AABW), which is formed by mixing of cold Antarctic Shelf Water with warmer Circumpolar Deep Water (Piepgras and Wasserburg, 1987, Orsi et al., 1999). Upwelling processes along the Antarctic Circumpolar Current (ACC) transport deep water to the ocean surface in the Atlantic sector of the Southern Ocean, which subsequently mixes with warm surface waters from the Indian Ocean and is transported northward as warm and salty water across the equator (Fig. 1) (Kuhlbrodt et al., 2007). Paleoclimate records indicate that changes in this circulation system had strong impacts on the climate in the past (e.g. Broecker at al., 1985, Rahmstorf, 2002, Alley, 2007, Böhm et al., 2015).

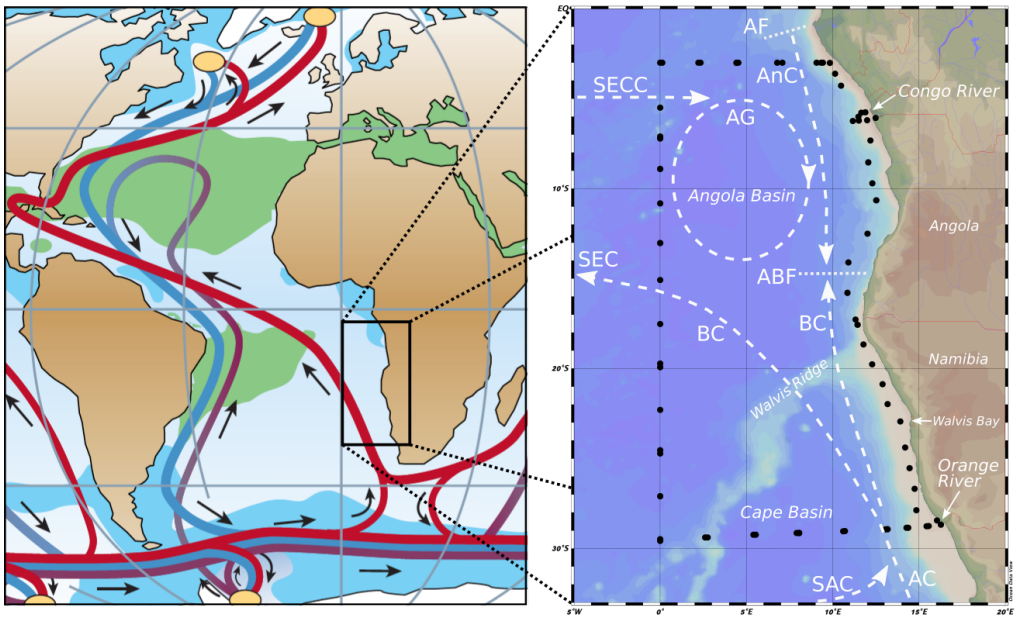

Fig. 1: Left figure: sketch of the AMOC with surface currents (red), deep currents (blue) and bottom currents (purple). Deep water formation areas are illustrated in yellow color (after Rahmstorf et al. (2002) and Kuhlbrodt et al. (2017)). Right figure: Southeastern Atlantic Ocean with the Angola and Cape Basins. The white dashed lines indicate the surface currents including the SAC = South Atlantic Current, AC = Agulhas Current, BC = Benguela Current, SEC = South Equatorial Current, SECC = South Equatorial Counter Current, AG = Angola Gyre, AnC = Angola Current, AF = Angola Front, ABF = Angola Benguela Front. Black dots represent the stations of cruise M121 that started and ended in Walvis Bay (Namibia).

1. INTRODUCTION

The southeastern Atlantic Ocean which includes the more than 5000 m deep Angola and Cape Basins is a key region to investigate ocean circulation processes as its prevailing water masses form important parts of the return flow of the AMOC. The Angola and Cape Basins developed by rifting and breakup processes of the Gondwana continent as a consequence of the South Atlantic opening in the Early Cretaceous (Peron-Pinvidic et al., 2013, Naafs and Pancost, 2014) (Fig. 1). The two basins are separated by the Walvis Ridge, which is a more than 3000 km long and aseismic ridge extending from the Mid-Atlantic Ridge to the African coast. It either formed synchronously with the opening of the south Atlantic as a consequence of a mantle hot spot or independently of the opening by later uplift processes (Goslin et al., 1974 and references therein). The ridge almost completely prevents the northward advection of cold bottom waters originating from the south. Only limited leakage of AABW across the deep Walvis Passage occurs near 37 °S and 7 °W (Connary and Ewing, 1974, Shannon and Chapman, 1991). Larger amounts of AABW enter the Angola Basin further north through the Romanche Fracture Zone located at the equator at ~15 °W (Metcalf et al., 1964). Main parts of deep waters of the Angola and Cape Basins are occupied by NADW, whereas above 1300 m water depth AAIW is dominant (van Bennekom and Berger, 1984). AAIW is formed by mixing of Sub-Antarctic Surface Water with sinking Antarctic Surface Water in the South Atlantic Ocean (Suga and Talley, 1995). However, the Southern Ocean component in the AAIW decreases from about 70 % in the Cape Basin to about 45 % at the equator (Broecker and Takahashi, 1981).

Upper layers of the southeastern Atlantic Ocean are occupied by South Atlantic Central Water (SACW), Subtropical Surface Water (STSW) and Tropical Surface Water (TSW). SACW of the subtropical gyre originates from Subantarctic Mode Water in the Subantarctic Zone and is transported within the South Atlantic Current that feeds into the Benguela Current (BC) (Fig. 1). Parts of the SACW originate from Indian Central Water, which is advected into the Atlantic Ocean by the Agulhas Current (AC). SACW of the subtropical Atlantic is covered by high saline STSW, whereas SACW of the tropical Atlantic is overlain by fresh TSW (Tomczak and Godfrey, 1994, Stramma and England, 1999). The BC feeds into the South Equatorial Current, which flows in a northwesterly direction across the entire South Atlantic. Near the Brazilian coast it

changes direction and then flows eastward across the South Atlantic as the South Equatorial Counter Current that feeds into the cyclonic Angola Gyre (AG) (Stramma and England, 1999). A second branch of the BC flows northward along the West African coast until it meets the southward flowing Angola Current (AnC) at the Angola Benguela Front. The AnC originates from the Angola Front near the equator. South of the Angola Basin, between the Walvis Ridge and Cape Agulhas at 34◦S, the southeasterly winds cause strong coastal upwelling (Meeuwis and Lutjeharms, 1990) (Fig. 1).

The geochemical compositions of water masses of the Angola and Cape Basins are influenced by continental inputs such as dust (e.g. Chester et al., 1972, Mahowald et al., 2005), particulate and dissolved sedimentary (e.g. Noble et al., 2012, Zheng et al., 2016) and riverine inputs (e.g. Eisma et al., 1984, Bayon et al., 2004, Coynel et al., 2005, Bayon et al., 2009, Laraque et al., 2009, Denamiel et al., 2013) as well as by advection of water masses with different chemical properties from the Indian and Southern Ocean (e.g. Franzese et al., 2006, Beal et al., 2016, D'Addezio et al., 2016, Durgadoo et al., 2017, Amakawa et al., 2019). However, data investigating the impact of these external components on the hydrography and chemical composition of water masses of the southeastern Atlantic Ocean are scarce. Radiogenic neodymium (Nd) and hafnium (Hf) isotopes as well as rare earth element (REE) concentrations are widely used for the reconstruction of present and past water mass mixing processes and as tracers of weathering inputs into the ocean, which will be introduced in the following sections.

1.2. Principles of radiogenic neodymium and hafnium isotopes as water mass tracers

1.2.1. Samarium-neodymium isotope evolution

Terrestrial rocks and minerals contain various trace elements including the rare earth elements and Hf. The rare earth element Nd has seven naturally occurring stable isotopes (^{142}Nd, ^{143}Nd, ^{144}Nd, ^{145}Nd, ^{146}Nd, ^{148}Nd and ^{150}Nd), whereas the High Field Strength Element Hf has 6 naturally occurring isotopes (^{174}Hf, ^{176}Hf, ^{177}Hf, ^{178}Hf, ^{179}Hf and ^{180}Hf). Among these isotopes, ^{143}Nd is the product of the radioactive decay of ^{147}Sm

(half life = 1.06x10^11 y) and ^{176}Hf is the decay product of ^{176}Lu (half life = 3.6x10^10 y). Commonly, radiogenic ^{143}Nd and ^{176}Hf are normalized to the primordial isotopes ^{144}Nd and ^{177}Hf, respectively and the $^{143}Nd/^{144}Nd$ and $^{176}Hf/^{177}Hf$ isotope ratios are expressed in the ε-notation

$$\varepsilon_{Nd} = \left[\frac{\left(\frac{143_{Nd}}{144_{Nd}} SAMPLE\right) - \left(\frac{143_{Nd}}{144_{Nd}} CHUR\right)}{\frac{143_{Nd}}{144_{Nd}} CHUR}\right] * 10{,}000$$

$$\varepsilon_{Hf} = \left[\frac{\left(\frac{176_{Hf}}{177_{Hf}} SAMPLE\right) - \left(\frac{176_{Hf}}{177_{Hf}} CHUR\right)}{\frac{176_{Hf}}{177_{Hf}} CHUR}\right] * 10{,}000$$

where CHUR represents the Chondritic Uniform Reservoir ($^{143}Nd/^{144}Nd$ = 0.512638 and $^{176}Hf/^{177}Hf$ = 0.282769) (Jacobsen and Wasserburg, 1980, Nowell et al., 1998) and the evolution Hf and Nd isotope compositions of the bulk earth (Fig. 2).

During partial melting or fractional crystallization of the Earth's mantle, Nd and Hf preferentially accumulate in the melt fraction, whereas Sm and Lu preferentially stay in the residuum. The melt with low Sm/Nd and Lu/Hf ratios is incorporated into the Earth's crust and crystallizes. Consequently, the Earth's crust is characterized by lower $^{143}Nd/^{144}Nd$ and $^{176}Hf/^{177}Hf$ isotope ratios than the Earth's mantle (Fig. 2A) and consequently crustal rocks such as granites and metamorphites have less radiogenic ε_{Nd} and ε_{Hf} values than mantle rocks such as basalts and gabbros (Fig. 2B). The rocks' ε_{Nd} and ε_{Hf} signature varies both as a function of the age of the rock and as a function of the Sm/Nd and Lu/Hf ratio and is indicative for different continental regions. The Nd and Hf isotope compositions of most terrestrial rocks display a strong positive correlation, which is defined as the "terrestrial array" (Vervoort et al., 1999) (Fig. 3).

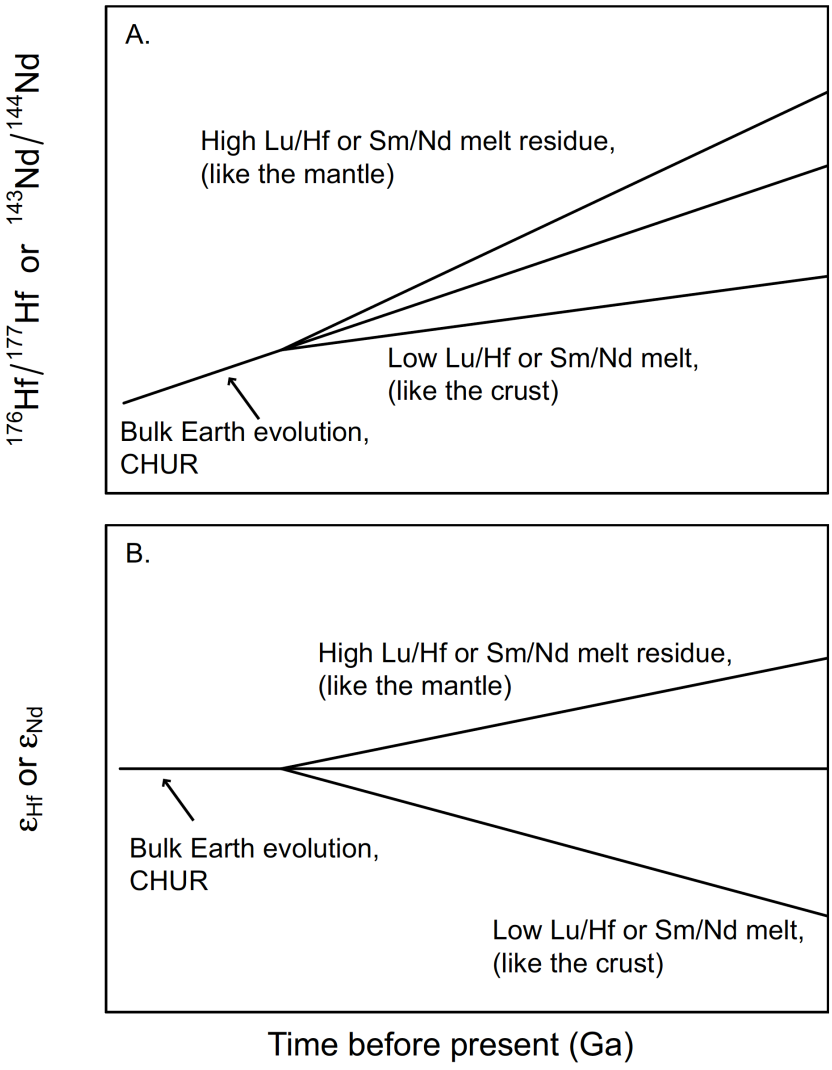

Figure 2: Nd and Hf isotope evolution of Bulk Earth (CHUR) over time. With the onset of the Earth's differentiation, higher Lu/Hf and Sm/Nd ratios and thus higher ε_{Nd} and ε_{Hf} values evolved in the mantle than in the crust (after Rickli, 2009).

1.2.2. Neodymium and hafnium isotopes and continental weathering

Physical and chemical weathering lead to decomposition of rocks and minerals. Due to similar chemical characteristics and ionic radii of Sm and Nd, most rock-forming minerals have homogeneous Sm/Nd ratios and thus the Nd isotope composition of the weathered material and weathering solutions does not differ significantly from that of the source rocks. This process is called congruent weathering. Nd is delivered into the oceans by fluvial and eolian dust inputs (e.g. Goldstein et al., 1984) but exchange between seawater and continental deposits on shelves is also a major contributor to the Nd budget of the oceans (Lacan and Jeandel, 2005b).

In contrast, Lu and Hf are chemically different causing highly variable Lu/Hf ratios in different minerals. Minerals such as zircons are resistant to weathering processes and retain their low Lu/Hf ratios and low ε_{Hf} signatures, which has been termed as the "zircon effect" (cf. van de Flierdt et al., 2007). Thus, the Hf isotope composition of weathered material and weathering solutions can differ significantly from the bulk rock isotope composition of the source rock, which is termed incongruent weathering. Hf is transported into the oceans mainly via riverine inputs (e.g. Bayon et al. 2006), while some authors have proposed significant inputs by hydrothermal venting (Bau and Koschinsky, 2006). Data from ferromanganese crusts and nodules (Albarède et al., 1998, David et al., 2001, van de Flierdt et al., 2006, Bayon et al., 2009) and from seawater (Rickli et al., 2009, Zimmermann et al., 2009, Stichel et al., 2012b) exhibit a more radiogenic Hf isotope composition for a given Nd isotope value resulting in the "seawater array" (Fig. 3). This offset is most likely mainly caused by the effects of incongruent weathering, as mentioned above.

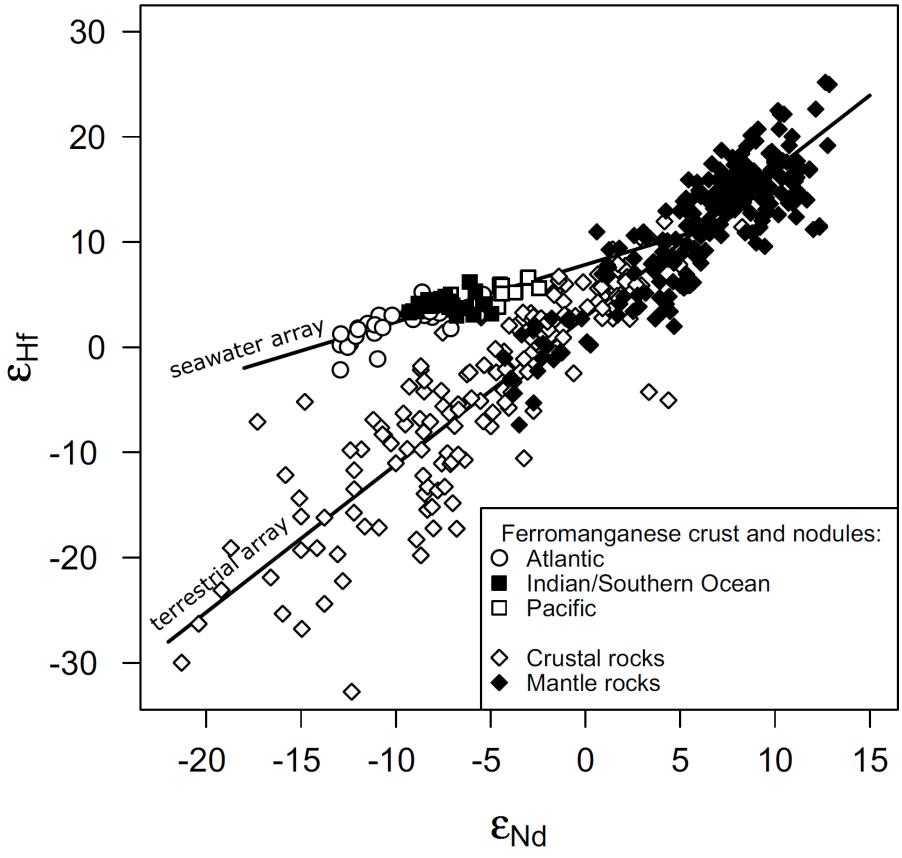

Figure 3: Hf and Nd isotope compositions of crustal and mantle rocks represent the terrestrial array. Hf and Nd isotope compositions of Fe-Mn crusts in the Atlantic, Indian/Southern Ocean and Pacific represent the seawater array, which for a given ε_{Nd} value has a more radiogenic ε_{Hf} value (after Rickli, 2009).

1.2.3. Dissolved Nd and Hf isotopes as water mass tracers

Water masses of the oceanic basins are labelled by Nd and Hf isotope compositions resulting from isotopically different inputs from the adjacent continents and their geological formations (Jeandel, 2007). These signatures allow to trace the pathways and mixing of the water masses. The intermediate oceanic residence time of Nd (600-2000 years) (Jeandel et al., 1995, Tachikawa et a., 1999, Tachikawa et al., 2003) results in a quasi-conservative behavior of Nd in the open ocean as well as in long distance transport of deep-water mass Nd isotope signatures (Frank, 2002, Goldstein and Hemming, 2003). The oceanic residence time of Hf (250-7500) is less well constrained than that of Nd, but several studies suggested that the lower end of the above estimate is most realistic (Firdaus et al., 2008, Godfrey et al., 2009, Rickli et al., 2009). Therefore, Hf isotopes have been used as a tracer of continental weathering inputs and water mass mixing on shorter basin scales (Stichel et al., 2012b, Filippova et al., 2017).

However, dissolved Nd and Hf isotope signatures of seawater are not only controlled by continental inputs and mixing processes. While radiogenic Nd and Hf isotopes are not fractionated by biological processes and evaporation (Frank, 2002), preformed isotope compositions can vary due to particle-seawater interactions, a process that has been termed "boundary exchange" (Lacan and Jeandel, 2005). Processes and locations of boundary exchange include release of large amounts of particles at river mouths, resuspension of shelf sediments, submarine groundwater discharge and subterranean estuaries (Jeandel, 2016). While this leads to changes in the dissolved Nd isotope compositions, dissolved Nd concentrations remain constant due to the competition between release of Nd through dissolution and Nd removal through precipitation or adsorption. On the other hand, while Nd isotope compositions behave quasi conservatively in the subsurface ocean, Nd concentrations in the water column generally increase with depth. The decoupling of Nd concentrations and isotopic compositions is defined as the "Nd paradox" (Nozaki and Alibo, 2003, Siddall et al., 2008).

1.2.4. Dissolved rare earth elements in seawater

The rare earth elements (REEs) are a group of transition metals including all lanthanides as well as yttrium and scandium. Elements with similar chemical behavior are subdivided into three groups: the light (L)REEs (from lanthanum to europium), the (M)REEs (from gadolinium to dysprosium) and the (H)REEs (from holmium to lutetium). LREEs are more compatible in the melt fraction while HREEs preferentially remain in the solid mantle, which results in fractionation during magmatic processes (Hofmann, 1988). Therefore, depending on the type and evolution of the lithologies, characteristic REE concentration patters are established. At the Earth's surface, the REEs are mobilized by chemical and physical weathering and are introduced into the oceans mainly by rivers and dust (e.g. Byrne and Sholkovitz, 1996, Tachikawa et al., 1999, Frank, 2002).

REE patterns are key parameters to investigate the origin of continental inputs, their transport processes, as well as the interactions between seawater and sediment particles and pore waters at land ocean interfaces and in the open ocean (Elderfield et al., 1990, Haley et al., 2003, Grasse al., 2012, Grenier et al., 2013, Garcia-Solsona et al., 2014, Abbott et a., 2015). To detect subtle differences in REE-patterns, REE concentrations are commonly normalized to the Post Archean Australian Shale (PAAS, McLennan 2001). While fresh lithogenic continental material has flat shale-like PAAS-normalized REE patterns (Elderfield, 1990), river inputs are characterized by a mid REE (MREE) enrichment (cf. Elderfield, 1990, Osborne et al., 2015, Laukert et al., 2017). Upon contact with seawater the LREEs are removed preferentially by coagulation of river-borne colloids at low salinities (Sholkovitz, 1993, Rousseau, 2015, Tepe and Bau, 2016). Preferential release of HREEs from resuspended particles and sediments in estuaries at higher salinities can further enhance the HREE enrichment in seawater (Sholkovitz and Szymczak, 2000, Sholkovitz 1994) but is not observed everywhere (cf. Laukert et al., 2017). Recent studies have proposed that REE fractionation already occurs in the rivers, because colloidal and truly dissolved pools have different REE patterns. Thus, dissolved seawater REE patterns can be a combination of both intra-oceanic and riverine processes (Pourret and Tuduri, 2017). PAAS-normalized seawater REE patterns are depleted in LREEs and have a pronounced Ce anomaly due to the oxidation of Ce^{3+} to insoluble Ce^{4+} (e.g. Elderfield and Greaves, 1982).

1.3. Previous work, motivation and research questions

1.3.1. Previous work

The hydrography of the southeast Atlantic Ocean including the Benguela upwelling has been intensively investigated and described (e.g. van Bennekom, 1984, Shannon et al., 1985, Lutjeharms and Meeuwis, 1987, Stramma and Peterson, 1989, Meeuwis and Lutjeharms, 1990, Peterson and Stramma, 1991, Stramma and England, 1999). However, studies investigating dissolved Nd and Hf concentrations and isotope compositions as well as REE and nutrient concentrations in the Angola and Cape Basins are scarce (Rickli et al., 2009, Rickli et al., 2010, Noble et al., 2012, Stichel at al., 2012a and Zheng et al., 2017.)

The first dissolved Hf and Nd isotope data of seawater from the Angola Basin have been reported by Rickli et al. (2009) and Rickli et al. (2010). These investigations confirmed the existence of the seawater array and concluded that the seawater Hf budget is dominated by continental inputs rather than by hydrothermal fluxes. According to these studies, Hf and Nd isotope compositions of intermediate and deep waters of the Angola Basin do not behave conservatively and are influenced by terrestrial inputs from the west African coast. Unradiogenic Nd isotope compositions of surface waters in the Angola Basin were concluded to result from reduction of Fe-Mn coatings of sediment particles originating from the Congo River.

Stichel et al., 2012A conducted the first combined study of surface water Hf and Nd isotope compositions as well as Hf and REE concentrations in the Atlantic sector of the Southern Ocean. The northernmost station of the cruise track is located southwest of Cape Town in the Cape Basin. There, surface waters are characterized by high Nd concentrations and unradiogenic ε_{Nd} values as low as -18.9, which were ascribed to terrigenous inputs from South Africa and advected via the Agulhas Current.

Zheng et al., 2016 reported dissolved REEs (dREEs) along a full-depth east-west section at ~12 °S off the Angolan Coast that was occupied during the CoFeMUG (KN195-2) cruise. These authors showed that while dissolved REE concentrations in deep waters are mostly controlled by preformed dREEs and indicate conservative behavior, significant dREE additions in bottom waters near the continent-ocean interface were observed. Elevated dREE concentrations in surface waters near the

Angolan coast likely resulted from dissolution of Fe-Mn-oxides in the oxygen minimum zone. Noble et al. (2012) found elevated surface water concentrations of micronutrients such as cobalt, iron and manganese along the same CoFeMUG section. The major sources of these metals are reductive dissolution and particle resuspension of coastal sediments within the oxygen minimum zone, advected offshore by wind driven upwelling.

More recently, Vieira et al. (2020) used radium isotopes to trace the flux of dissolved iron (dFe) introduced into the Angola Basin by the Congo River Plume for over 1000 km from the Congo outflow. Extremely high Fe input into the Congo-shelf-zone and lateral transport causes a large offshore dFe flux of 5.8 ± 2.1 x 10^8 mol yr^{-1}, which likely impacts phytoplankton growth in the South Atlantic Ocean.

1.3.2. Motivation and research questions

The work presented in this thesis is embedded in the international GEOTRACES program (www.geotraces.org). The program investigates the sources, sinks and biogeochemical cycling of trace elements and their isotopes (TEIs), including micronutrients, in the world oceans to reconstruct present and past oceanic processes. The combined measurements of a large range of key TEIs along sections crossing chemical gradients improved the understanding of oceanic processes and is a central feature of the GEOTRACES program (Fig. 4). International laboratory measurements of TEIs are intercalibrated to ensure comparable and robust data sets, which are provided by the participants of the GEOTRACES programme to the scientific community (Schlitzer et al., 2018).

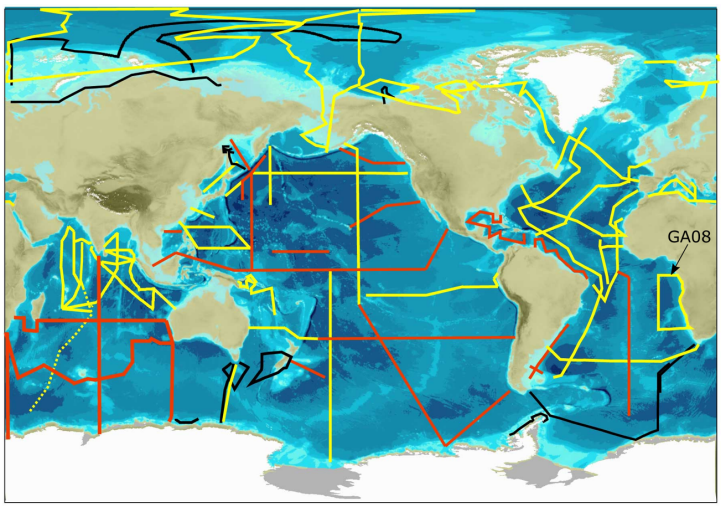

Figure 4: Global GEOTRACES sections. Yellow sections such as GA08 (M121) have been successfully completed.

The motivation of this thesis is a detailed investigation of the distribution of dissolved Nd, Hf isotope compositions and concentrations, as well as of REE concentrations in the southeastern Atlantic Ocean, where important parts of the return flow of the AMOC are located. This thesis also aims at identifying the potential sources of external TEI inputs and to improve the understanding of the behavior of TEIs in the Angola and Cape Basins. The following major research questions are therefore raised:

1. Do dissolved Nd isotope compositions serve as quasi-conservative tracers of water mass mixing in the Angola and Cape Basins and which external Nd inputs can be identified that influence the Nd isotope compositions and concentrations.

2. Which impact does the Congo River plume have on the distribution of Nd and Hf isotope compositions and REE concentrations in the southeastern Atlantic Ocean and which exchange processes between the fresh water plume, particles and seawater occur?

3. Which impact do sediments of the coastal area of Angola and Namibia have on the Nd isotope composition and REE concentrations of the southeastern Atlantic Ocean, and how does the Benguela upwelling influence the composition of the coastal waters?

1.3.3. Outline of the thesis

The thesis is divided into three main chapters providing the main results and discussions. All chapters are presented in the form of scientific manuscripts, of which chapter I is already published, chapter II has been submitted and is currently under review and chapter III is in preparation for submission to a peer-reviewed journal.

Chapter I presents the distribution of Nd isotope compositions and concentrations in the Angola and Cape Basin along two full water column sections. Based on the data, mixing relationships of the main water masses and the impact of non-conservative inputs of REEs and Nd isotopes were investigated. This chapter has been published in the journal Earth and Planetary Science Letters (EPSL), authored by Peer Rahlf, Ed Hathorne, Georgi Laukert, Marcus Gutjahr, Syee Weldeab and Martin Frank under the title: **Tracing water mass mixing and continental inputs in the southeastern Atlantic Ocean with dissolved neodymium isotopes** (https://doi.org/10.1016/j.epsl.2019.115944).

The contributions to this article are the following: Martin Frank proposed the study. Collection and pre-concentration of the water samples on board of RV Meteor was carried out by Jutta Heinze and myself. I carried out the chemical treatment, the column chemistry as well as the Nd concentration and isotope measurements in the laboratory of the GEOMAR. I wrote the manuscript, which was improved by contributions from and discussions with the co-authors.

Chapter II investigates the mixing behavior of dissolved Nd, Hf isotope compositions and concentrations as well as REE concentrations of the Congo River Plume with ambient seawater. The fluxes of REEs and Hf to the northeastern Angola Basin introduced by freshwater advection of the Congo plume were quantified and vertical exchange and particle release processes associated with the plume and its suspended particles were assessed. This chapter has been submitted to the journal Geochimica et Cosmochimica Acta (GCA) authored by Peer Rahlf, Georgi Laukert, Ed Hathorne, Lúcia H. Vieira and Martin Frank under the title **The Congo River Plume: Tracing continental inputs with rare earth elements and dissolved neodymium and hafnium isotopes**.

The contributions to this article are the following: Martin Frank proposed the study. Collection and pre-concentration of the water samples on board of the Meteor was carried out by Jutta Heinze and myself. I did the chemical treatment, the column chemistry, the REE and Hf concentration as well as the Nd and Hf isotope measurements in the laboratory of GEOMAR. Ed Hathorne helped with the analyses, in particular of the REE data. I wrote the manuscript, which then was improved by contributions from and discussions with all co-authors.

Chapter III examines the Nd isotope compositions and REE concentrations of waters along the coast of Angola and Namibia. Terrestrial inputs as well as the effects of the Benguela upwelling, influencing the distribution of REEs and Nd isotope compositions are identified. This chapter will be prepared for submission to a peer-reviewed journal by the authors Peer Rahlf, Ed Hathorne and Martin Frank under the title**: Release of Rare Earth Elements and unradiogenic neodymium from the West African coast to surface waters of the Angola Basin.**

The contributions to this article are the following: Martin Frank proposed the study. Collection and pre-concentration of the water samples on board of RV Meteor was carried out by Jutta Heinze and me. I did the chemical treatment, the column chemistry, the REE concentration as well as the Nd isotope measurements in the laboratory of GEOMAR. Ed Hathorne helped with the analyses of the REE data and Georgi Laukert helped with the analyses of the Nd isotope data. I wrote the manuscript, which was improved by discussions with Ed Hathorne and Martin Frank.

2. METHODS

2.1. Sampling and pre-concentration

Overall 208 seawater samples from the entire water column were collected during GEOTRACES cruise GA08 (RV Meteor cruise M121) in November/December 2015. The cruise started in Walvis Bay (Namibia) and went along the coast of Namibia, Angola, Congo and Gabon. The cruise continued offshore along 3°S and then southward along the Zero Meridian until 30 °S when it turned east until approaching the coast of South Africa. RV Meteor turned north again and went back to Walvis Bay along the coast of Namibia (Fig. 1).

Surface water samples were recovered with a towed stainless steel fish, when the ship was underway. Samples from the full water column were collected with 10 l Niskin bottles attached to a stainless steel CTD rosette. All samples were then treated in the onboard laboratory strictly following recommended GEOTRACES protocols (van de Flierdt et al., 2012). Each 20 L sample was filtered through a nitro-cellulose acetate filter (0.45 µm pore diameter) into an acid-cleaned LDPE-cubitainer with a peristaltic pump within 2 h after sample collection, and subsequently acidified with ~20 mL concentrated, distilled HCl. For Nd concentration measurements, 2 L aliquots from each filtered sample were collected in acid-cleaned 2-liter PE-bottles. To each large volume sample 400 µl $FeCl_3$ solution (~200 mg Fe/mL) were added and the sample was left to equilibrate for 24 h. Ammonia solution (25 %, Merck Suprapur®) was then added to raise the pH from about 2 to 7.5-8.0. After 48 h, the trace elements co-precipitated with the FeOOH had settled to the bottom of the cubitainers and the supernatant was syphoned off. The precipitates were transferred into 2 L wide mouth LDPE-bottles for transport to the home laboratory at GEOMAR.

Three Congo River water samples at zero salinity were collected in May, July and October 2017 by boat. The samples were collected in 10 L plastic canisters and filtered within 2 hours after collection through AcroPak™500 Capsules containing Supor® membrane (pore size: 0.8/0.2 µm) filter cartridges. The samples were acidified with distilled concentrated HCl to pH ~2 and 20 mL of aliquots from each sample were separated into acid-cleaned Zinsser® HDPE vials for Nd- and Hf-concentration measurements. 1 L of each sample was separated and 1 mL $FeCl_3$ solution (~200 mg Fe/mL). After equilibration suprapure ammonia solution (25 %) was added to raise the pH to 7.5-8.0. After 48 hours, the supernatant water was separated from the FeOOH-co-precipitated trace elements.

2.2. Chemical procedures including chromatographic purification

In the home laboratory at GEOMAR all precipitates were centrifuged and rinsed three times with deionized water (MilliQ, 18.2 MΩcm) in 50 mL centrifuge tubes to remove major seawater ions. After dissolution in 6 M HCl/0.5 M HF and transfer into Teflon vials the samples were evaporated to dryness. To remove organic compounds, the samples were treated with aqua regia at 120 °C for 24 h. After evaporation to dryness, the samples were dissolved in 4 mL 6 M HCl and were checked for the presence of a jelly-like precipitate, which can contain up to ~90 % of the Hf in the samples (Stichel et al. 2012b). These precipitates were separated by centrifugation, dissolved in 2 M HF at 100 °C, dried down and dissolved in 1M HCl/0.05M HF. Before this precipitate was added to the main sample again, the latter was washed with pre-cleaned di-ethyl ether to remove 99 % of the Fe (Stichel at al., 2012b). The samples were dried down and dissolved in 4 mL 6 M HCl/1 M HF. The rare earth elements (REEs) were chromatographically separated from matrix elements using cation exchange resin AG 50W-X8 (200-400 µm mesh size, 1.4 mL resin bed) following a modified scheme of Stichel (2010) (Table 1). Neodymium was then separated from the other REEs for isotope measurements using Eichrom®LN-Spec resin (50-100 µm mesh size, 2 mL resin bed) following a modified protocol of Pin and Zalduegui (1997) (Table 2). To remove residual traces of the resin and organic compounds, the Nd cuts were treated with 100 µl quartz distilled HNO_3 and 100 µl H_2O_2 (30 wt.%, Merck Suprapur®).

Hafnium was further purified by column chemistry using AG1-X8 resin (200-400 μm mesh size, 4 cm height and 0.8 cm ∅) and Eichrom®LN-Spec resin (100-150 μm mesh size, 8.3 cm height and 0.4 cm ∅), following a modified procedure of Chu et al. (2002) (Table 3, 4). The Hf cuts were finally treated with 1 mL 0.5 M HNO_3/0.1 M HF to remove residual resin and organics.

Table 1: AG50W-X8 (200-400 μm mesh-size, 1.4 mL resin bed) column chemistry (modified after Stichel, 2010).

volume	reagent	stage
10 mL	6MHNO_3/0.5 M HF	pre-clean
2*1 mL	MQ	change the acid
0.5 mL	1MHCl/0.05 HF	pre-clean
1 mL	1MHCl/0.05 HF	pre-condition
1 mL	1MHCl/0.05 HF (sample)	load and directly collect Hf
1.5 mL	1MHCl/0.05 HF	collect Hf
5 mL	3M HCl	elute Fe
2*1 mL	MQ	change the acid
10 mL	2M HNO_3	elute Ba
6.5 mL	6M HNO_3	collect Nd/REE
10 mL	6M HNO_3/ 0.5M HF	clean
2+3 mL	MQ	pass/store

Table 2: LN-Spec resin (50-100 μm mesh size, 2 mL resin bed) column chemistry (modified after Pin and Zalduegui, 1997).

volume	reagent	stage
8 mL	6M HCl	pre-clean
0.5 mL	0.1 M HCl	pre-condition
1 mL	0.1 M HCl	pre-condition
0.5 mL	0.1 M HCl (sample)	load the sample
0.5 mL	0.1 M HCl	wash and elute Ba
9 mL	0.25 M HCl	elute LREE
10 mL	0.25 M HCl	collect Nd
8 mL	6M HCl	Clean
1 mL	0.3M HCl	pass
1 mL	0.3M HCl	store

Table 3: AG1-X8 (200-400 μm mesh-size, 4 cm height and 0.8 cm ∅) column chemistry (modified after Chu et al., 2002)

volume	reagent	stage
8 mL	9 M HCl/1 M HF	clean
2 x 1 mL	4 M HF	pre-condition
2 mL	4 M HF	loading sample
8 mL	4 M HF	eluting matrix
9 mL	6 M HCl/1 M HF	collecting Ti, Zr, Hf + HREE
8 mL	9 M HCl/1 M HF	clean
2 mL	MQ	store

Table 4: Ln-Spec resin (100-150 μm mesh-size, 8.3 cm height and 0.4 cm ∅) column chemistry (modified after Chu et al., 2002).

volume	reagent	stage
12 mL	6 M HCl/1 M HF	clean
2 x 3 mL	2.2 M HCl/1 % H2O2	pre-condition
0.5 mL	2.2 M HCl/1 % H_2O_2	loading sample (Ti, Zr, Hf)
3.5 mL	2.2 M HCl/1 % H_2O_2	eluting Ti
12 mL	6 M HCl	eluting HREE
7 mL	1 M HF	collecting Hf-Zr
12 mL	6 M HCl/1 M HF	clean
2 mL	1 M HCl	store

2.3. Nd and Hf isotope measurements

Neodymium isotope compositions were measured on a NU Plasma (Nu Instruments Limited) and on a Neptune Plus (Thermo Scientific) MC-ICP-MS at GEOMAR, Kiel. A gain calibration of the Faraday cups was carried out directly before the measurements. Nd samples were introduced into the mass spectrometers in 0.5 M HNO_3 and in case of the Hf samples in 0.5 M HNO_3/0.1 M HF. Sample concentrations were determined coarsely by measuring of a small fraction of the sample together with a number of standards with known different Nd or Hf concentrations.

The $^{143}Nd/^{144}Nd$ ratios of 38 samples were measured on a Nu Plasma MC-ICPMS and were corrected for instrumental mass bias to $^{146}Nd/^{144}Nd = 0.7219$, using an exponential mass fractionation law. 174 seawater samples measured on our Neptune

Plus MC-ICPMS, the $^{143}Nd/^{144}Nd$ ratios were double-corrected for instrumental mass bias with $^{146}Nd/^{144}Nd = 0.7219$ and $^{142}Nd/^{144}Nd = 1.141876$ following the approach of Vance and Thirlwall (2002).

Isobaric interferences between ^{144}Sm and ^{144}Nd were corrected by measuring the abundance of the interference-free isotope ^{147}Sm and by calculating the potential ^{144}Sm contribution on mass 144 from the natural abundance of Sm. Mass bias corrected $^{143}Nd/^{144}Nd$ ratios (normalized to a $^{146}Nd/^{144}Nd$ of 0.7219) of the JNdi-1 standard ranged from 0.512046 to 0.512086 on the Nu Plasma MC-ICPMS and from 0.512009 to 0.512080 on the Neptune Plus MC-ICPMS. The mass bias corrected $^{143}Nd/^{144}Nd$ of all samples were normalized to the accepted JNdi-1-standard value of 0.512115 (Tanaka et al., 2000).

The external reproducibility of the Nd isotope measurements was estimated by repeated measurements of in-house Nd standard solutions. For the Neptune Plus, the in-house standard gave reproducibilities between 0.1 and 0.35 ε_{Nd} units (2SD). For the Nu Plasma, the reproducibility of the in-house standard was between 0.2 and 0.4 ε_{Nd} units (2SD).

The $^{176}Hf/^{177}Hf$ ratios of 19 water samples were measured on a Neptune Plus MC-ICPMS and corrected for instrumental mass bias to $^{179}Hf/^{177}Hf = 0.7325$ applying an exponential mass fractionation law. The $^{176}Hf/^{177}Hf$ ratios were normalized to the accepted JMC 475 standard value of 0.28216 (Nowell et al., 1998). The external reproducibility was estimated by repeated measurements of the JMC 475 standard and ranged from 0.59 to 2.76 ε_{Hf} units (2SD) depending on sample size. All samples were corrected for isobaric interferences of lutetium (Lu) and ytterbium (Yb) on mass 176 by monitoring ^{175}Lu and ^{172}Yb.

2.4. Nd and Hf concentration measurements by isotope dilution

2.4.1. Chemical treatment and spike addition

For precise determination of Nd and Hf concentrations based on an isotope dilution method (Rickli et al., 2009), a 1 L aliquot of each water sample was spiked with a pre-weighed ^{150}Nd and ^{180}Hf spike and 15µl of an $FeCl_3$ solution (~200 mg Fe/mL). After

5 days of equilibration Suprapure ammonia solution (25 %) was added to raise the pH to 7.5-8.0 for coprecipitation. Precipitates were chemically treated and chromatographically purified as the precipitates for the Nd isotope separation (section 2.2., Table 1).

Hafnium was further purified by column chemistry using AG1-X8 resin (200-400 μm mesh size, 1.6 ml resin bed), following a modified procedure of Sahoo et al. (2006) (Table 5).

Table 5: AG1-X8 resin (200-400 μm mesh size, 1.6 ml resin bed) column chemistry.

volume	reagent	stage
8 ml	9 M HCl/1 M HF	cleaning
8+8 ml	MQ	cleaning
8 ml	0.1 M HF	pre-condition
2 ml	0.1 M HF (sample)	load the sample
4 ml	0.1 M HF + 2% H_2O_2	elute Fe, Ti
3 ml	1 M HF + 0.2% H_2O_2	elute Zr, Ti (Hf)
3 ml	MQ	wash resin
6+2 ml	6M HCl	collect Hf
8 ml	9M HCl/1 M HF	cleaning, elute W
2+3 ml	MQ	pass/store

2.4.2. Mass spectrometry

Isotope dilution measurements of the Nd and Hf concentrations based on $^{150}Nd/^{144}Nd$ and the $^{178}Hf/^{180}Hf$ ratios were carried out on a Nu Plasma MC-ICPMS. Prior to the concentration measurements, Nd and Hf samples were diluted in 0.5 ml 0.5 M HNO_3 and 0.5 ml 0.5 M HNO_3/0.5 M HF, respectively. Isobaric interferences between Nd and Sm on masses 144, 148 and 150 and the instrumental mass bias were corrected by an iterative correction method Stichel (2010). The mass bias was corrected by a fictional mass fractionation factor, which was used for the initial iteration. After five iterations, no significant changes were observed anymore and the factor was applied for the correction. Isobaric interferences of ^{180}Hf and ^{180}W were corrected by measuring the interference free isotope ^{182}W. Mass bias corrected $^{178}Hf/^{180}Hf$ ratios were corrected for instrumental mass bias by applying an exponential mass fractionation law.

Replicates for each element yielded an external reproducibility of better than 1% for Nd and better than 5% for Hf.

2.5. Rare earth element measurements

REE concentrations were measured with a SeaFAST system (Elemental Scientific Inc.) connected to a Thermo Element XR ICP-MS (Hathorne et al., 2012). In brief, 7 mL of undiluted and acidified seawater samples were each spiked with 70 µl of a 10 ng/g In solution. A 4 mL sample loop was filled before the samples were preconcentrated online on the ion exchange resins within the SeaFAST system while most of the matrix was washed to waste. The REEs were then eluted directly into the ICP-MS spray chamber and data collected in time resolved analysis mode. Raw data were processed with the computer software iolite© to average the intensity peaks for each mass. GEOTRACES inter-calibration samples BATS 15 m and BATS 2000 m (van de Flierdt et al., 2012) were measured to monitor the external reproducibility, which is given as 2 SD for each REE. Neodymium concentrations determined by the seaFAST technique and isotope dilution (n = 44) were identical within the 95% confidence limits as observed with previous seaFAST methods (Hathorne et al., 2012).

3. PUBLICATION AND MANUSCRIPTS

CHAPTER I

Tracing water mass mixing and continental inputs in the southeastern Atlantic Ocean with dissolved neodymium isotopes

Published as: *Rahlf, P., Hathorne, E., Laukert, G., Gutjahr, M., Weldeab, S., & Frank, M., 2020. Tracing water mass mixing and continental inputs in the southeastern Atlantic Ocean with dissolved neodymium isotopes. Earth and Planetary Science Letters, 530, 115944. https://doi.org/10.1016/j.epsl.2019.115944.*

Abstract

In contrast to the vigorous deep ocean circulation system of the north- and southwestern Atlantic Ocean, no systematically sampled datasets of dissolved radiogenic neodymium (Nd) isotope signatures exist to trace water mass mixing and provenance for the more restricted and less well ventilated Angola Basin and the Cape Basin in the southeastern Atlantic Ocean, where important parts of the return flow of the Atlantic Meridional Overturning Circulation are generated. Here, to improve our understanding of water mass mixing and provenance, we present the first full water column Nd isotope (expressed as ε_{Nd} values) and concentration data for a section across the western Angola Basin from 3° to 30° S along the Zero Meridian and along an E-W section across the northern Cape Basin at 30° S sampled during GEOTRACES cruise GA08. Compared with the southwestern Atlantic basin we find overall less radiogenic ε_{Nd} signatures reaching -17.6 in the uppermost 200 m of the Angola and Cape basins. In the western Angola Basin these signatures are the consequence of the admixture of a coastal plume originating near 13 °S and carrying an unradiogenic Nd signal that likely resulted from the dissolution of Fe-Mn coatings of particles formed in river estuaries or near the West African coast. The highly unradiogenic Nd isotope signatures in the upper water column of the northern Cape Basin, in contrast, originate

from old Archean terrains of southern Africa and are introduced into the Mozambique Channel via rivers like the Limpopo and Zambezi. These signatures allow tracing the advection of shallow waters via the Agulhas and Benguela currents into the southeastern Atlantic Ocean. The Nd isotope compositions of the deep water masses in both basins primarily reflect conservative water mass mixing with the only exception being the central Angola Basin, where the signatures are significantly overprinted by terrestrial inputs. Bottom waters of the Cape Basin show excess Nd concentrations of up to 6 pmol/kg (20%), originating from resuspended bottom sediments and/or dissolution of dust, but without significantly changing the isotopic composition of the waters due to similar ε_{Nd} values of particles and bottom waters ranging between -9.6 and -10.5. Given that bottom waters within the Cape Basin today are enriched in Nd, non-conservative Nd isotopic effects may have been resolvable under past glacial boundary conditions when bottom waters were more radiogenic.

1. Introduction

The Atlantic Meridional Overturning Circulation (AMOC) controls meridional heat and salt transport in the Atlantic Ocean and thus exerts important control on present and past global climate. It is also responsible for the transfer of gases such as O_2 and CO_2 from the atmosphere to the deep ocean and thus controls the ventilation and alkalinity of the deep Atlantic Ocean. The AMOC is known to have undergone major changes in the recent past as well as on longer time scales during the Late Quaternary, and its reconstruction based on different geochemical tools has been a major objective of paleoceanographic research (cf. Curry and Oppo, 2005; Böhm et al., 2015).

Radiogenic neodymium (Nd) isotopes are widely used as tracers for present and past large-scale water mass mixing processes. This is possible due to the quasi-conservative behavior of Nd and its average oceanic residence time of 300-1000 yr (Arsouze et al., 2009; Rempfer et al., 2011; Tachikawa et al., 2003). Nd is introduced into the oceans via particulate and dissolved loads of rivers and aeolian dust (Goldstein et al., 1984; Frank, 2002; Goldstein and Hemming, 2003) as well as through exchange with shelf and slope sediments (Lacan and Jeandel, 2001, 2005b). The Nd isotope ratio ($^{143}Nd/^{144}Nd$) of

water masses is commonly expressed as $\varepsilon_{Nd} = [(^{143}Nd/^{144}Nd)_{sample}/(^{143}Nd/^{144}Nd)_{CHUR} -1] \times 10^4$ with CHUR = 0.512638 (Jacobsen and Wasserburg, 1980).

Neodymium isotope data for the Atlantic Ocean, recently extended and refined by the international GEOTRACES program, closely track conservative intermediate and deep water mass mixing of the AMOC (Stichel et al., 2012a, b Lambelet et al., 2016, van de Flierdt et al., 2016, Zieringer et al., 2019). North Atlantic Deep Water (NADW) formed by mixing of source waters in the Labrador and Nordic Seas is characterized by an ε_{Nd} signature of -13.2 to -13.5 (Piepgras and Wasserburg, 1987, Lacan and Jeandel, 2005a, Lambelet et al., 2016). In the subtropical and tropical Atlantic, NADW mixes with Antarctic Intermediate Water (AAIW) and Antarctic Bottom Water (AABW) (Naveira-Garabato et al. 2002). AAIW is formed by mixing of Sub-Antarctic Surface Water with sinking Antarctic Surface Water in the South Atlantic Ocean and is characterized by an average ε_{Nd} signature of -8.7 (Jeandel, 1993), whereas AABW is formed by mixing of cold Antarctic Shelf Water with warmer Circumpolar Deep Water (Orsi et al., 1999) having ε_{Nd} values ranging between -8.6 and -9.6 (Jeandel, 1993; Stichel et al., 2012b).

The application of radiogenic Nd isotopes as conservative water mass tracers is, however, not possible in places such as ocean boundaries, where significant continental inputs of Nd occur via rivers, dust or sedimentary exchange processes (Lacan and Jeandel, 2005b). Nevertheless, pronounced changes in the mixing between Southern Ocean waters and Northern Component waters in the restricted Angola Basin and the Cape Basin of the southeastern Atlantic Ocean (Fig. 1.1) during the Late Quaternary have been inferred from deep water ε_{Nd} signatures obtained by leaching of sedimentary Fe-Mn oxyhydroxides (Jonkers et al., 2015, Klevenz et al., 2008, Piotrowski et al., 2005, Wei et al., 2016). In the modern water column of the Angola Basin, highly unradiogenic ε_{Nd} signatures varying between -13.9 and -11.1 are found for AAIW, which cannot be explained by conservative mixing. Instead, partial dissolution of ferromanganese oxides originating from the Congo River under low oxygen conditions (Rickli et al., 2009, 2010) or near the African shelf (Zheng et al., 2016) have been invoked. Relatively unradiogenic Nd isotope compositions of AAIW have also been found southwest of Africa (ε_{Nd} of -9.3) and have been associated with entrainment of the Agulhas Current (AC) (Stichel et al., 2012a). The lack of seawater Nd isotope and concentration data from the Angola and Cape Basins has, however,

hindered a systematic assessment of the contribution of Nd from the AC, which represents the main surface return flow of the AMOC from the Indian Ocean.

Here we present the first detailed study of the distribution of dissolved Nd isotopic compositions and concentrations in the Angola Basin and in the northern Cape Basin based on filtered seawater samples from 20 full water column profiles collected during GEOTRACES cruise GA08 (Fig. 1.1). We constrain the potential origins of unradiogenic Nd isotopic signatures of surface and deep waters and demonstrate that dissolved Nd isotopes can serve to reliably trace deep water mass mixing in most parts of the southeastern Atlantic Ocean, where deep circulation is more restricted than that of the western South Atlantic.

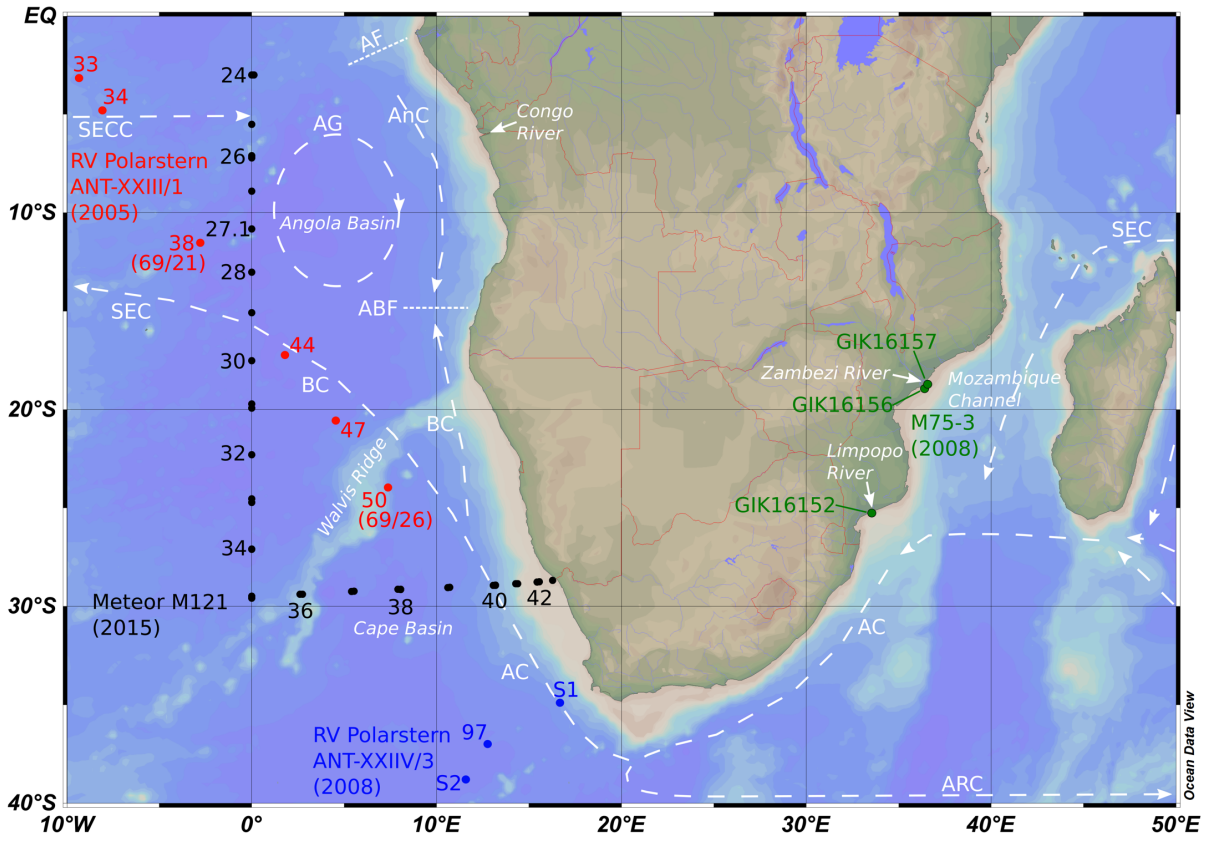

Figure 1.1: Surface circulation map of the Angola Basin, Cape Basin and Mozambique Channel. Black dots represent stations from this study. Red dots represent stations from cruise RV Polarstern ANT-XXIII/1 (2005) (Rickli et al., 2009, 2010). Blue dots represent stations from cruise RV Polarstern ANT-XXIIV/3 (2008) (Stichel et al., 2012a,b). Green dots represent stations from Cruise M75-3 (2008). White dashed arrows indicate surface currents: AC = Agulhas Current, BC = Benguela Current, SEC = South Equatorial Current, ABF = Angola Benguela Front, AF = Angola Front, SECC = South Equatorial Counter Current, AG = Angola Gyre, AnC = Angola Current. (For interpretation of the colors in the figure(s), the reader is referred to the web version of this article.)

1.1. Hydrography

The Benguela Current (BC) is the dominant surface current of the southeastern Atlantic Ocean, originating from the Agulhas Current and introduced via the Agulhas Leakage (Stramma and England, 1999). The BC flows north along the West African coast until it meets the Angola Current at the Angola-Benguela Front (ABF) near 15 °S. A second branch of the BC feeds into the South Equatorial Current, which flows in a northwesterly direction across the entire South Atlantic. Near the Brazilian coast it changes direction and then flows eastward across the South Atlantic as the South Equatorial Counter Current that feeds into the cyclonic Angola Gyre (AG) (Stramma and England, 1999) (Fig. 1.1). The AG is bordered by the Angola Front in the north and by the ABF in the south. South of the Angola Basin, between the Walvis Ridge and Cape Agulhas (34 °S), the southeasterly winds cause strong coastal upwelling (Meeuwis and Lutjeharms, 1990).

Surface waters in the northern part of the Angola Basin are dominated by Tropical Surface Water (TSW), which is characterized by temperatures near 27°C (station 24, 25) (Fig. 1.2) and constitutes the mixed layer of most of the tropical Atlantic. The mixed layer of the southern part of the Angola Basin and the Cape Basin is occupied by Subtropical Surface Water (STSW) as indicated by temperatures near 20°C (Fig. 1.2). TSW and STSW are underlain by South Atlantic Central Water (SACW) (Fig. 1.2) (Sverdrup et al., 1942, Stramma and England, 1999). SACW is transported into the subtropical gyre by the South Atlantic Current, which feeds into the BC. SACW in the tropical Atlantic partly originates from Indian Central Water (ICW), which is advected into the Atlantic Ocean by the Agulhas Current (Stramma and Schott, 1999). Intermediate waters are characterized by a low salinity ranging between 34.3 and 34.6, potential temperatures between 4 and 6 °C and neutral densities of 27.13 kg/m^3 ≤ γ^n ≤ 27.55 kg/m^3, which are typical for nutrient-rich Antarctic Intermediate Water (AAIW) (Fig. 1.2) (Whitworth and Nowlin, 1987). The AAIW in the western South Atlantic originates from the surface of the Antarctic Circumpolar Current (ACC) and is subducted northwards at the Polar Front between 50° and 40°S. In the South East Atlantic Ocean (SEAO), AAIW originates from the Indian Ocean and is advected as part of the Agulhas Current leakage (Roman and Lutjeharms, 2010, Stramma and England, 1999). Northward propagation of AAIW occurs between 500 and 1200 m

water depth (Talley, 1996). Below AAIW, Upper Circumpolar Deep Water (UCDW) prevails at salinities between 34.8 and 34.6, potential temperatures between 3 and 4°C and neutral densities of 27.55 kg/m^3 ≤ γ^n ≤ 27.8 kg/m^3 (Fig. 1.2). The oxygen-poor and nutrient-rich UCDW also originates from the ACC, propagates northwards and loses its characteristics through mixing by the time it reaches the equator (Stramma and Schott, 1999). In the Angola Basin, deep and bottom waters below AAIW are dominated by North Atlantic Deep Water (NADW), characterized by higher salinities between 34.8 and 35, potential temperatures between 2 and 3 °C and neutral densities of 27.8 kg/m^3 ≤ γ^n ≤ 28.12 kg/m^3 (Fig. 2). NADW is advected into the SEAO via a branch of the Deep Western Boundary Current that forms near the equator (Rhein et al., 1995) and enters the Angola Basin across the Romanche Fracture Zone. Bottom waters of the Cape Basin predominantly consist of Lower Circumpolar Deepwater (LCDW) (γ^n ≥ 28.12 kg/m^3), which is markedly distinct from the Angola Basin due to the fact that the Walvis Ridge prevents northward advection of LCDW and Antarctic Bottom Water (AABW) (Fig. 1.2) (e.g. Rickli et al., 2009).

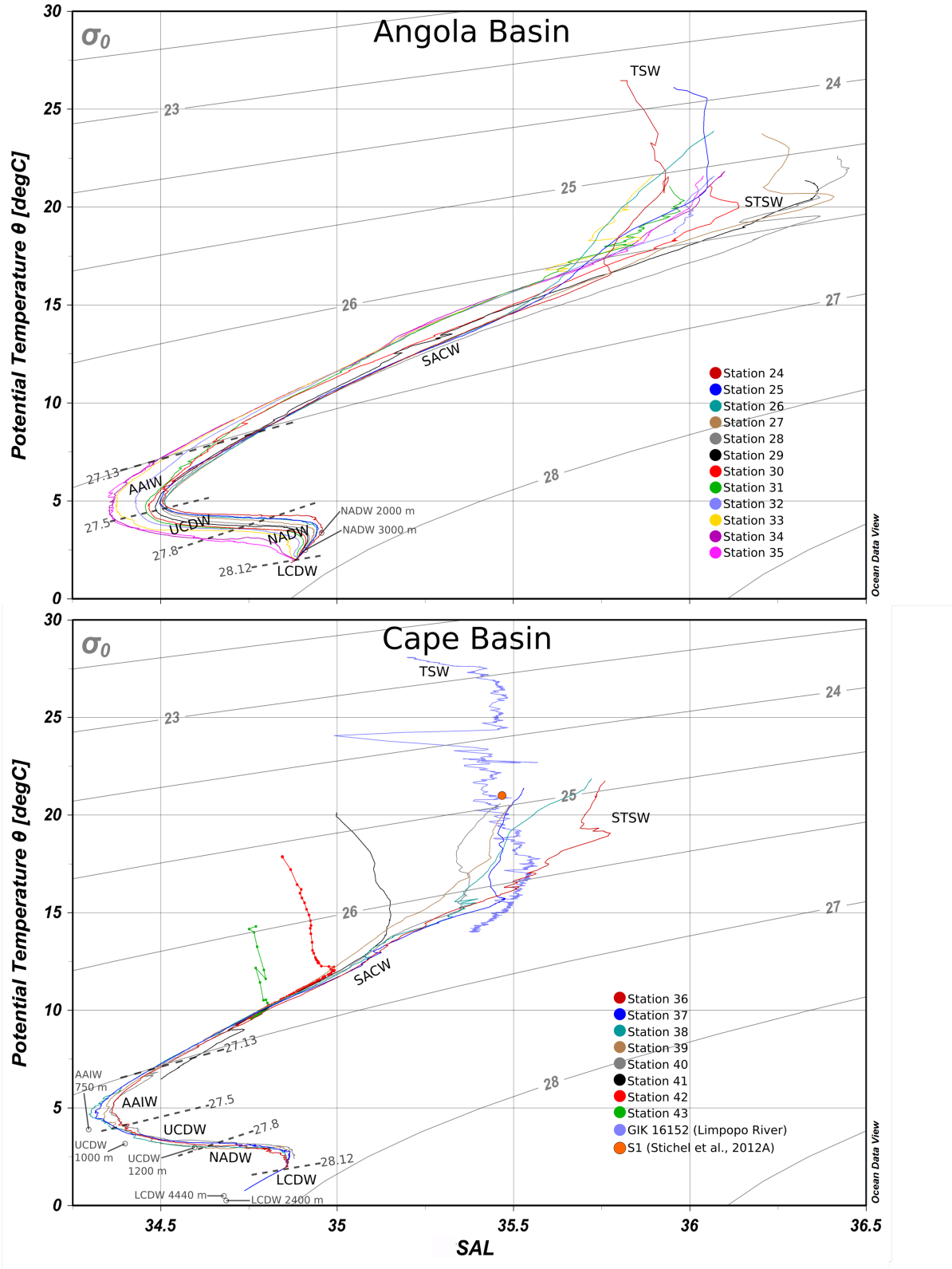

Figure 1.2: T-S plots with stations from this study. The dashed lines indicate neutral densities (γ^n). The water mass endmembers used for mixing calculations (Fig. 1.6) are marked with circles. Bottom waters of the Angola Basin mainly consist of North Atlantic Deep Water (NADW), whereas bottom waters of the Cape Basin consist of a significant portion of Lower Circumpolar Deepwater (LCDW). Surface waters of the Cape Basin are South Atlantic Central Water (SACW) and Subtropical Surface Water (STSW), while surface waters of the Angola Basin are mainly Tropical Surface Water (TSW). The TSW from the Limpopo River area mixes with the STSW from the Cape Basin.

The Agulhas Current is the largest boundary current in the world's ocean and originates from the South Equatorial Current in the tropical Indian Ocean, which is a mixture of contributions from the Tasmanian leakage, the Indonesian Throughflow, the Red Sea and the Arabian Sea (Durgadoo et al., 2017). It bifurcates near the northeastern tip of Madagascar and feeds warm and saline waters into the Madagascar and Mozambique currents (Stramma and Lutjeharms, 1997) (Fig. 1.1). The Agulhas Current then flows along the east coast of South Africa, detaches from the continent at the Agulhas Bank and is partly retroflected into the Indian Ocean as the Agulhas Return Current. The remaining waters are advected into the SEAO via the Agulhas Leakage, as cyclonic and anticyclonic eddies and filaments, thereby feeding the surface return flow of the AMOC (Loveday et al., 2014).

The main water masses in the Mozambique Channel contributing to the upper water column and ultimately to the Agulhas Current are Tropical Surface Water (TSW) and Subtropical Surface Water (STSW) (Ullgren et al., 2012). The TSW or Equatorial Surface Water (Sæter and Jorge da Silva, 1984) is a warm (28 °C) and low salinity water mass (<34.5), carried by the South Equatorial Current-into the central Mozambique Channel (Tomczak and Godfrey, 1994). The STSW is also a warm (21-28 °C), but highly saline water mass (35.2-35.5) (Ullgren et al., 2012) that prevails in the upper 300 m of the southern Channel (Sæter and Jorge da Silva, 1984).

2. Methods

Seven near surface water samples were taken during Meteor Cruise M75-3 in 2008 from the runoff-influenced areas of the Zambezi and Limpopo Rivers in the Mozambique Channel. 106 water samples from the Angola and Cape Basin were taken during GEOTRACES cruise GA08 (RV Meteor cruise M121) in November/December 2015 along the Zero Meridian between 3°S and 30°S, followed by an E-W section along 30°S between 0° and 17°E near the South African coast (Fig. 1.1). Samples from the full water column were collected with 10 l Niskin bottles attached to a stainless steel CTD rosette, while surface water samples were recovered with a towed stainless steel fish. The samples were then treated in the onboard laboratory strictly following recommended GEOTRACES protocols (van de Flierdt et al., 2012). Each 20 L sample

was filtered through a nitro-cellulose acetate filter (0.45 µm pore diameter) into an acid-cleaned LDPE-cubitainer with a peristaltic pump within 2 h after sample collection, and subsequently acidified with ~20 ml concentrated, distilled HCl. For Nd concentration measurements, 2 L aliquots from each filtered sample were collected in acid-cleaned 2-liter PE-bottles. To each large volume sample 400 µl $FeCl_3$ solution (~200 mg Fe/ml) were added and the sample was left to equilibrate for 24 h. Ammonia solution (25 %, Merck Suprapur®) was then added to raise the pH from about 2 to 7.5-8.0. After 48 h, the trace elements co-precipitated with the FeOOH settled to the bottom of the cubitainers and the supernatant was syphoned off.

The precipitates were transported to the home laboratory at GEOMAR in 2 L bottles and were centrifuged and rinsed three times with deionized water (MilliQ, 18.2 MΩcm) in 50 ml centrifuge tubes to remove major seawater ions. After dissolution in 6 M HCl/0.5 M HF and transfer into Teflon vials the samples were evaporated to dryness. To remove organic compounds, the samples were treated with aqua regia at 120 °C for 24 h. Most of the Fe was subsequently removed via liquid–liquid extraction with pre-cleaned di-ethyl ether (Stichel at al., 2012b). The rare earth elements (REEs) were chromatographically separated from matrix elements using cation exchange resin AG 50W-X8 (1.4 ml, 200-400 µm) and following a modified protocol of Münker et al. (2001). Neodymium was then separated from the other REEs for isotope measurements using Eichrom®LN-Spec resin (2 ml, 50-100 µm) following a modified protocol of Pin and Zalduegui (1997). To remove residual traces of the resin and organic compounds, the Nd cuts were treated with 100 µl quartz distilled HNO_3 and 100 µl H_2O_2 (30 wt.%, Merck Suprapur®).

For the determination of Nd concentrations, 1 L aliquots were spiked with a pre-weighed ^{150}Nd spike and then purified with the same cation column chemistry that was used for the Nd isotope separation. Nd concentrations were then determined via isotope dilution on a Nu Plasma MC-ICPMS (Nu Instruments).

The $^{143}Nd/^{144}Nd$ ratios of 25 samples were measured on a Nu Plasma MC-ICPMS and were corrected for instrumental mass bias to $^{146}Nd/^{144}Nd = 0.7219$, using an exponential mass fractionation law. Isobaric interferences between ^{144}Sm and ^{144}Nd were corrected by measuring the abundance of the interference-free isotope ^{147}Sm and

by calculating the potential ^{144}Sm contribution on mass 144 from the natural abundance of Sm. Mass bias corrected $^{143}Nd/^{144}Nd$, normalized to a $^{146}Nd/^{144}Nd$ of 0.7219, for the JNdi-1 standard on the Nu Plasma MC-ICPMS ranged from 0.512046 to 0.512086 and on the Neptune Plus MC-ICPMS ranged from 0.512009 to 0.512080. The mass bias corrected $^{143}Nd/^{144}Nd$ of all samples were normalized to the accepted JNdi-1-standard value of 0.512115 (Tanaka et al., 2000). In the case of the 81 seawater samples measured on our Neptune Plus MC-ICPMS, the $^{143}Nd/^{144}Nd$ ratios were double-corrected for instrumental mass bias with $^{146}Nd/^{144}Nd$ = 0.7219 and $^{142}Nd/^{144}Nd$ = 1.141876 following the approach of Vance and Thirlwall (2002). The external reproducibility of the Nd isotope measurements was estimated by repeated measurements of in-house Nd standard solutions. For the Neptune Plus, the in-house standard gave reproducibilities between 0.1 and 0.35 ε_{Nd} units (2SD). For the Nu Plasma, the reproducibility of the in-house standard was between 0.2 and 0.4 ε_{Nd} units (2SD). The external reproducibility for Nd concentration measurements was 2 % (2SD, n = 4 sample replicates).

3. Results

Neodymium isotope compositions and concentrations are listed in supplementary Table A1 and are plotted together with previously published data from one station in the Angola Basin (69/21) and one station in the Cape Basin (69/26) (Rickli et al., 2009) in Fig. 1.3. The data from the two cruises show consistent distributions. In addition, our data are displayed in a section plot together with Nd isotope and concentration data from the Southern Ocean obtained during Polarstern cruise ANT-XXIV/3 (Stichel et al., 2012a, b) (Fig. 1.4).

3.1. Surface waters

Surface waters in the Angola Basin, and Cape Basin between stations 26 and 40, have highly unradiogenic ε_{Nd} values of -14.5 to -17.6 (Fig. 1.3). Between stations 41 and 43, in the Benguela Upwelling area above the South African shelf, the εNd signatures are significantly more radiogenic (-8.3 to -13.5) (Fig. 1.3). Surface water Nd concentrations

in the Angola Basin range between 9.8 pmol/kg and 36.1 pmol/kg, with highest concentrations prevailing at station 28 (Fig. 1.3). The surface water concentrations in the Cape Basin range between 7.5 and 21.9 pmol/kg, with the highest concentrations observed near the coast at station 43 (Fig. 1.3).

Surface waters off the Zambezi River mouth have ε_{Nd} signatures of -15.5 (GIK16156) and -14.7 (GIK16157) and Nd concentrations reach 50.6 and 63.9 pmol/kg, respectively. Surface waters off the Limpopo River mouth are characterized by ε_{Nd} signatures near -22 and concentrations between 54 and 97 pmol/kg (Supplementary Table A2).

3.2. Intermediate waters

Intermediate waters between 500 and 1500 m have the lowest ε_{Nd}-value of -13.2 in the central Angola Basin (station 28) and the signatures become more radiogenic southwards, reaching ε_{Nd} values of up to -10.4 at station 35 (Figs. 3, 4). Nd concentrations for these waters range between 11.6 pmol/kg (station 35) and 18.5 pmol/kg (station 28). In contrast, the ε_{Nd} signatures of intermediate waters along the Cape Basin section are essentially invariant at values around -10 and Nd concentrations near 12 pmol/kg (Figs. 3, 4).

3.3. Deep and bottom waters

Deep waters in the southern and central Angola Basin between 1500 and 4000 m depth are characterized by ε_{Nd} values between -11 (station 35) and -14.4 (station 28), respectively. In the northern part of the basin, ε_{Nd} values are near -13 and hence are close to typical values for NADW (station 24) (Figs. 3, 4). In contrast, deep Cape Basin waters in the density range of NADW are more radiogenic (ε_{Nd} = -11 to -12.5). At 1500 m water depth, Nd concentrations vary between 13.9 and 22.3 pmol/kg in the Angola Basin, while Nd concentrations of all stations in the Cape Basin are constant at ~14 pmol/kg (Fig. 1.4). Both basins exhibit a nearly linear increase in Nd concentration with water depth to ~25 pmol/kg at 4000 m (Fig. 1.4).

Bottom waters in the Angola Basin show ε_{Nd} values between -11.7 and -13 and Nd concentrations between 24.6 and 29.8 pmol/kg (Fig. 1.3), whereas the signatures of bottom waters in the Cape Basin are significantly more radiogenic (ε_{Nd} ~ -10) and the Nd concentrations increase to 37 pmol/kg between 4000 and 5000 m water depth (Fig. 1.3).

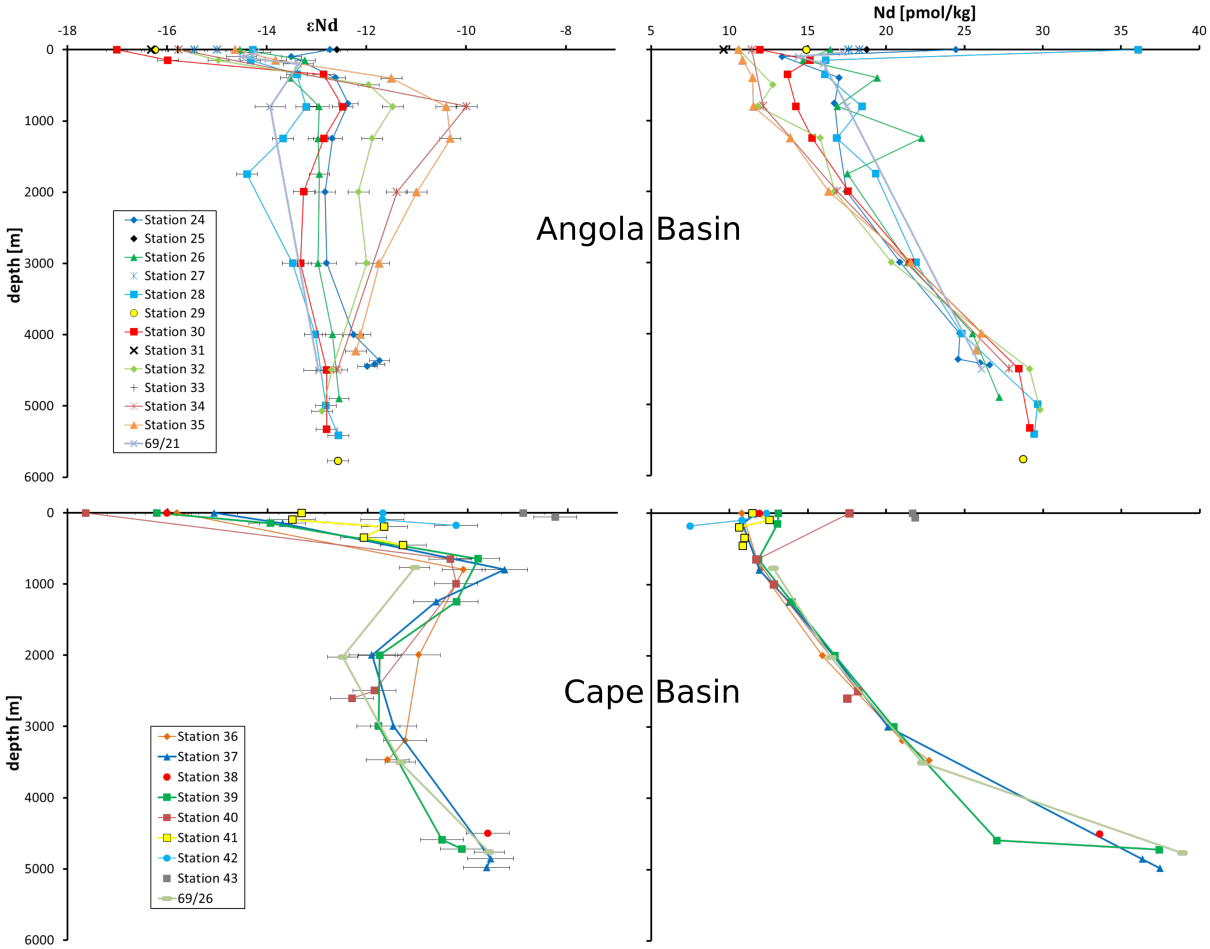

Figure 1.3: Profiles of the Nd isotopic compositions (ε_{Nd}) and concentrations from the Angola and Cape Basins. Surface waters of both basins have highly unradiogenic ε_{Nd} values of up to -17.6, whereas intermediate waters have ε_{Nd} values between -10 and -14. Bottom waters of the Cape Basin are more radiogenic (ε_{Nd} -10) than those of the Angola Basin (ε_{Nd} -13). Surface water concentrations of the basins are between 10 and 20 pmol/kg but have a peak concentration of 36 pmol/kg in the Angola Basin at station 28. Isotope compositions and concentrations of stations 69/21 and 69/26 (Rickli et al., 2009) are similar to the values we measured.

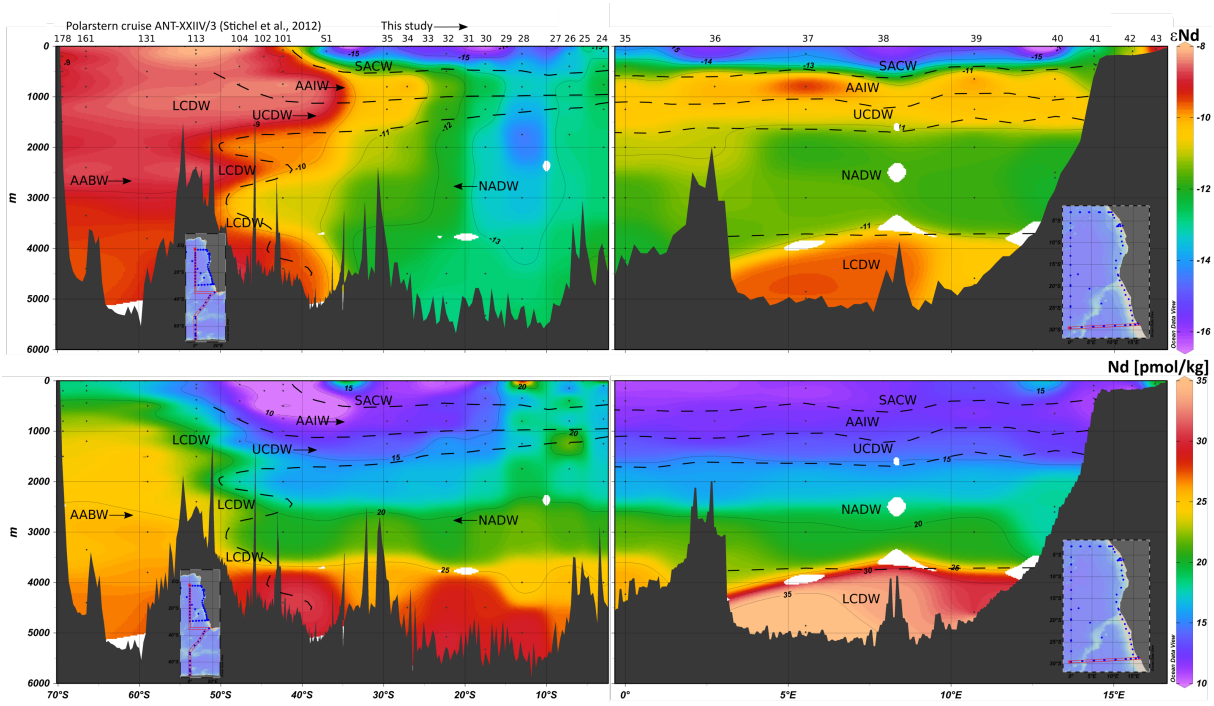

Figure 1.4: Nd isotopic compositions and Nd concentrations of the Angola Basin and Cape Basin from this study, together with data from cruise ANT-XXIII/3 (Stichel et al., 2012 a,b). Dashed lines indicate approximate boundaries of the prevailing water masses. Sections were produced using Ocean Data View (Schlitzer, 2019) and modified manually.

4. Discussion

4.1. Sources of unradiogenic Nd

The highly unradiogenic ε_{Nd} values of surface waters in the Angola Basin and Cape Basin of up to -17.6 cannot be explained by water mass mixing processes, and must at least partly be the result of regional terrestrial Nd inputs originating from old continental source rocks. Below we discuss the potential sources of such unradiogenic Nd inputs.

4.1.1. Aeolian dust

A possible source of terrestrial material with unradiogenic neodymium isotope signatures is aeolian dust (Goldstein et al., 1984, Tachikawa et al., 1997, 1999). The Sahara-Sahel Dust Corridor (SSDC) between 12°N and 28°N is the world's largest source of desert-derived dust, reaching an annual production of 400-700 million tons/year (Middleton and Goudie, 2001, Moreno et al., 2006). The dust is transported

across the Atlantic Ocean by the trade wind belts (Grousset et al., 1988). However, the deposition of Saharan dust mainly occurs between 10° N and 30° N (Karyampudi et al., 1999, Mahowald et al., 2005, Moreno et al., 2006) and does not pass the inter tropical convergence zone to reach the South Atlantic Ocean. Furthermore, ε_{Nd} signatures of -8.5 and -14.6 in the dust (Goldstein et al., 1984, Grousset et al., 1988) are too radiogenic to explain the surface water signatures of the Angola and Cape Basin. While dust from the Namib and Kalahari desert in southern Africa is transported into the SEAO, the dust concentrations above this region are relatively low (0.06 to 0.23 $\mu g/m^3$) (Chester et al., 1972) compared to the Sahara (Mahowald et al., 2005). Most importantly, ε_{Nd} signatures of dust collected above the Angola Basin range between -9.1 and -10.4 and are thus also far too radiogenic to explain the observed highly unradiogenic surface seawater values (Goldstein et al., 1984, Grousset, et al., 1988, Rickli et al., 2010). Based on these observations, aeolian dust input is unlikely to be a major source of the unradiogenic dissolved surface water Nd isotope signatures in the Angola Basin.

4.1.2. Sedimentary Fe-Mn oxides in the Angola Basin

Fe-Mn oxide coatings of marine sediment particles are important carriers of Nd and other REEs and release these elements to ambient seawater under low oxygen conditions (Haley and Klinkhammer, 2003). Nd isotope compositions of Fe-Mn oxides in Congo fan sediments and in Congo River borne shelf and slope sediments further south at 13 °S have an average ε_{Nd} value of -16.3 and -22.9, respectively (Bayon et al., 2004, 2009). Lateral advection of Nd released by the reduction of Fe-Mn coatings of suspended particles in the oxygen minimum zone of the Angola Basin, between 100 and 700 m water depth (Rickli et al., 2010), is a suitable potential source of unradiogenic Nd to the waters of the upper water column and provides a viable explanation for the high surface Nd concentrations at station 28. This is further supported by the observation of a trace metal enriched plume originating from the African coast and extending 2500 km into the subtropical gyre between 11 and 15 °S (Noble et al., 2012, Zheng et al., 2016).

4.1.3. Surface waters of the Cape Basin

With ε_{Nd} values of up -17.6, surface waters in the Cape Basin are less radiogenic than those of the Angola Basin. However, along the Cape Basin transect there is no evidence for a trace metal enriched plume extending from the coast. The Nd isotope compositions of shelf and slope sediments from the Cape Basin (ε_{Nd} = -13.3) and of dust particles (ε_{Nd} = -10.9) (Bayon et al., 2009) are too radiogenic to cause the observed near surface water signatures. Similarly, with ε_{Nd} values varying between -14 to -12 (Franzese et al. 2006), the Nd isotope compositions of sediments along the proximal South African coast are too radiogenic to explain the observed highly unradiogenic signatures. However, Nd isotope signatures of -9 to -13 of surface waters at stations 41-43 are likely caused by partial dissolution of suspended sediments from the Orange River, which have similar ε_{Nd} signatures (Weldeab et al., 2013).

4.1.4. The Mozambique Channel and the Agulhas Current

Surface waters near southwestern South Africa are marked by highly unradiogenic ε_{Nd} signatures as revealed by one sample yielding a value of -18.9 (S1, Fig. 1.1), which is consistent with the influence of the Agulhas Current receiving its unradiogenic signature from particle dissolution close to the eastern coast of southern Africa (Stichel et al., 2012a). A potential source region for these particles is the Mozambique Channel, which receives large amounts of sediments from the Zambezi and Limpopo Rivers. Surface waters of the Zambezi discharge area have ε_{Nd} signatures between -14.7 (GIK16157) and -15.5 (GIK16156) (Supplementary Table A2), whereas the river suspended load is less radiogenic and has a mean ε_{Nd} value of -16.7. Surface sediments directly at the river mouth have ε_{Nd} values as negative as -17.7 (van der Lubbe et al., 2016). The dissolved and particulate river loads are only slightly more radiogenic than the isotopic signatures of the near surface Cape Basin. It is, however, likely that the signatures released, for example from resuspension induced by deep reaching eddies, can also be less radiogenic depending on the exact origin of the sediment particles transported by the Agulhas Leakage into the Cape Basin either in particulate or dissolved form.

Surface waters at the Limpopo River mouth have ε_{Nd} signatures as negative as -22.4 (GIK16152, Supplementary Table A2). According to the T-S-relationships these mix with water of Station S1 (Stichel et al., 2012a) and SACW encountered at stations 36-40 of the Cape Basin (Fig. 1.2). We selected Station S1 as an endmember and calculated mixing relationships between S1 (Stichel et al., 2012a), SACW of the Cape Basin and TSW/STSW of the Angola Basin (Fig. 1.5). For the Agulhas Current endmember represented by station S1 (Stichel et al., 2012a) we chose an ε_{Nd} signature of -18.9 and a salinity of 35.47. For SACW, an ε_{Nd} value of -9.6 and a salinity of 34.79 was adopted (Jeandel, 1993). For TSW/STSW an ε_{Nd} of -12.8 and a salinity of 36.39 was used (Zieringer et al., 2019). As a result, we find that a mixture between SACW from the Cape Basin and waters from S1 can explain the unradiogenic surface water signatures, noting that waters from S1 are likely influenced by even less radiogenic waters from the Mozambique Channel (Fig. 1.5). Station 43 in the Cape Basin consists of almost pure SACW, whereas station 40 located only 164 nautical miles further offshore to the west is most influenced by waters of the Agulhas Current (Fig. 1.5). The Nd isotopic compositions of surface waters from the western Cape Basin and Angola Basin are less radiogenic than the mixing line between SACW and TSW/STSW (Fig. 1.5) and clearly indicate admixture of the unradiogenic Agulhas Current (Fig. 1.5). The compositions of stations 27 to 30 and fish 44 (Rickli et al., 2009) are close to the mixing line between TSW/STSW and S1, indicating that these stations are also strongly influenced by the Agulhas Current. Overall, our Nd data track the Agulhas Current entering the Cape Basin at station 40, flowing across the Angola Basin, passing the location of fish 44 (Rickli et al., 2010) and exiting the basin close to station 30 (Fig. 1.1).

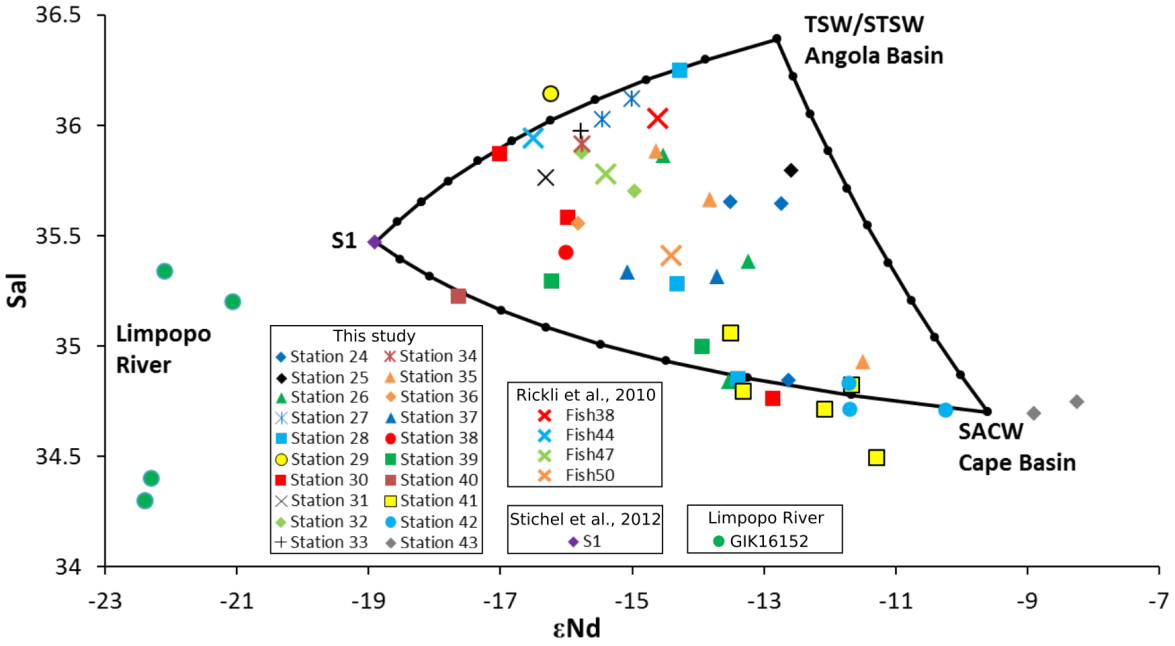

Figure 1.5: Salinity versus ε_{Nd} for shallow waters between 0 and 400 m water depth, showing mixing relationships between regional endmembers S1 (Stichel et al., 2012a), SACW of the Cape Basin and TSW/STSW of the Angola Basin. For the Agulhas Current endmember represented by station S1 (Stichel et al., 2012a) we chose an ε_{Nd} signature of -18.9 and a salinity of 35.47. For SACW, an ε_{Nd} value of -9.6 and a salinity of 34.79 were adopted (Jeandel, 1993). For TSW/STSW an ε_{Nd} of -12.8 and a salinity of 36.29 was used (Zieringer et al., 2019). The plot indicates that near surface waters of the Cape Basin and Angola Basin are a mixture of SACW, TSW/STSW and unradiogenic waters from the Mozambique Channel.

4.2. Intermediate waters

Mixing relationships between the intermediate and deep water masses NADW, AAIW and UCDW were calculated in order to evaluate to what extent the Nd isotope and concentration data reflect conservative mixing in the Angola and Cape basins (Figs. 6a, b). We chose regional water mass endmembers prevailing at the northern and southern borders of the research area, which mix at the corresponding depths according to the TS-relationships (Fig. 1.2). The northernmost station of the Angola Basin (station 24, 2000 m, ε_{Nd} = -12.8, Nd = 17.5 pmol/kg, salinity = 34.95) was selected for the regional NADW endmember signature. The regional AAIW- and UCDW-endmember compositions (ε_{Nd} = -8.2, Nd = 10.9 pmol/kg, salinity = 34.28 and ε_{Nd} = -8.5, Nd = 11.8 pmol/kg, salinity = 34.37, respectively) were adopted from station 101 in the southern Cape Basin (Stichel et al. 2012b). In the Angola Basin the contribution of NADW decreases southward, reflecting gradual dilution with southern sourced AAIW and UCDW (Fig. 1.6a). However, all stations have a less radiogenic ε_{Nd} signature than expected from the mixing lines, except station 35 (1248 m) (Fig. 1.6a).

To quantify the variability not related to conservative water mass mixing, we calculated the difference $\Delta\varepsilon_{Nd}$ between measured ε_{Nd} values and the corresponding ε_{Nd} values resulting from pure water mass mixing of the two previously defined regional endmembers. The same was done for Nd concentrations (Δ_{Nd}). We defined deviations from conservative mixing exceeding ±0.5 ε_{Nd} units and ±0.8 pmol/kg Nd as indicating non-conservative behavior. This is based on the max 2SD uncertainties of the Nd isotope measurements and on a 2 % uncertainty of the highest measured Nd concentration. The patterns of $\Delta\varepsilon_{Nd}$ and Δ_{Nd} for all samples below 500 m are shown in Fig. 1.7. Intermediate waters of the Angola Basin are 1 to 2.5 ε_{Nd} units less radiogenic and reach elevated Nd concentrations of up to 30 % (1 to 5 pmol/kg) (Fig. 1.7), compared with calculated values assuming conservative mixing. The highest $\Delta\varepsilon_{Nd}$ and Δ_{Nd} occur in the northern and central part of the basin above 3500 m water depth, where low oxygen conditions are likely responsible for the reduction of Fe-Mn oxyhydroxides near the coast and the associated release of unradiogenic Nd to intermediate waters (Rickli et al., 2010) (see 4.1.2).

The intermediate waters of the Cape Basin constitute a well constrained mixture of 90 % AAIW and 10 % NADW between 650 and 800 m water depth and a mixture of 60-80 % AAIW/UCDW and 40-20 % NADW between 1000 and 1200 m water depth (Fig. 1.6b). However, water samples between 650 and 800 m do not exactly fall on the mixing line and are slightly less radiogenic ($\Delta\varepsilon$Nd ~ -1), whereas Nd concentrations remain constant (Fig. 1.7). These intermediate waters likely acquired their unradiogenic Nd isotope signatures remotely via reversible scavenging (Siddall et al., 2008), partial dissolution of sinking particles or boundary exchange processes in the Mozambique Channel and subsequent advection of this unradiogenic Nd into the Cape Basin via the Agulhas Leakage.

4.3. Deep waters

Deep water mixing relationships were calculated between NADW and UCDW/LCDW in the Angola Basin, (Fig. 1.6c, d). For mixing calculations at 2000 m water depth, we again used the regional NADW endmember from the northernmost station of the Angola Basin (station 24, 2000 m depth) and the regional UCDW

endmember from station 104 (1200 m, ε_{Nd} = -8.5, Nd = 13.82 pmol/kg, salinity = 34.63) (Stichel et al. 2012b). For mixing calculations at 3000 m water depth, NADW at station 24 at 3000 m water depth (ε_{Nd} = -12.8, Nd = 20.89 pmol/kg, salinity = 34.9) and LCDW at station 113 (2400 m depth) (ε_{Nd} = -8.5, Nd = 24.51 pmol/kg, salinity = 34.68) (Stichel et al. 2012b) were used as regional endmembers. While deep waters in the northern Angola Basin are composed of almost pure NADW, the southern Angola Basin waters represent a conservative mixture of 30-40 % UCDW and LCDW (Fig. 1.6c). Deep water masses of the central Angola Basin (station 28, 30) exhibit an unradiogenic Nd isotope excess ($\Delta\varepsilon_{Nd}$ ~ -1.5) (Fig. 1.7). At the same time Nd concentrations are slightly elevated by a maximum of 10 % (ΔNd ~ +1 pmol(kg) between 2000 and 3000 m water depth and are essentially in agreement with the water mass mixing relationship and similar to modeled ΔNd values from the Angola Basin at ~12 °S (cf. Zheng et al., 2016). This can be explained by partial dissolution of Fe-Mn oxides originating from surface waters (see 4.1.2). Lateral transport of dissolved Nd originating from sediments of the African shelf may also contribute to the observed patterns (Zheng et al., 2016). In contrast, deep waters of the northern and southern Angola Basin are not marked by significant $\Delta\varepsilon_{Nd}$ and ΔNd values and thus are dominantly controlled by preformed REE concentrations thus reflecting essentially conservative water mass mixing (Figs. 6c, 7).

Deep waters of the eastern Cape Basin contain a NADW fraction of up to 80-90 %, whereas NADW in deep waters of the western Cape Basin (station 36) is mixed with up to 40 % UCDW/LCDW (Fig. 1.6d). This is consistent with the notion that these deep waters from 3000 m depth in the Cape Basin are directly mixed with NADW (Rickli et al., 2009), which can be explained by exchange across gaps in the Walvis Ridge. Differences between measured and calculated Nd isotopic compositions and concentrations in deep waters of the Cape Basin are within the defined uncertainty range ($\Delta\varepsilon_{Nd}$ = ±0.5, ΔNd = ± 0.8), again suggesting essentially conservative water mass mixing (Fig. 1.7). However, at ~3000 m depth near the slope area, a significant Nd loss of up to 18 % (ΔNd ~ -4) is observed, which likely results from Nd scavenging by resuspended shelf sediments.

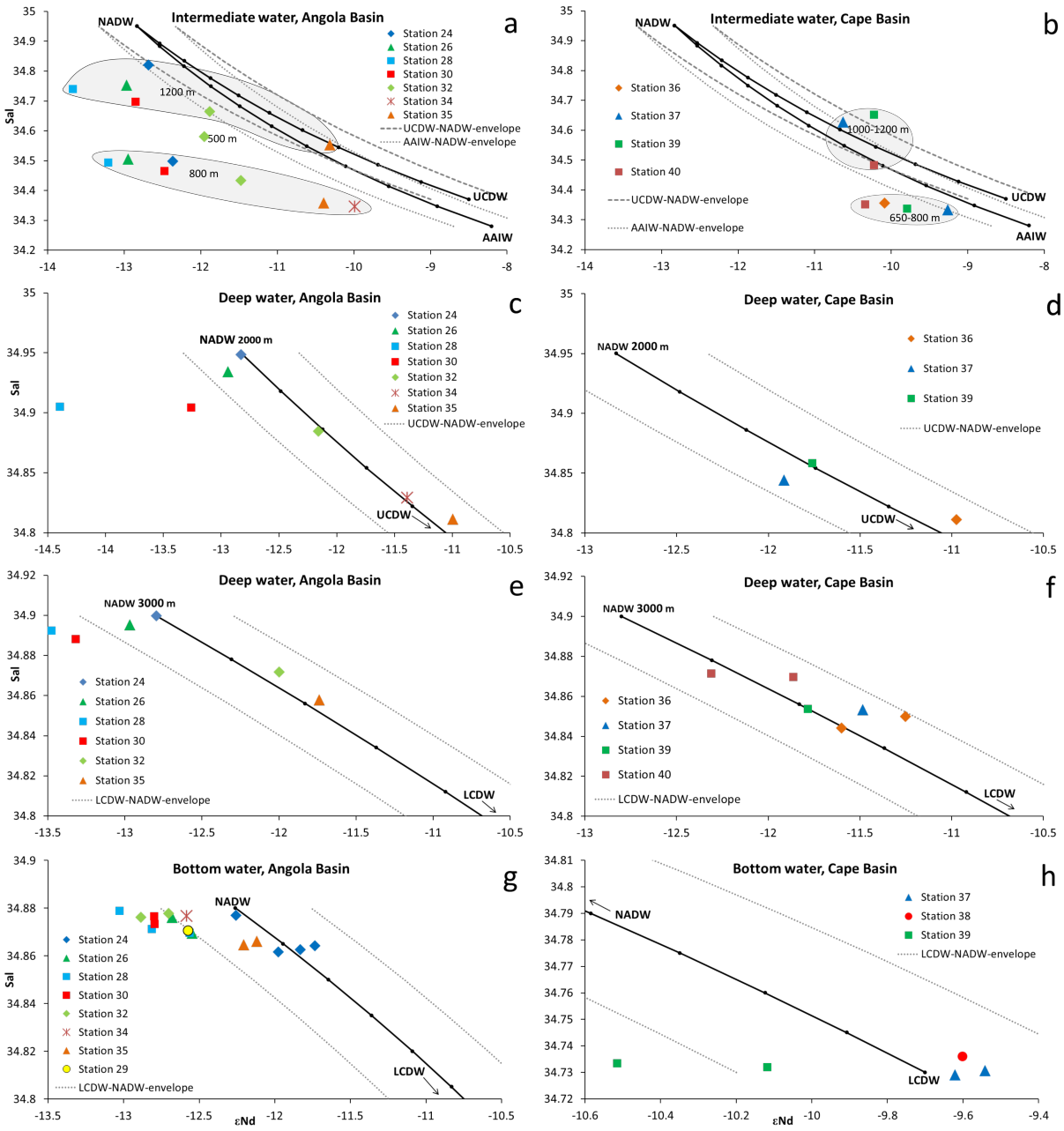

Figure 1.6: Salinity versus ε_{Nd} diagrams for all water masses of the Angola and Cape Basin.

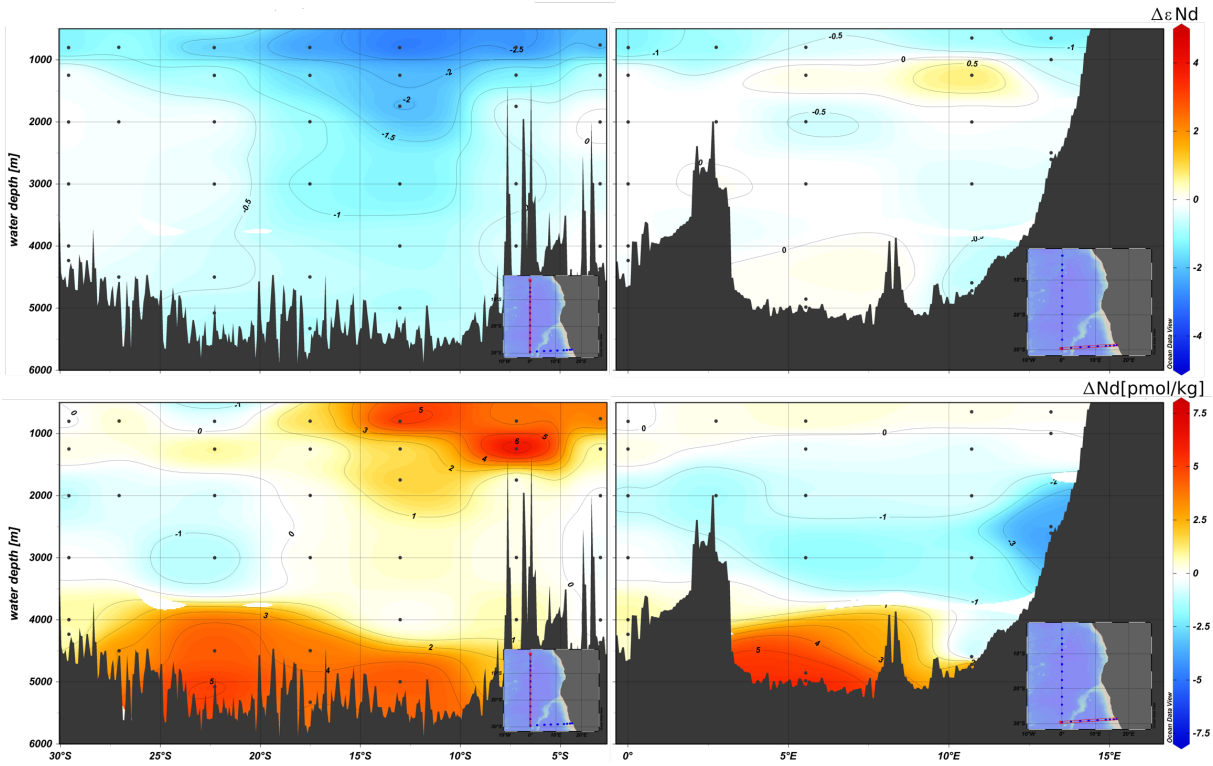

Figure 1.7: $\Delta\varepsilon_{Nd}$ and ΔNd values mark the differences between measured ε_{Nd} values and Nd concentrations and those calculated based on conservative water mass mixing. White areas reflect conservative mixing within the uncertainty ranges of $\Delta\varepsilon_{Nd}$ ±0.5 ε_{Nd} and ΔNd ±0.8 pmol/kg, respectively. Red colors indicate an excess of radiogenic Nd and of Nd concentrations. Blue colors indicate an excess of unradiogenic Nd and removal of Nd.

4.4. Bottom waters

For mixing relationships of the bottom waters, the same NADW regional endmember as for the deep waters was chosen and the LCDW regional endmember was adopted from station 104 (4440 m depth, ε_{Nd} = -8.7, Nd = 27,9 pmol/kg, salinity of 34.69 (Stichel et al. 2012b). Bottom waters of the Angola Basin are composed of almost pure NADW (Fig. 1.6e), but are slightly less radiogenic than expected from the conservative mixing relationships and exhibit excess Nd concentrations of up to 20 % (ΔNd = ~+5 pmol/kg) (Fig. 1.7). This excess can be explained by release of REEs from particles sinking from surface waters into the hydrographically isolated deep Angola Basin (Rickli et al., 2009, Zheng et al. 2016).

Cape Basin bottom waters are composed of pure LCDW, based on hydrographic parameters (Stichel et al., 2012b) and on Nd isotope compositions (Fig. 1.6h) but also show an excess Nd concentration (ΔNd = ~+6 pmol/kg) (Fig. 1.7), which is about 20 % higher than the calculated expected concentration for conservative LCDW (Fig.

1.6h). However, at the same time no significant change of the Nd isotope composition ($\Delta\varepsilon_{Nd}$) is observed (Fig. 1.7). The Nd excess likely originates from partial dissolution of resuspended sediments and/or dust particles from the Namib or Kalahari deserts, which have isotope compositions of -9.8 to -11.4 and -9.3 to -10.9 (Bayon et al., 2004), respectively, similar to those of Cape Basin bottom waters (-9.6 to -10.5) (Fig. 1.6). A simple mass balance calculation reveals that the dissolved sediment or dust would need to have an ε_{Nd} signature above -7.2 or below -12.7 to change the isotope composition of LCDW beyond ±0.5 ε_{Nd} units, assuming that particle dissolution results in similar excess Nd concentrations mixed with LCDW as today. This indicates that terrigenous inputs with extremely low or high Nd isotope compositions are required to significantly alter the Nd isotope compositions of the bottom waters in the study area in the modern regional deep water mass configuration. Available evidence from detrital sediment compositions in the Cape Basin (Dausmann et al., 2017) suggests that the ε_{Nd} range between -7.2 and -12.7 was not exceeded over the past 12 Myr. Thus, while local additions affect the Nd concentration in the deep Cape Basin, water mass mixing exerts the key control over the Cape Basin bottom water Nd isotope composition in the modern regional deep water mass configuration. However, the non-conservative Nd isotope effect may have been more pronounced under glacial boundary conditions such as the Last Glacial Maximum (LGM), when NADW contributions to Cape Basin deep water were significantly lower resulting in a more radiogenic signature of the bottom waters of ~-6 as extracted from sediments (Piotrowski et al., 2004). Without non-conservative Nd addition in the Cape Basin, the ambient glacial bottom water value may hence have been somewhat more radiogenic than -6.

4.5. Comparison of the eastern and western South Atlantic Basins

We compare our Nd isotope compositions from the Angola and Cape basins with Nd isotope measurements from full water profiles at 30°0’ S, 1°25’W (station 217, eastern South Atlantic) and at 33°15’S, 41°45’W (station 302, western South Atlantic) (Jeandel 1993). Although station 217 is located at a distance of only 80 nautical miles from our station 35, surface waters at station 217 are three ε-units more radiogenic than at station

35 but interestingly match the isotope compositions of surface waters in the eastern Cape Basin (Fig. 1.8). AAIW at station 217 (εNd -6) also shows a more radiogenic value than presented in Stichel at al. (2012b) and the values we detected for the Angola and Cape basins, but for NADW similar values at all locations are observed (Fig. 1.8). The large differences between the AAIW measurements may be due to the fact that Jeandel (1993) at the time used unfiltered seawater samples, so that release from more radiogenic particles during seawater acidification may have contributed to these more positive signatures. The western South Atlantic water masses, except NADW, are generally more radiogenic than the Angola and Cape basins in the east. This can be explained by the unrestricted admixture of more radiogenic Pacific waters advected through the Drake Passage (Jeandel, 1993, Rickli et al. 2009).

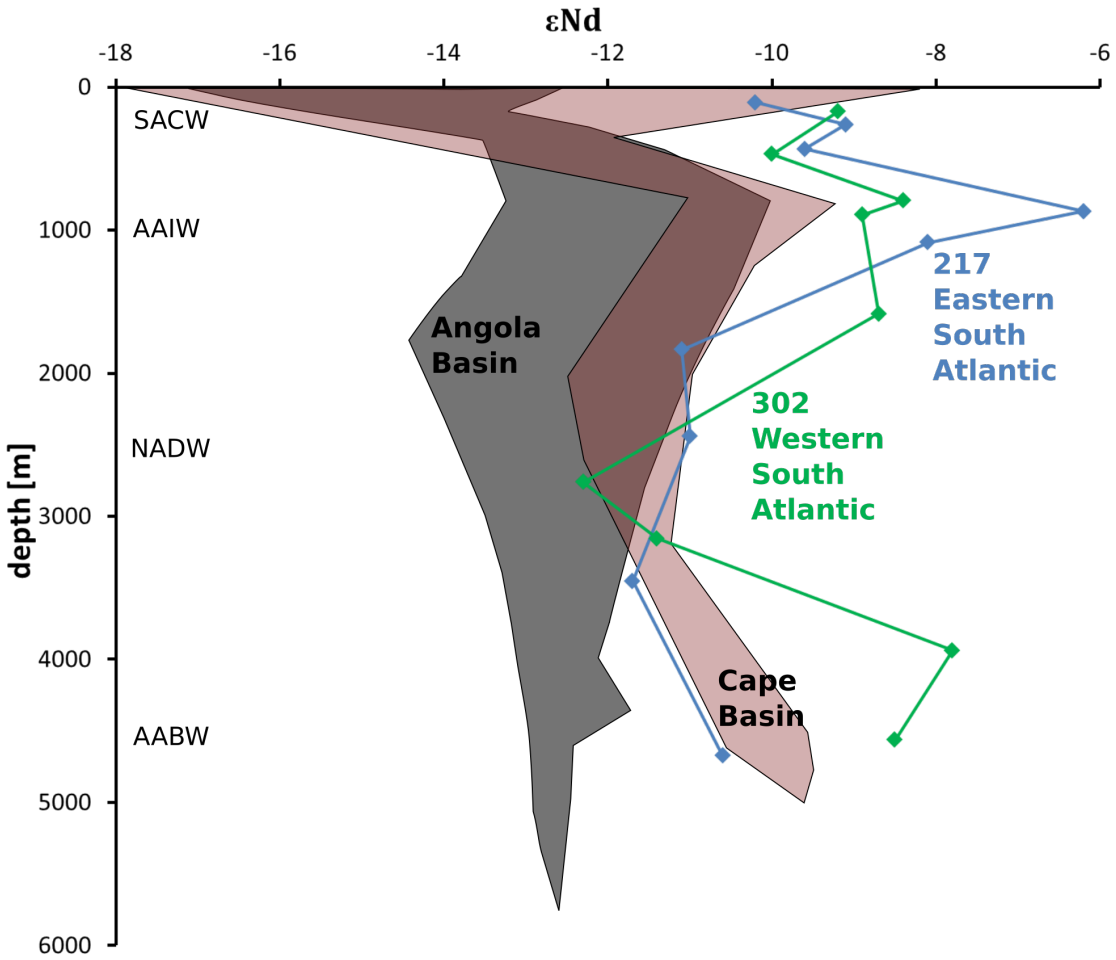

Figure 1.8: Range of Nd isotope compositions in the Angola and Cape basins from our study compared with two water column profiles of the eastern and western South Atlantic (Jeandel, 1993).

4.6. Nd isotope composition of seawater and sediments from the Walvis Ridge and Cape Basin

Comparison between the Nd isotope compositions of benthic foraminifera from core top sediments from the Cape Basin side of the Walvis Ridge (Klevenz et al., 2008) and seawater of our stations 36 and 37 in the Cape Basin from similar depths reveal a close correspondence (Fig. 1.9). This suggests that the authigenic fraction in these sediments faithfully reflects today's Nd isotope distribution of the main water masses in the Cape Basin. Core top sediments from the southern Cape Basin record ε_{Nd} values of -9.9 in good agreement with extracted Holocene NADW signatures (Wei et al., 2016), which are only slightly more radiogenic than the modern signature of the core of NADW we find in the southern Angola Basin and eastern Cape Basin (ε_{Nd} -11). Overall, the comparison of our water column Nd isotope data with the surface sediment signatures indicates that authigenic sedimentary Nd isotopes in the SE Atlantic reliably reflect paleo water mass compositions.

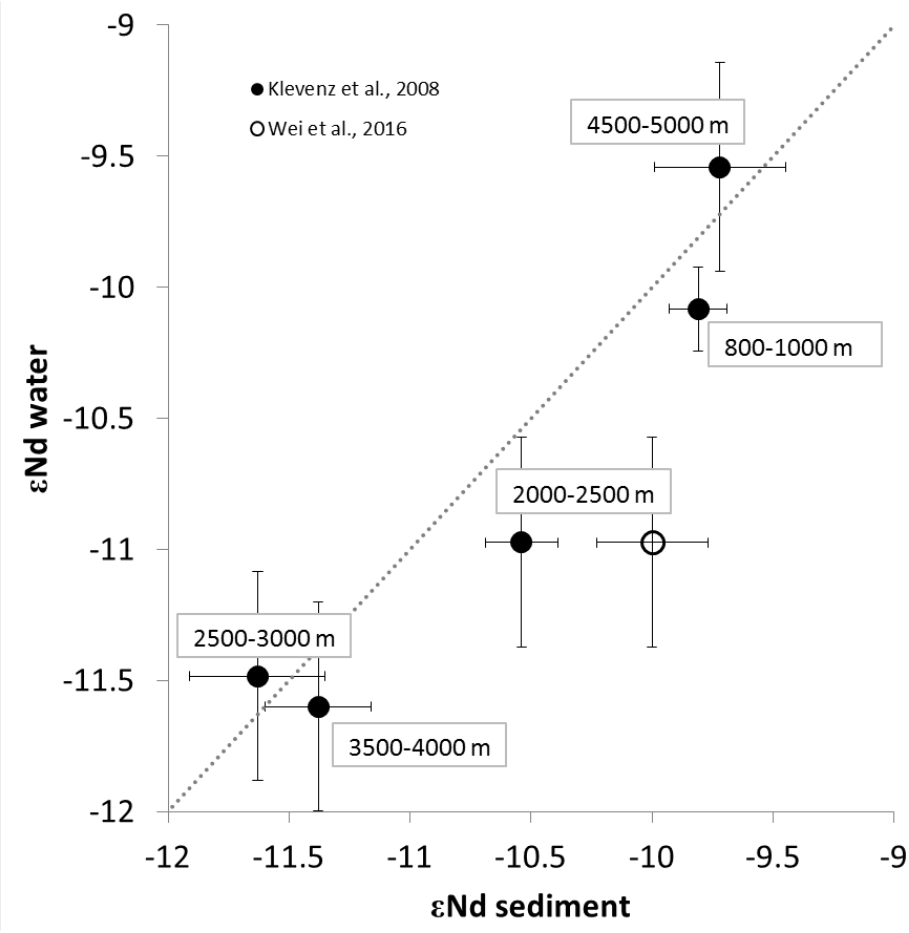

Figure 1.9: Comparison of Nd isotope compositions of water masses in the Cape Basin and core top sediments of the Walvis Ridge (Klevenz et al., 2008) and of the southern Cape Basin (Wei et al., 2016) reveals good agreement for the corresponding water depths.

5. Conclusions

Dissolved Nd isotopic compositions and Nd concentrations were determined along a N-S and an E-W full water column section across the Angola Basin and the northernmost Cape Basin in the SE Atlantic, which were sampled during GEOTRACES cruise GA08.

We found ε_{Nd} signatures as unradiogenic as -17 in surface waters of the Angola Basin and -17.6 in surface waters of the Cape Basin, which must originate from local or regional terrestrial inputs. In the central Angola Basin sediment particles from the African shelf and slope are transferred into the oxygen minimum zone and release unradiogenic Nd by reductive dissolution of their Fe-Mn oxyhydroxide coatings resulting in altered surface and intermediate water Nd isotope signatures. In contrast, surface waters of the Cape Basin are dominated by unradiogenic Nd isotope signatures originating from dissolved and particulate inputs of large rivers in the Mozambique Channel, from where they are advected by the Agulhas Current.

Deep water Nd isotope compositions in the northern and southern Angola Basin and in the western Cape Basin between 2000 and 4000 m essentially suggest that compositions are controlled by conservative water mass mixing, whereas the Nd isotopic composition of the deep central Angola Basin is overprinted by unradiogenic Nd likely released by dissolution of Fe-Mn oxides on sinking particles. At the deep eastern margin of the Cape Basin Nd is scavenged and removed from ambient seawater without significantly altering the Nd isotope compositions, most likely a consequence of resuspension of shelf and slope sediments.

Due to the hydrographic isolation of bottom waters in the Angola Basin, unradiogenic Nd released from sinking particles accumulates below 4000 m water depth. Bottom waters of the well ventilated Cape Basin hint at excess Nd concentrations below 4000 m water depth, originating from resuspended bottom sediments and/or dissolution of particles, increasing the Nd concentrations of the bottom waters. However, this addition does not significantly affect the seawater Nd isotope compositions expected from conservative mixing, due to similar ε_{Nd} values of the sediments and bottom waters, which today range from -9.6 to -10.5.

We conclude that Nd isotopes are a reliable quasi-conservative tracer of present and past deep water mass mixing in the southern and northern Angola Basin and in the Cape Basin, whereas the Nd isotope compositions of surface and bottom waters of the Angola Basin, as well as the entire water column of the central Angola Basin are affected by non-conservative addition of Nd from terrestrial inputs. The non-conservative additions to the Cape Basin water column are too small to significantly modify its Nd isotope compositions today, but may have been more significant in the past such as during glacial maxima.

Acknowledgments

We thank Jutta Heinze, Ana Kolevica and Christopher Siebert for all their support in the laboratory. We thank the crew and captain of RV Meteor for their support during cruises M75-3 and M121. We thank Patricia Jovičevič Klug and Niklas Meinicke for measuring the Nd isotope compositions of the samples from the Mozambique Channel and relating them to the local hydrography. Special thanks are expressed to the reviewers Derek Vance and Alex Piotrowski who helped to significantly improve the quality of the manuscript.

CHAPTER II

Dissolved neodymium and hafnium isotopes and rare earth elements in the Congo River Plume: Tracing and quantifying continental inputs into the southeast Atlantic

Submitted to Geochim. Cosmochim. Acta. as: *Rahlf, P., Laukert, G., Hathorne, E., Vieira, L.H., Frank, M., 2020. Dissolved neodymium and hafnium isotopes and rare earth elements in the Congo River Plume: Tracing and quantifying continental inputs into the southeast Atlantic.*

Abstract

The Congo River is the second largest river by discharge in the world and a major source of element inputs into the South Atlantic Ocean. Yet, the element fluxes and transport mechanisms across and beyond its estuary and their impacts on the marine distribution and cycling of many major and trace elements are not well understood. We present the first combined dissolved neodymium (Nd) and hafnium (Hf) isotope and rare earth element (REE) concentration distributions following the Congo River plume along its flow path off the West African coast and along a connected offshore latitudinal section at 3°S. The Congo River freshwater itself is characterized by extraordinarily high Nd and Hf concentrations of up to 4000 pmol/kg and 54 pmol/kg, and by Nd (ε_{Nd}) and Hf (ε_{Hf}) isotope compositions that range between -15.6 and -16.4 and between 0.35 and -1.4, respectively. Our near- and offshore data indicate that at salinities above 23 conservative mixing of Congo-derived Nd and Hf concentrations and isotopic signatures with ambient surface seawater occurs for at least 1000 km to the northwest of the river mouth. The impact of non-conservative behavior related to estuarine REE/Hf removal and release from or exchange with particulate phases at lower salinities cannot be assessed based on $\varepsilon_{Nd}/\varepsilon_{Hf}$ given that dissolved and suspended riverine pools have identical isotopic compositions and due to the lack of low salinity samples. However, a comparison between dissolved Nd/Hf fluxes from the Congo River and the shelf zone estimated based on radium isotope

compositions indicate that release from Congo-derived particulate phases likely balances strong estuarine REE/Hf removal in the low salinity zone. The combined riverine and shelf zone flux for Nd is almost twice as high as that estimated for the Amazon River, despite that the Amazon discharge is about five times higher than that of the Congo River. Even the offshore Nd flux estimated for the 3 °S transect based on radium isotope compositions still corresponds to ~40 % of the Congo-shelf-zone flux and reaches 150±50 Mg/year for Nd. Moreover, intermediate and deep waters below the plume and in the open northern Angola Basin are strongly affected by inputs from the Congo River given that Nd isotope signatures are inconsistent with values expected from large-scale water mass mixing and instead support unradiogenic Nd release either from sinking or deposited Congo-derived detrital material.

1. Introduction

The understanding of the distribution and cycling of major and trace elements and their isotopes in the oceans requires the identification of their sources and sinks, the quantification of input fluxes, as well as their transport processes. Rivers are major sources transporting dissolved trace elements to the oceans, whereas estuarine and shelf sediments at the same time act as a major sink responsible for scavenging and boundary exchange processes (Goldstein and Jacobsen, 1987, Say and Jeandel, 2005b). The Congo River entering the southeast Atlantic at 6°S and 12.3°E has the second largest water discharge in the world (after the Amazon River) of approximately 42,800 $m^3 s^{-1}$, draining a continental area of $3.7x10^6$ km^2 (Savoye et al., 2009). Distributions of sea surface temperature, salinity, chlorophyll, and mean sea level anomaly fields indicate that the main axis of its plume is subject to seasonal variability but usually extends between 400 und 1000 km in northwesterly direction as forced by wind driven currents and the Benguela Coastal Current (Denamiel et al., 2013, Hopkins et al., 2013). The river supplies high dissolved and particulate loads within its surface water plume but also affects material transport near the sea floor as sourced by resuspension and turbidity flows in the Congo canyon (Vangriesheim et al., 2009). Whilst several studies have previously investigated the biogeochemical implications of the Congo inputs on nutrient and carbon cycling in the coastal discharge region (Eisma and van Bennekom, 1978, Vangriesheim et al., 2009), recent work has also focused on inputs and fluxes of

trace elements originating from the Congo and their influence on the nearby and more distal South East Atlantic (Menzel Barraqueta et al., 2019, Vieira et al., 2020).

REE patterns have been demonstrated to provide valuable information on the origin of continental inputs and the biogeochemical cycling of elements in the open ocean (Elderfield et al., 1990). While dissolved REEs in seawater advected over distances of hundreds of kilometers typically show a heavy-REE (HREE) enriched pattern (all patterns discussed in this study are normalized to PAAS (Post-Archean Average Shale, McLennan, 2001)), fresh lithogenic continental inputs (dust, detrital particles) release shale-like REE patterns, whereas river inputs are generally characterized by a mid REE (MREE) enrichment (e.g. Osborne et al., 2015, Laukert et al., 2017). Light REEs (LREE) in river waters entering the ocean are removed preferentially by coagulation of river-borne colloids at low salinities (Sholkovitz, 1995, Rousseau et al., 2015, Tepe and Bau, 2016). Preferential release of HREEs from resuspended particles and sediments in estuaries at higher salinities can further enhance the HREE enrichment in seawater (Sholkovitz and Szymczak, 2000, Sholkovitz et al., 1994). Recent studies have proposed that REE fractionation and HREE enrichment already occur in the rivers because colloidal and truly dissolved riverine pools have different REE patterns (Pourret and Tuduri, 2017, Merschel et al., 2017b). Thus, seawater REE patterns could be the result of a combination of intra-oceanic and riverine processes.

In addition, dissolved radiogenic hafnium (Hf) and neodymium (Nd) isotope compositions in seawater provide information on present and past ocean circulation and weathering conditions on land (e.g. Rickli et al., 2009, 2010, Stichel et al., 2012a). Neodymium isotopes have been widely used as a long-distance tracer of water mass advection and mixing, enabled by its ocean residence time of 300-1000 years (Jeandel et al. 1995, Tachikawa et al., 1999, Tachikawa et al., 2003, Siddall et al., 2008, Arsouze et al., 2009, Rempfer et al., 2011). The radiogenic Nd isotope ratio ($^{143}Nd/^{144}Nd$) is expressed as $\varepsilon_{Nd} = [(^{143}Nd/^{144}Nd)_{sample}/(^{143}Nd/^{144}Nd)_{CHUR} -1] \times 10^4$ with CHUR = 0.512638 (Jacobsen and Wasserburg, 1980). In contrast, the ocean residence time of Hf is likely only few hundred years (Rickli et al., 2009, Zimmermann et al., 2009b) and therefore Hf isotopes have been used as a tracer for continental weathering inputs and water mass mixing on shorter basin scales (Stichel et al., 2012a, Filippova et al., 2017). The radiogenic Hf isotope ratio is expressed as ε_{Hf} =

$[(^{176}Hf/^{177}Hf)_{sample}/(^{176}Hf/^{177}Hf)_{CHUR} -1] \times 10^4$ with CHUR = 0.282785 (Bouvier et al., 2008). In the Angola Basin, partial dissolution of particulate inputs from the shelves, which include authigenic riverine signatures, have been demonstrated to not only affect the present and past water column Nd isotope signatures close to the coast but also in the open ocean (Bayon et al., 2004, Rickli et al., 2009, Noble et al., 2012, Kraft et al, 2013, Zheng et al., 2016, Rahlf et al., 2020). The riverine flux of Nd to the oceans is poorly constrained due to variability in the removal of "dissolved" Nd during estuarine coagulation and the subsequent release of Nd from suspended sediments (Rousseau et al., 2015, and references therein). The behavior of Hf during estuarine mixing is only known for the Hudson River where removal by coagulation amounts to about 50 % in surface waters and 75 % in near bottom waters (Godfrey et al., 2008). The Hudson surface waters then exhibit an increase in Hf concentrations reaching a broad peak at salinities between 5 and 15 that may indicate release from particles, but a similar peak in Ag concentrations has been suggested to reflect a possible anthropogenic source (Godfrey et al., 2008).

To better understand the inputs of riverine Nd and Hf to the ocean and their impact on the open ocean we collected filtered seawater samples from 16 full water column profiles along the Congo River plume at the coast of Congo and Gabon and along an offshore section at 3°S, complemented by three freshwater samples collected directly from the Congo River (Fig. 2.1). We quantify for the first time REE/Hf fluxes and the modification of Nd and Hf concentrations and isotope compositions within the Congo River plume. In addition, we investigate the effects of vertical and horizontal mixing on dissolved Nd and Hf isotope compositions near the West African coast given that previous studies found evidence for continental inputs significantly affecting the radiogenic isotope composition of the entire water column of the Angola Basin (Rickli et al., 2009, 2010, Rahlf et al., 2020). We finally evaluate how far the Congo River plume is traceable by these geochemical parameters, how it contributes to their budgets in the South East Atlantic Ocean, and to which degree the Nd/Hf isotope and REE distributions can be used as water mass tracers in areas of high continental inputs.

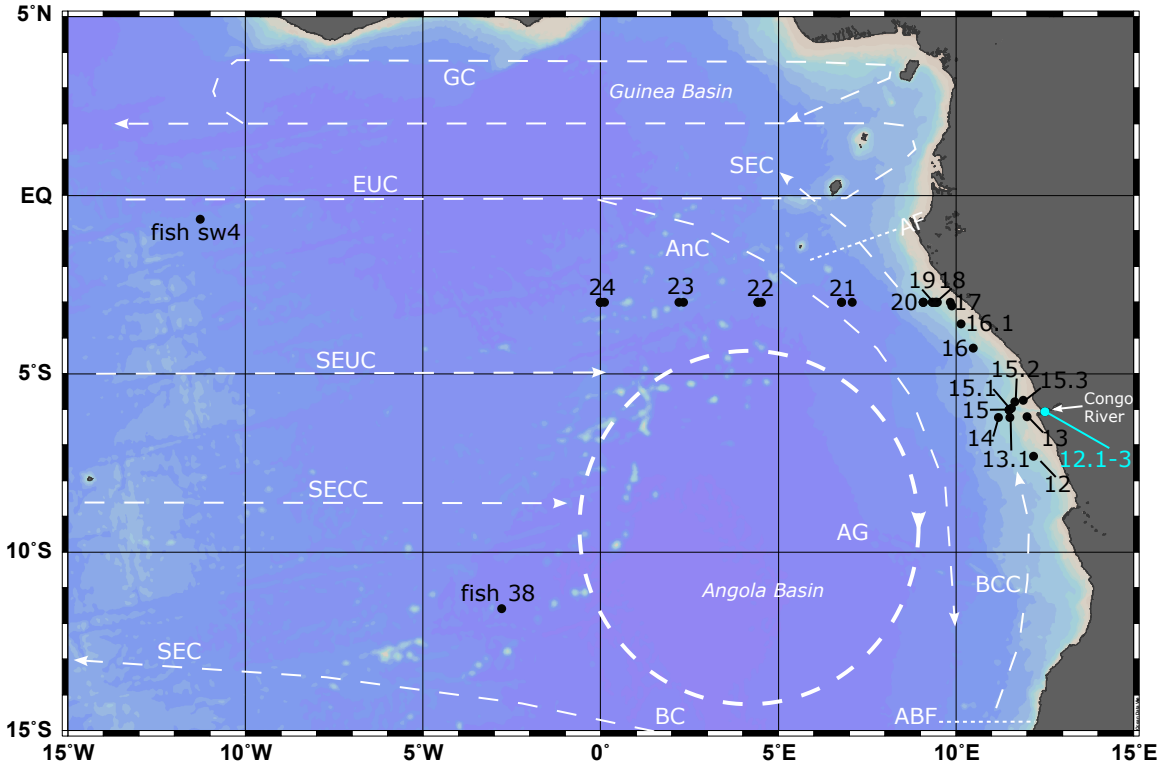

Figure 2.1: Surface water currents of the Angola Basin and sampling locations. Black dots represent stations 12-24 from this study and stations fish sw 4 and fish 38 from Rickli et al. (2010). Water samples from stations 12-24 were recovered in 2015 during GEOTRACES cruise GA08, whereas the Congo River samples of station 12.1-12.3 were taken by boat in May, July and October 2017. Currents shown are abbreviated as GC = Guinea Current, EUC = Equatorial Under Current, SEC = South Equatorial Current, AnC = Angola Current, AF = Angola Front, SEUC = South Euqatorial Under Current, SECC = South Equatorial Counter Current, AG = Angola Gyre, BC = Benguela Current, BCC = Benguela Counter Current, ABF = Angola Benguela Front.

1.2. Hydrography

The surface ocean circulation in the central and northern Angola Basin is part of the eastern boundary current system of the South Atlantic Ocean and is divided into a northern and a southern current system (Mohrholz et al. 2001). The southern system is dominated by the Benguela Current (BC) originating from the warm and saline Agulhas Current (AnC), which bifurcates at the Angola Benguela Front (ABF) into the Benguela Coastal Current (BCC) and the South Equatorial Current (SEC) (Fig. 2.1). The BCC flows north along the coast of Angola and entrains the Congo River plume. The SEC flows northwest across the South Atlantic Ocean, changes its direction near the Brazilian Coast and flows back eastward as the South Equatorial Counter Current (SECC), now as part of the northern current system. This current system also consists of the eastward flowing Guinea Current (GC), the Equatorial Undercurrent (EUC), the South Equatorial Countercurrent (SECC) and the South Equatorial Undercurrent (SEUC). The EUC feeds the southward flowing Angola Current (AnC) (Stramma and

England, 1999, Mohrholz et al. 2001). The AnC flows southward along the coast of Angola until it meets the BC at the ABF. Between the northern and southern current systems the cyclonic Angola Gyre forms a separate circulation cell, which extends to a depth of about 300 m (Mohrholz et al. 2001) (Fig. 2.1).

The uppermost 20 m of the eastern and northern Angola Basin are occupied by warm (27 °C) Tropical Surface Water (TSW) (Fig. 2.2). Between about 20 and 100 m depth, the mixed layer is characterized by Subtropical Underwater (STUW) at temperatures between 16 and 24°C and salinities between 35.7 and 36. Waters between about 100 and 500 m depth are dominated by South Atlantic Central Water (SACW), which is characterized by a linear T-S relationship (Fig. 2.2), salinities between 34.8 and 35.7 and potential temperatures between 8.5 and 15.8°C (Sverdrup et al., 1942, Stramma and England, 1999). Below 500 m depth Antarctic Intermediate Water (AAIW) has low salinities between 34.6 and 34.8 and potential temperatures between 4.6 and 8.5°C resulting in neutral densities of 27.13 kg/m^3 ≤ γ^n ≤ 27.55 kg/m^3. Waters below AAIW are composed of Upper Circumpolar Deep Water (UCDW) at salinities between 34.5 and 34.9, potential temperatures between 4.3 and 4.6°C and neutral densities of 27.55 kg/m^3 ≤ γ^n ≤ 27.8 kg/m^3. Bottom and deep waters of the northern Angola Basin (stations 21-24) are composed of North Atlantic Deep Water (NADW) characterized by salinities between 34.9 and 34.97, potential temperatures between 1.8 and 4.3°C and neutral densities of 27.8 kg/m^3 ≤ γ^n ≤ 28.12 kg/m^3 (Fig. 2.2). Antarctic Bottom Water (AABW) (γ^n ≥ 28.12 kg/m^3) is not present in the study area.

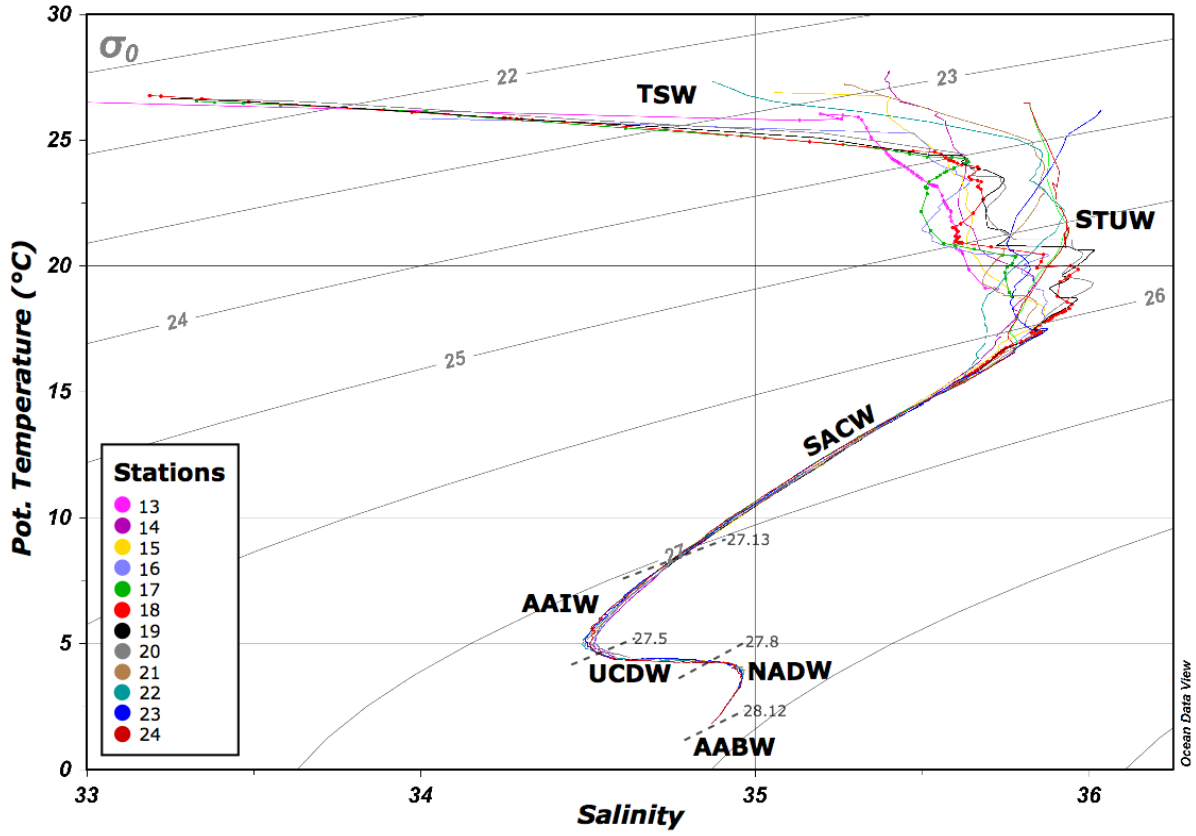

Figure 2.2: T-S-density plot including all stations from this study above a salinity of 33. Surface waters are represented by Tropical Surface Water (TSW) and subsurface waters by Subtropical Under Water (STUW). Intermediate water masses are identified as South Atlantic Central Water (SACW) and Antarctic Intermediate Water (AAIW). Deep waters are composed of Upper Circumpolar Deep Water (UCDW) and North Atlantic Deep Water (NADW). Undiluted Antarctic Bottom Water (AABW) and Lower Circumpolar Deep Water (LCDW) are not present in the northern Angola Basin. This figure was produced using Ocean Data View (Schlitzer, 2020) and modified manually.

2. Methods

2.1. Sampling, neodymium and hafnium isotope analysis

Water samples from the Congo River Plume were collected during GEOTRACES cruise GA08 with German RV Meteor (M121) in November/December 2015 with a stainless steel CTD rosette and a towed fish for surface waters and were immediately transferred into 20 L cubitainers. Each sample was filtered through a nitro-cellulose acetate filter (0.45 µm pore diameter) into a LDPE-cubitainer using a peristaltic pump and was then acidified with concentrated distilled HCl resulting in a sample pH of about 2. For Nd- and Hf-concentration measurements, filtered two L aliquots of each sample were separately stored and acidified in PE-bottles. To each 20 L sample, 400 µl $FeCl_3$ solution (~200 mg Fe/mL) was added and left to equilibrate for 24 hours. High-

purity ammonia solution (25 %) was subsequently added to raise the pH to 7.5-8.0. After 48 hours, the co-precipitated trace elements settled to the bottom of the cubitainers together with FeOOH and the supernatant water was syphoned off.

River water end-member samples from the Congo River at zero salinity were taken upstream by boat in May, July and October 2017 near the center of the river at ~6 °S and ~12.5 °E (stations 12.1-12.3). The samples were collected in 10 L plastic bottles and filtered within 2 hours after collection through AcroPak™500 cartridges containing Supor Membrane filters (pore size: 0.8/0.2 µm). The sample pH was adjusted to ~2 by addition of distilled concentrated HCl. In the home laboratory at GEOMAR, 20 mL of aliquots of each sample were separated into acid-cleaned HDPE vials for Nd- and Hf-concentration measurements. 1 L of each sample was mixed with 1 mL of the same $FeCl_3$ solution as above and was then treated like the 20 L seawater samples for co-precipitation.

The precipitates were centrifuged and rinsed three times with deionized water (MilliQ, 18.2 MΩcm) in 50 mL centrifuge tubes to remove major seawater ions. The precipitates were transferred into 60 mL PFA vials with 4 mL 6 M HCl/1 M HF and then evaporated to dryness. To remove organic components, the samples were boiled in aqua regia at 120 °C for 24 h. After evaporation to dryness, the samples were dissolved in 4 mL 6 M HCl and were checked for presence of any jelly-like precipitate, which can contain up to ~90 % of the Hf in the samples (Stichel et al. 2012b). The jelly precipitates were separated by centrifugation, dissolved in 2 M HF at 100 °C, dried down and dissolved in 1M HCl/0.05M HF. Before this solution was merged again with the main sample, the latter was washed with pre-cleaned di-ethyl ether to remove 99 % of the Fe (Stichel at al., 2012b). The samples were dried down and dissolved in 4 mL 6 M HCl/1 M HF. The REEs were separated chromatographically from matrix elements with cation exchange resin AG 50W-X8 (1.4 mL, 200-400 µm) and Nd was further separated from the other REEs for isotope measurements using Eichrom®LN-Spec resin (2 mL, 50-100 µm) following previously established procedures (Münker et al., 2001, Pin and Zalduegui, 1997). Hafnium was further purified by a Bio-Rad AG1-X8 (200-400 µm) and an Eichrom®LN-Spec resin (100-150 µm) following a modified procedure of Chu et al. (2002). To destroy residual traces of the resin and organic compounds, the Nd cuts were finally treated with 100 µl quartz distilled HNO_3 and

100 µl H_2O_2 (30 wt.%, Merck Suprapur®). Hf cuts were treated with 1 mL 0.5 M HNO_3/0.1 M HF before measurement.

The $^{143}Nd/^{144}Nd$ ratios of 13 samples (station 12.1-16.1) were measured on a Nu Plasma MC-ICPMS and were single-corrected for instrumental mass bias to $^{146}Nd/^{144}Nd = 0.7219$ using an exponential mass fractionation law. The $^{143}Nd/^{144}Nd$ ratios of the remaining 44 samples were measured on a Neptune Plus MC-ICPMS and were double-corrected for instrumental mass bias to $^{146}Nd/^{144}Nd = 0.7219$ (Vance and Thirwall, 2002). Isobaric interferences between ^{144}Sm and ^{144}Nd were corrected by measuring the abundance of the interference free isotope ^{147}Sm and by calculating the potential ^{144}Sm contribution on mass 144 from the natural abundance of Sm. The $^{143}Nd/^{144}Nd$ ratios of all samples were normalized to the accepted JNdi-1-standard value of 0.512115 (Tanaka et al., 2000). The external reproducibility of the Nd isotope measurements as estimated by repeated measurements of the JNdi-1-standard was between 0.15 and 0.31 ε_{Nd} units (2SD) on the Neptune Plus and between 0.42 and 0.63 ε_{Nd} units (2SD) on the Nu Plasma.

The $^{176}Hf/^{177}Hf$ ratios of 19 samples (stations 12.1-16.1) were measured on a Neptune Plus MC-ICPMS and corrected for instrumental mass bias to $^{179}Hf/^{177}Hf = 0.7325$ applying an exponential mass fractionation law. The $^{176}Hf/^{177}Hf$ ratios were normalized to the accepted JMC 475 standard value of 0.28216 (Nowell et al., 1998). The external reproducibility was estimated by repeated measurements of the JMC 475 standard and ranged from 0.59 to 2.76 ε_{Hf} units (2SD) depending on sample size.

2.2. Neodymium and hafnium concentration analysis

For precise determination of Nd- and Hf-concentrations of the 19 river plume samples between (stations 12.1 to 16.1), 1 L aliquots of these samples were spiked with pre-weighed ^{150}Nd and ^{180}Hf spikes and were then mixed with 15µl of $FeCl_3$ solution. After 5 days of equilibration, high-purity ammonia solution (25 %) was added to raise the pH to 7.5-8.0. After 48 hours, trace elements co-precipitated with the FeOOH and settled to the bottom and the supernatant water was syphoned off. The precipitates were transferred into 50 mL centrifuge tubes and were centrifuged und rinsed three times with deionized water (MilliQ, 18.2 MΩcm) to remove major seawater ions. Then they were transferred into 7 mL Teflon vials in 1 mL 3 M HCl/0.2 M HF and

evaporated to dryness. The samples were then heated in aqua regia at 120 °C for 24 h to destroy organic components before they were dissolved in 1 mL 1 M HCl/0.05 M HF. High Field Strength Elements (HFSEs) were separated from REEs by ion chromatography using AG 50W-X8 resin (1.4 mL, 200-400 µm) following a modified recipe by Münker et al. (2001). Nd cuts were evaporated to dryness in 0.5 mL 2% HNO_3 + 100 µl H_2O_2 and then dissolved in 0.5 mL 2% HNO_3 for Nd concentration measurements. Hf cuts were dissolved in 2 mL 0.1 M HF for further purification using AG 1-X8 resin (1.6 mL, 200-400 µm), following a modified procedure of Sahoo et al. (2006). The isotope dilution measurements of the Nd and Hf concentrations based on $^{150}Nd/^{144}Nd$ and the $^{178}Hf/^{180}Hf$ ratios were carried out on a Nu Plasma MC-ICPMS. Replicates for each element yielded an external reproducibility of better than 2% for Nd and 5% for Hf (2 SD).

2.3. Rare earth elements

All REE concentrations were measured with a SeaFAST system (Elemental Scientific Inc.) connected to a Thermo Element XR ICP-MS (Hathorne et al., 2012). In brief, 7 mL of undiluted and acidified seawater samples were each spiked with 70 µl of a 10 ng/g indium solution. A 4 mL sample loop was filled before the samples were preconcentrated online while the matrix was mostly washed to waste. The REEs were then eluted directly into the ICP-MS spray chamber and data collected in time resolved analysis mode. Raw data were processed with the computer software iolite© to average the intensity peaks for each mass. GEOTRACES inter-calibration samples BATS 15 m and BATS 2000 m (van de Flierdt et al., 2012) were measured to monitor the external reproducibility, which is given as 2 SD in supplementary Table A4 for each REE. Nd concentrations for stations 17 to 23 (45 samples) were obtained by SeaFAST measurements only. Neodymium concentrations determined by the seaFAST technique and isotope dilution (n = 44) were identical within the 95% confidence limits as observed with previous seaFAST methods (Hathorne et al., 2012).

3. Results

All data reported here are provided in tables 1 and 2 with corresponding hydrographic information and are accessible through the PANGAEA database (Link will be provided after the acceptance of the manuscript).

3.1. Neodymium and hafnium concentrations

The highest Nd and Hf concentrations were determined in three Congo River freshwater samples collected during summer, autumn and winter of 2017 and correlate with the seasonal variations of the river discharge (cf. Chao et al., 2015). During low discharge in summer, Nd (Hf) concentrations reach ~1900 (33) pmol/kg (station 12.1), whereas during the high discharge period in autumn, Nd (Hf) concentrations are as high as ~3900 (54) pmol/kg (station 12.2) (Fig. 2.3a,c). Spring samples have intermediate Nd and Hf concentrations (station 12.3). Surface waters along the nearshore plume section (stations 12 – 16.1) have significantly lower but highly variable concentrations (Fig. 2.3a,c). Highest concentrations are found in the surface waters with the lowest salinity (S ~23) of stations 15.1-3 located nearest to the river mouth and reaching ~430 pmol/kg for Nd and ~13 pmol/kg for Hf, whereas the lowest nearshore concentrations are observed at station 14 (S = 35.9) and reach only 33 pmol/kg for Nd and 0.4 pmol/kg for Hf. Along the offshore section (stations 17 – 24), surface water Nd concentrations vary between 14 pmol/kg (station 23, S = 35.8) and 63 pmol/kg (station 19, S = 33.8) (Fig. 2.3a). At 100 m water depth, Nd concentrations at all offshore stations decrease to a minimum of ~13 pmol/kg, which is followed by an increase to slightly higher values at 500 m depth. Between 1000 and 4000 m depth, Nd concentrations range between 14 and 21 pmol/kg and bottom waters are marked by higher Nd concentrations between 23 and 30 pmol/kg (Fig. 2.3a). All REEs except Ce show depth profiles essentially identical to Nd albeit at different concentrations (see section 3.3). Offshore Hf concentrations are available for station 24 only and vary between 0.2 pmol/kg at the surface and 1.1 pmol/kg at 3000 to 4000 m depth. We note that the deep water sample at ~4400 m depth has a significantly lower Hf concentration (~0.2 pmol/kg) than deep and bottom water samples collected immediately above and below (Fig. 2.3c).

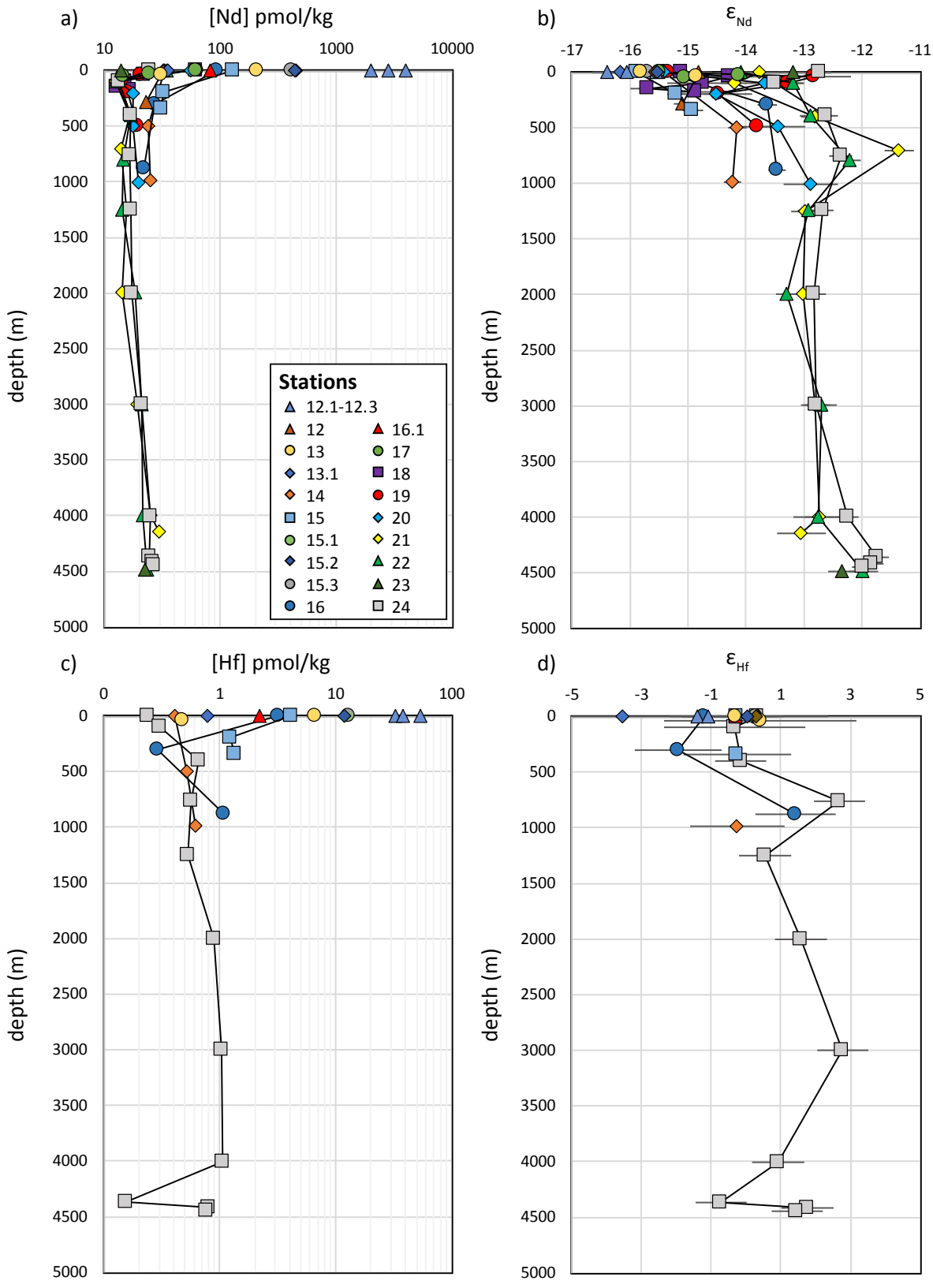

Figure 2.3: Nd and Hf isotope compositions and concentrations versus depth for all stations. For a better illustration of the variability of the concentrations, logarithmic scales are used. The Nd isotope and concentration profiles of station 24 have previously been published in Rahlf et al. (2020).

3.2. Neodymium and hafnium isotopic compositions

Congo River Nd and Hf isotope signatures only exhibit a small seasonal variability between -16.4 and -15.5 and between -1.4 and +0.4, respectively (supplementary Table A3). For Hf isotopes the most radiogenic value was associated with the highest concentrations in autumn. Surface waters along the nearshore section have similarly unradiogenic ε_{Nd} values ranging between -16.2 and -15.4 and ε_{Hf} values ranging between -3.55 and +0.3 (Fig. 2.3b,d). Within the upper 500 m of the nearshore stations at the Congo mouth, the Nd isotope signatures overall become more radiogenic with increasing water depth, whereas Hf isotope signatures remain essentially constant. Below 500 m depth, Nd and Hf isotope compositions do not vary significantly.

Along the offshore section between stations 17 and 24, the surface water ε_{Nd} and ε_{Hf} evolve to more radiogenic values with distance from the coast (Fig. 2.3b,d). The upper water column (< 500 m water depth) is marked by highly variable ε_{Nd} and ε_{Hf} values, which below 500 m depth become systematically more radiogenic and reach ε_{Nd} = -11.4 (station 21) and ε_{Hf} = +2.7 (station 24) in the core of AAIW at ~700 m depth (Fig. 2.3b,d). Below AAIW, the ε_{Nd} values are essentially constant at ~ -13 reflecting the presence of NADW, while bottom waters influenced by the admixture of AABW or LCDW have slightly more radiogenic Nd isotope signatures (~ -12). The ε_{Hf} signatures of the deep and bottom waters vary between -0.7 (~4400 m) and +2.8 (~3000 m), with the least radiogenic value corresponding to the lowest Hf concentration (Fig. 2.3d). The intermediate and deep water Nd and Hf isotope signatures are thus markedly more radiogenic than those of the Congo River.

3.3. REE distribution patterns

Depth profiles of the concentrations of all REEs are reported in supplementary Table A4. The PAAS-normalized (Post-Archean Average Shale, McLennan, 2001) REE patterns for surface-, intermediate-, deep- and bottom waters are shown in Figure 4 and compared to BATS 15 m and BATS 2000 m reference waters from the Bermuda Atlantic Time Series (van de Flierdt et al., 2012). The Congo River freshwater (station 12.1) has the highest REE concentrations and an essentially flat REE pattern typical for river waters. The surface sample of station 15.3 collected closest to the Congo River mouth (S = 24) has significantly lower REE concentrations and is marked by a weak

LREE depletion. All other surface samples at salinities > 33 have markedly lower REE concentrations and REE patterns similar to that of BATS 15 m, characterized by a clear LREE depletion and a negative Ce anomaly (Fig. 2.4a). The intermediate, deep and bottom water samples have REE patterns similar to BATS 2000 m and show the most pronounced LREE depletions and negative Ce anomalies (Fig. 2.4b).

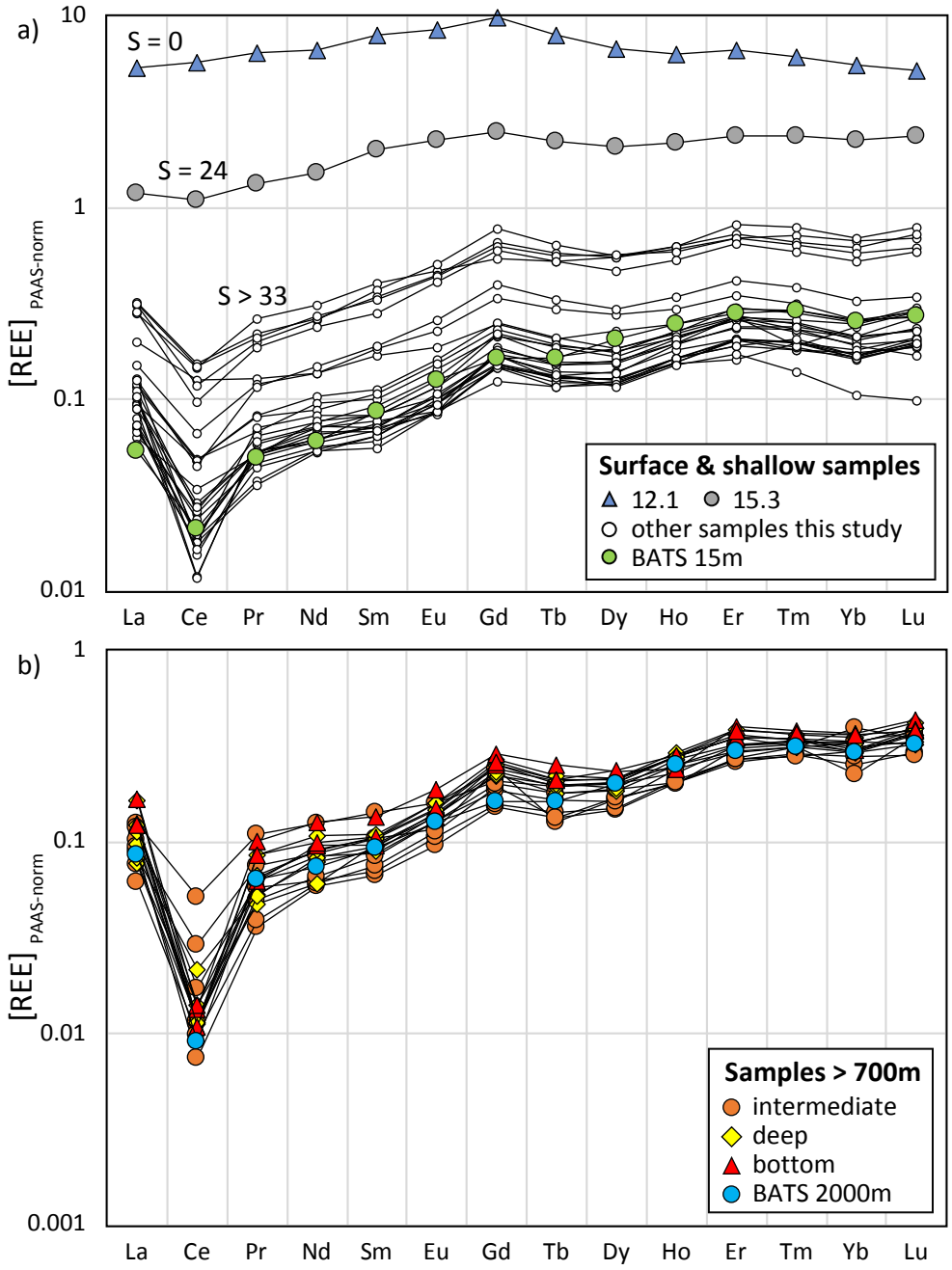

Figure 2.4: PAAS normalized REE patterns for a) surface and b) intermediate, deep and bottom waters. The PAAS normalized REE patterns of BATS 15 m and BATS 2000 m from the western North Atlantic (van de Flierdt et al., 2012) are shown for comparison.

Differences in the REE patterns of the surface waters are reflected by HREE/LREE ratios ranging between 0.9 and 2.9 (HREE/LREE = $([Tm]_N+[Yb]_N+[Lu]_N)/([La]_N+[Pr]_N+[Nd]_N)$, whereby subscript N refers to PAAS-normalized concentrations) (Fig. 2.5a). The lowest HREE/LREE ratios reflecting a flat REE pattern are found at the Congo River station (12.1), at the nearshore stations 13.1 and 15.3 close to the Congo River mouth, and at station 23 located in the open Angola Basin far from the discharge area. Stations 12.1, 13.1 and 15.3 are also marked by a very weak Ce anomaly (Ce/Ce* = [CeN]/[([La]N+[Pr]N)/2]) between ~0.8 and ~1, which is higher than all other stations (Ce/Ce* = 0.4-0. 6) (Fig. 2.5c) and than BATS 15 m (Ce/Ce* = 0.4). The strongest MREE enrichment (MREE/MREE* = $([Gd]_N+[Dy]_N)/([Yb]_N+[Nd]_N)$) is observed in surface samples between stations 21 and 23 (MREE/MREE* = 1.4-1.8), which is identical to or higher than the MREE enrichment in the Congo River freshwater sample (MREE/MREE* = 1.4) (Fig. 2.5b). The MREE/MREE* ratios decrease with depth reaching lowest values in intermediate waters, which also have higher HREE/LREE ratios (Fig. 2.5a). Deep and bottom waters show lower HREE/LREE values again, but are enriched in LREEs relative to BATS 2000 m and thus have lower HREE/LREE ratios than BATS 2000. Intermediate waters at stations 14 and 16 show significantly weaker Ce anomalies than all other intermediate depth samples (Fig. 2.5c).

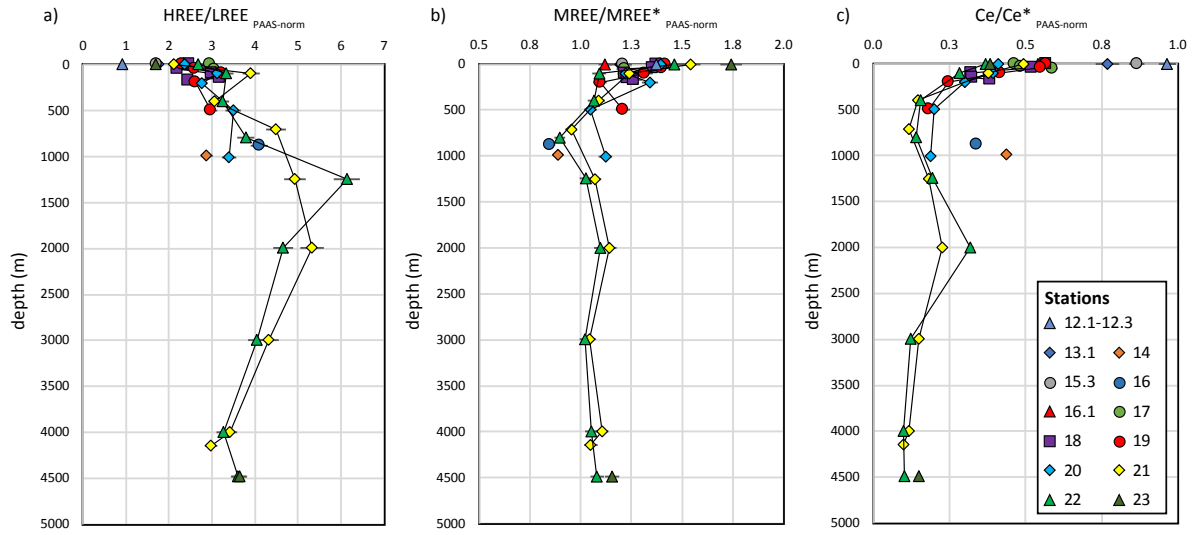

Figure 2.5: PAAS-normalized HREE/LREE, MREE/MREE* and Ce/Ce* depth profiles of all stations.

4. Discussion

4.1. Surface and subsurface waters

4.1.1. REE and Hf contributions of the Congo River to the southeastern Atlantic

The REE concentrations of our Congo River freshwater samples (stations 12.1-12.3) are similar to concentrations determined previously upstream in the Congo River (Dupré et al., 1996) but are highly enriched in all REEs compared to seawater and other rivers (cf. Rousseau et al., 2015). The freshwater also exhibits a flat REE pattern and MREE enrichment, as well as low HREE/LREE and high Ce/Ce* ratios (Figs. 4 & 5), which are typical characteristics of some major rivers (Goldstein & Jacobsen, 1988, Elderfield et al., 1990, Osborne et al., 2015, Laukert et al., 2017, Rousseau et al., 2015). Low surface water salinities along the coast document the presence of the Congo River plume in the surface waters of the BC for at least 1000 km downstream. To investigate the mixing and behavior of riverine and seawater REEs along this route, we compare the Nd concentrations of all surface samples with salinity. The surface sample of station 12 is employed as the seawater end-member given that this station is located south of the Congo River mouth and thus can be assumed to be unaffected by the Congo River plume. We calculated conservative mixing between this end-member (S = 35.15, [Nd] = 32.4 pmol/kg) and the Congo River freshwater (S = 0 and average [Nd] = 2914 pmol/kg) to investigate non-conservative REE behavior.

Figure 6a shows that most surface water samples have Nd concentrations higher than that of the surface sample of station 12. Only the surface waters of the offshore stations 23 and 24 have lower Nd concentrations and their high salinities demonstrate that they are not reached by the Congo plume. The REE concentrations decrease in northwesterly direction along the flow of the plume until stations 21 and 22, which have surface water concentrations similar to station 12. These elevated concentrations and their spatial distribution indicate that the Congo River is the dominant riverine REE source in this region and that the Congo-derived REEs are advected for 1000 km from the river outflow to at least 3°S, 4°E. This supports evidence from the iron and aluminum distributions in the South Atlantic Gyre based on samples from the same cruise, which document a large long-range transport of other dissolved trace metals originating from the Congo River (Menzel Barraqueta et al., 2019, Vieira et al., 2020).

The continuous decrease in surface Nd concentrations can be attributed to mixing with ambient Atlantic water. However, except the surface sample of station 16, all samples systematically plot well below the mixing line between Congo River freshwater and surface water of station 12 (Fig. 2.6a). This depletion suggests that a large fraction of the dissolved riverine REEs has already been removed from the water column by salt-induced coagulation of river-borne colloids (Elderfield et al., 1990, Sholkovitz 1976, Boyle et al., 1977) at salinities below ~23 (i.e. before reaching station 15.1). Salinity and Nd concentrations of all surface samples are linearly correlated (R^2 = 0.98) indicating conservative behavior of Nd in waters exceeding a salinity of 23. Despite that we were unable to sample closer to the river mouth and thus do not have data for those salinities at which salt induced coagulation and subsequent release from particles begins in other estuaries (e.g. Rousseau et al., 2015 and references therein), simple interpolation of the mixing line defined by all surface samples to zero salinity results in an initial riverine Nd concentration of 1260 pmol/kg (Fig. 2.6a). Although this is a simplification that likely underestimates the removal given that the counter-acting release from particles is not considered (e.g. Rousseau et al., 2015), the difference between the extrapolated value and the average concentration of the Congo River (2910 pmol/kg) suggest that at least 57 % of the Nd has been removed in the low salinity range (S < 23). This removal is somewhat lower than the mean removal of ~70 % calculated for estuaries globally (Rousseau et al., 2015). Even given the lack of low salinity data, this suggests that there is much less removal of Nd in the Congo estuary than in those of other major tropical rivers like the Amazon where removal reaches > 90 % (Rousseau et al., 2015). An increase in the surface Nd concentration is only observed for station 16, which also shows an elevated Hf concentration and a distinct Hf isotopic composition, likely resulting from contributions of a local weathering source (see below and section 4.1.2).

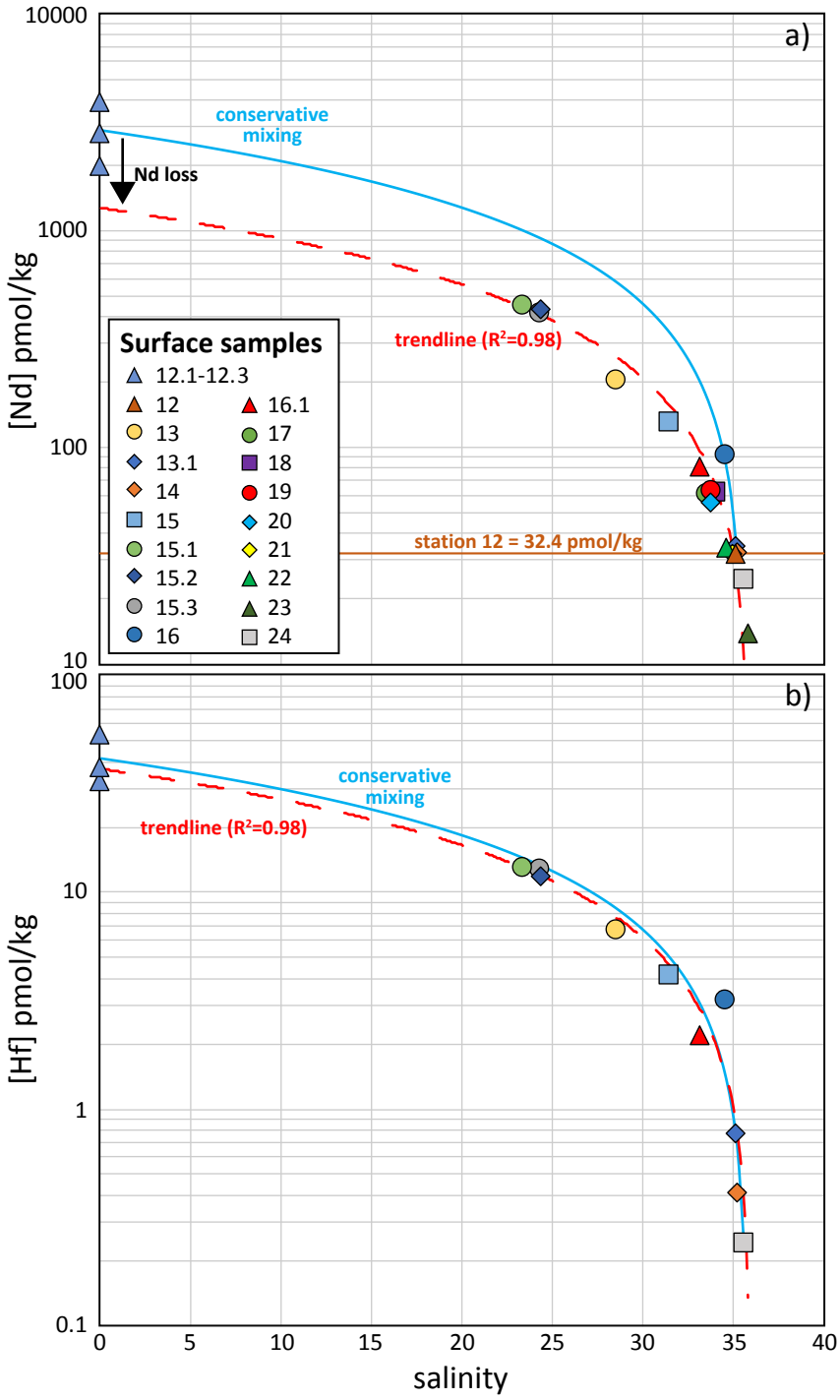

Figure 2.6: Nd and Hf concentrations of surface waters versus salinity. The blue lines represent conservative mixing between Congo River freshwater (average concentrations of station 12.1-12.3) and a marine end-member (surface samples of station 12 for Nd; surface sample of station 24 for Hf). Linear trendlines defined by all surface samples are shown in addition (red dashed lines). For a better visibility of the data distribution, logarithmic scales are used.

The same simplified extrapolation indicates little or no estuarine removal of Hf (Fig. 2.6b). Compared to the Hudson estuary, where initial drop and subsequent increase of surface Hf concentrations are observed at low salinities (0-5) (given that the potential contributions from anthropogenic sources are not considered, Godfrey et al., 2008), the observed mixing line in our study may also reflect the combined effect of initial Hf removal and subsequent release in the low salinity range. As Hf data at low salinities for the Congo and other rivers are not available, it is not possible to assess whether Hf removal occurs at low salinities. The surface sample of station 16 does not plot on the mixing line and has physical and geochemical characteristics that do not comply with those of other surface water samples. In particular, its low temperature (~25 °C) may be indicative of local entrainment of subsurface waters with elevated REE and Hf concentrations, which is not observed for surface waters prevailing at other stations that exhibit temperatures above 26 °C. Despite the inferred estuarine REE and Hf removal in the low salinity range, all above observations clearly indicate that freshwater of the Congo River has a strong (bio)geochemical impact on the surface waters of the eastern Angola Basin.

In order to further investigate estuarine REE/Hf behavior and to obtain an assessment of the Congo River's impact on the budgets of these elements in the South Atlantic Ocean, we determined Nd and Hf fluxes for the Congo River, the Congo-shelf-zone and the offshore section at 3°S (supplementary Table A5). The Congo River fluxes were calculated using the Nd and Hf concentrations in the Congo River and river discharge reported in Milliman and Farnsworth (2011). The Congo-shelf-zone and offshore fluxes were determined based on radium isotope (Ra) compositions following the approach described in Vieira et al. (2020). The similarity between REE/Hf and ^{228}Ra distributions (Vieira et al., 2020) suggests that the REE and Hf fluxes can be proportionally scaled with the ^{228}Ra flux (Charette et al., 2017). The calculated fluxes of Nd and Hf confirm large riverine contributions of REEs and Hf to the South Atlantic Ocean and moreover suggest non-conservative additions from particulate phases to the dissolved pool. The Congo-shelf-zone flux includes all dissolved Nd/Hf derived from the river dissolved phase and release from particulate phases (Vieira et al., 2020). Within uncertainties, this flux for both elements is identical to the flux estimated for the Congo River. For Nd, if we neglect release from particulate phases and assume that estuarine removal of at least 60 % occurs in the low salinity zone (see above), the

Congo-shelf-zone flux would amount to ~220 Mg (tonne) or 10^6 g/year. However, the determined Nd flux is almost twice as high (~387 Mg/year), which supports REE additions through release from Congo-derived particulate phases. A similar mechanism has to be invoked for Hf, given that strong Hf removal can be expected in the low salinity zone (cf. Godfrey et al., 2008). Compared to the Amazon River, whose discharge is five times higher than that of the Congo River, the Congo-shelf-zone Nd flux is higher by almost a factor of two (cf. Rousseau et al., 2015). Moreover, the offshore export of Congo-derived Nd along the 3 °S transect still amounts to 150 Mg/year, which corresponds to ~40 % of the Congo-shelf-zone flux and is remarkably high considering the 1000 km offshore transport. This suggests that the Congo River is more important for the global Nd budget than previously assumed (cf. Goldstein and Jacobsen, 1987) and accounts for 1-3 % (offshore flux) or 4-7 % (Congo-shelf-zone flux) of the missing global Nd flux of 5,500-11,000 Mg/year (Arsouze et al., 2009; Rempfer et al., 2011). Release from lithogenic suspended matter has been identified as a previously unconsidered but important additional REE supply mechanism for which a global Nd flux of 3,100-8,300 Mg/year was estimated (Rousseau et al., 2015), which is in the same range as the missing Nd flux but may be up to 3.5 times smaller based on the lower observed (3,100) and upper modeled (11,000) extremes. As we cannot determine the exact fraction of Nd or Hf release from lithogenic suspended matter for the Congo River we refrain here from further assessing global REE/Hf budgets or the role different supply mechanisms play for these budgets and instead emphasize the need of additional quantitative studies on both the particulate and dissolved fluxes from the Congo and other rivers.

4.1.2. Nd and Hf isotope behavior during estuarine mixing

Based on a conservative mixing model of Nd and Hf isotopes adopted from Rousseau et al. (2015), we investigate if these isotope systems supplied by the Congo River are mixed conservatively with open ocean waters as indicated by the conservative behavior of REE and Hf concentrations in surface waters with salinities above 23 (see section 4.1.1). For the Congo River end-member, we selected the seasonally variable ε_{Nd} and ε_{Hf} values in the surface river waters of station 12.1 (ε_{Nd} = -15.6, -16.4, -16.1 and ε_{Hf} = -1.1, -1.4 and 0.4, respectively), while surface waters of station sw4 (ε_{Nd} = -11.9,

ε_{Hf} = 1.9) (Rickli et al., 2010) and a salinity of 35.99 were applied as the open ocean surface water mixing end-member (Fig. 2.7). The mixing calculations reveal that both the ε_{Nd} and ε_{Hf} surface water signatures of essentially all samples plot within the range of the three mixing curves (Fig. 2.7a,b).

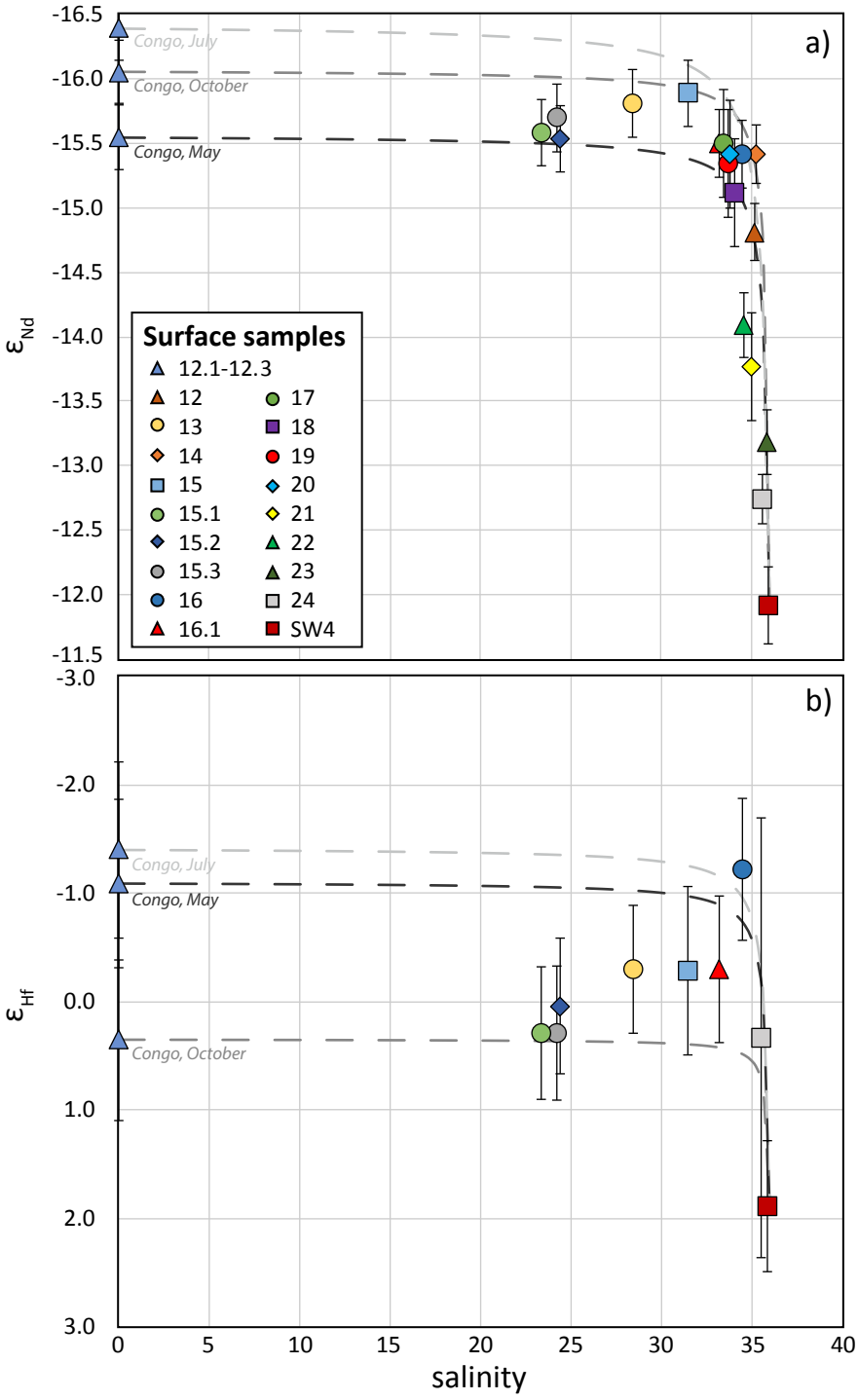

Figure 2.7: Mixing relationships between Nd and Hf isotopes and salinity of the Congo River and open ocean surface waters.

Isotopic compositions of samples with salinities below ~33 appear to be shifted towards less radiogenic signatures with increasing salinities but these signatures are within error of each other and with the conservative mixing lines and thus no significant trend can be validated based on our data. Only the surface sample of station 16 has a Hf isotope composition that is slightly less radiogenic than the other samples, likely as a consequence of subsurface water entrainment (see also section 4.1.1). Apart from this sample, these calculations suggest conservative Nd and Hf isotope behavior in the nearshore surface waters. However, in contrast to observations from the Amazon River (Rousseau et al., 2015), partial dissolution of Congo River particles would have no observable effect on the dissolved surface water isotope compositions given that these have ε_{Nd} signatures of -15.3 to -16.1 and ε_{Hf} signatures of +1.3 to -1.1 (Bayon et al., 2009, 2015, Allègre et al., 1996, Goldstein et al., 1984), which is identical to the dissolved isotope signatures at salinities below 33. The Congo River carries the second largest amount of terrestrial organic matter to the ocean after the Amazon (Coynel et al., 2015). Such organic particles bind Nd via surface-complexation and constantly exchange Nd with particles and the dissolved phase (Merschel et al., 2017a,b) resulting in identical dissolved and particulate Nd isotope compositions in the freshwater of the Congo River. While we cannot provide direct evidence for Nd release from or exchange with particulate phases, the elevated Congo-shelf-zone flux indeed indicates dissolution of Congo-derived particulate phases if we assume strong estuarine removal of REEs and Hf in the low salinity zone (see section 4.1.1). Even though the absence of strong REE removal and subsequent release has been inferred for other large estuaries (e.g. for high-latitude estuaries, see Laukert et al., 2017 and references therein), we argue that REE/Hf behavior in the Congo estuary will likely be similar to other tropical estuaries, such as the Amazon estuary. At salinities above 33 the isotope signatures change towards the marine end-member characterized by more radiogenic signatures than the riverine particles, supporting conservative mixing in the high-salinity range. Note that the surface sample of station 12 applied as an end-member in section 4.1.1 plots within this triangle and is thus not considered a distinct end-member in this section.

To identify any non-conservative estuarine impact on our mixing calculations, we introduced a third mid-salinity surface water end-member (station 13, salinity = 28.6, ε_{Nd} = -15.8, ε_{Hf} = -0.28). The calculation of a conservative, binary mixing

relationship between this end-member and our open ocean end-member (station sw4, salinity = 35.99, ε_{Nd} = -11.9, ε_{Hf} = 1.9) (Rickli et al., 2010) reveals that a third, less radiogenic water mass is required to explain the observed ε_{Nd} and ε_{Hf} values of the coastal stations (Fig. 2.8a,b). This water mass is likely represented by open ocean waters of more southerly origin (station fish 38, salinity = 36, ε_{Nd} = -14.6, ε_{Hf} = 0.9) (Rickli et al., 2010), which receive an unradiogenic Nd isotope signature from a trace metal enriched plume originating from the African coast (Noble et al., 2012, Zheng et al., 2016, Rahlf et al., 2020) admixed into the Congo River plume via the BCC (Fig. 2.1). Dust has also been discussed as an additional source (Menzel-Barraqueta et al., 2019). Saharan dust, however, usually does not reach that far south and carries a Nd isotope signature that is much less radiogenic than the required end-member (Grousset et al., 1998), whereas the Namibian dust source is too radiogenic to be considered as an additional source (Grousset et al., 1992, Rickli et al, 2009).

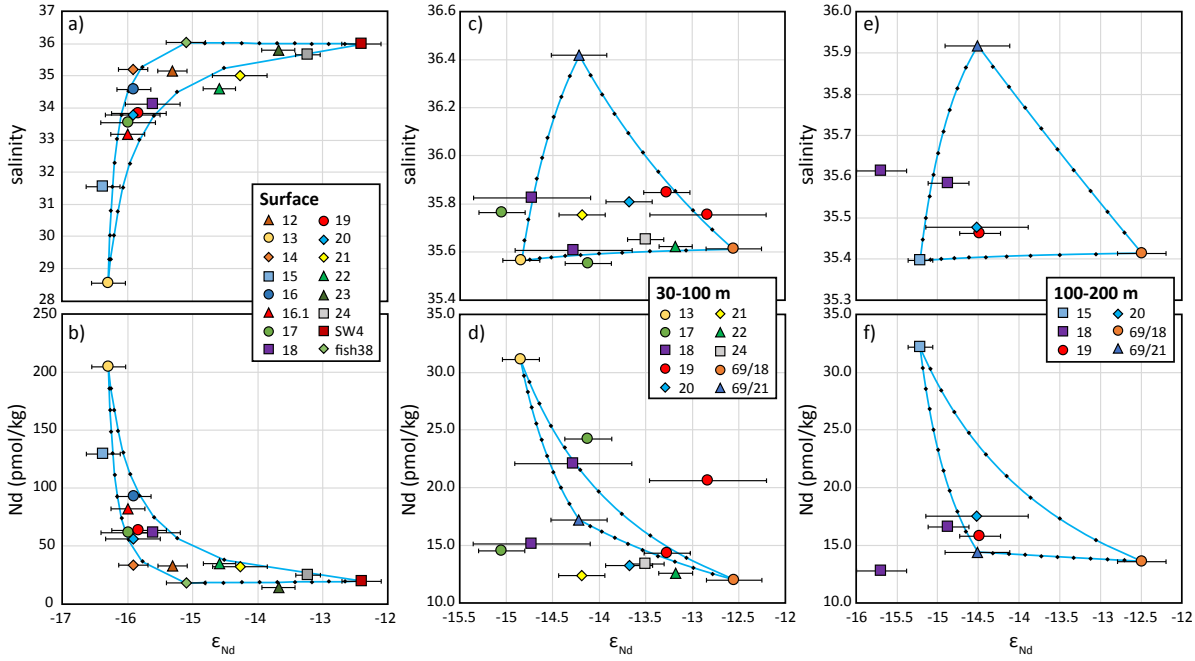

Figure 2.8: Conservative mixing is indicated by a ternary mixing relationship between three end-members for surface waters (a and b), for waters prevailing at 30-100 m depth (c and d), and 100-200 m depth (e and f).

We further applied the ternary mixing relationships for subsurface waters at 30-100 and 100-200 m water depth (Fig. 2.8). Between 30 and 100 m depth, most Nd isotope signatures plot within the ternary mixing diagrams (Fig. 2.8c), whereas most of the Nd concentrations indicate removal of Nd due to particle scavenging (Fig. 2.8d). Only two samples have higher Nd concentrations compared to those expected from conservative mixing (station 17, 30 m; station 19, 40 m), which may be a consequence

of local particle dissolution and will not be discussed any further. The Nd removal observed in many subsurface samples indicates that riverine REE removal is not limited to the surface layer. Waters between 100 and 200 m depths indicate conservative behavior of Nd isotopes and concentrations, except at station 18 that has less radiogenic Nd isotope signatures and is also marked by significant Nd removal (Fig. 2.8e, f).

4.1.3. Comparison of Nd and Hf isotope signature and incongruent weathering

The dissolved Nd and Hf signatures of the plume surface waters likely originate from pre-formed continental Fe-Mn oxides (Bayon et al., 2004), which are major components of particulate matter in the Congo River plume (Dupré et al., 1996). Continental pre-formed Fe-Mn oxides preferentially incorporate Hf (Bayon et al., 2009) with high ε_{Hf} for a given ε_{Nd} value, mainly as a consequence of the zircon effect (Piotrowski et al., 2000, van der Flierdt et al., 2002). The dissolved Nd and Hf isotope compositions of Congo River freshwater and surface waters between stations 12.1 and 16.1 plot at the unradiogenic end of the seawater array and overlap with leached Fe-hydroxide fractions from the Congo fan sediments (Bayon et al., 2009) (Fig. 2.9), which supports that dissolution of Fe-hydroxides mainly controls the radiogenic isotope signatures of the Congo River. The offset of ε_{Hf} values for a given ε_{Nd} value is indicative of incongruent weathering and preferential release of radiogenic Hf to the river waters (van de Flierdt et al., 2007, Bayon et al., 2009) supporting that the radiogenic Hf-Nd isotope fractionation observed for the seawater array already occurs on land and in rivers (cf. Merschel et al., 2017b). Samples from station 24 (full water column profile) plot at more radiogenic Nd and Hf isotope compositions of the seawater array (Fig. 2.9), which is in line with previously published data of Rickli et al. (2009, 2010) who showed that neither surface nor deep waters of this westernmost station of our study are directly affected by Hf and Nd originating from the Congo plume.

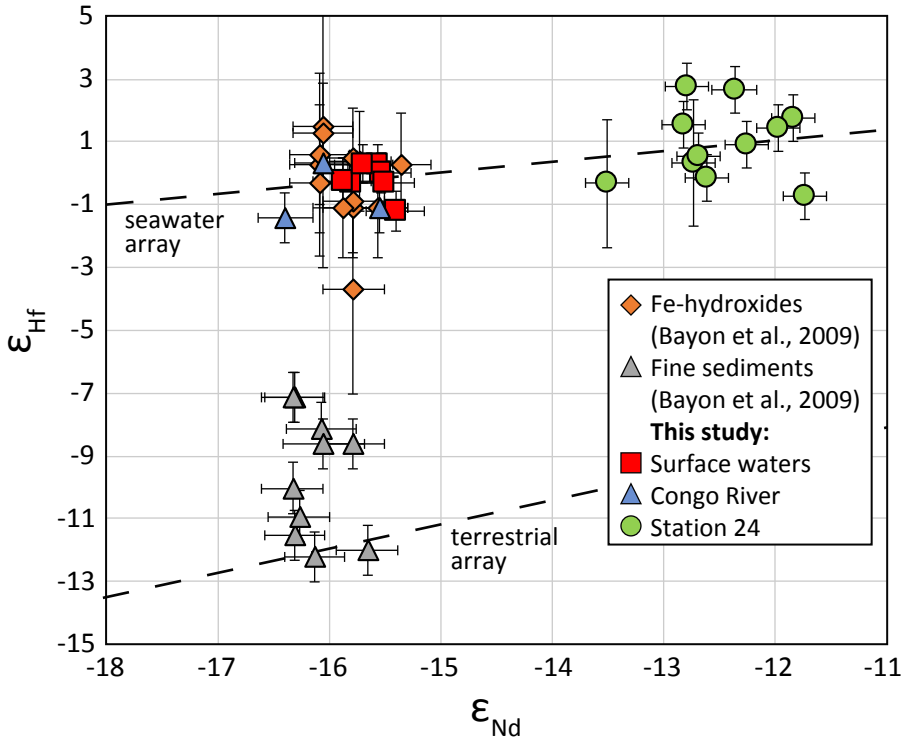

Figure 2.9: Nd isotope versus Hf isotope diagram of dissolved surface water isotope compositions shown together with fine sediments and leached Fe-hydroxides from Congo River fan sediments (Bayon et al., 2009), indicating that Fe-hydroxides mainly control the radiogenic isotope signatures of Congo River freshwater and nearshore surface waters.

4.2. Intermediate, deep and bottom waters

Mixing relationships between the intermediate, deep and bottom water masses UCDW, NADW and LCDW were calculated in order to evaluate to what extent the Nd isotope and concentration data reflect conservative mixing in the northern and northeastern Angola Basin (Fig. 2.10). We chose regional water mass end-members, which mix at the corresponding depths according to their TS-relationships (Fig. 2.2). The northwestern station of the Angola Basin occupied during M121 (station 24, 2000 m, ε_{Nd} = -12.8, Nd = 17.5 pmol/kg, salinity = 34.95) (Rahlf et al. 2020) was selected as the regional NADW end-member signature. The regional UCDW- and LCDW-end-member compositions (station 101, 1000 m, ε_{Nd} = -8.5, Nd = 11.8 pmol/kg, salinity = 34.37, station 113, 2400 m, ε_{Nd} = -8.5, Nd = 24.51 pmol/kg, salinity = 34.68 and station 104, 4440 m, ε_{Nd} = -8.7, Nd = 27,9 pmol/kg, salinity of 34.69, respectively) were adopted from the southern Cape Basin (Stichel et al. 2012b). To quantify variations not related to conservative water mass mixing, we calculated the difference $\Delta\varepsilon_{Nd}$ between measured ε_{Nd} values and the corresponding ε_{Nd} values expected from pure water mass

mixing of the two previously defined regional end-members. The same has been done for Nd concentrations (Δ[Nd]). We defined deviations from conservative mixing exceeding ±0.6 ε_{Nd} units and ±5 % of the Nd concentrations in pmol/kg as indicating contributions from non-conservative behavior following Rahlf et al. (2020). This is based on the maximum 2SD uncertainties of the Nd isotope measurements and on the 5 % uncertainty of the Nd concentration measurements.

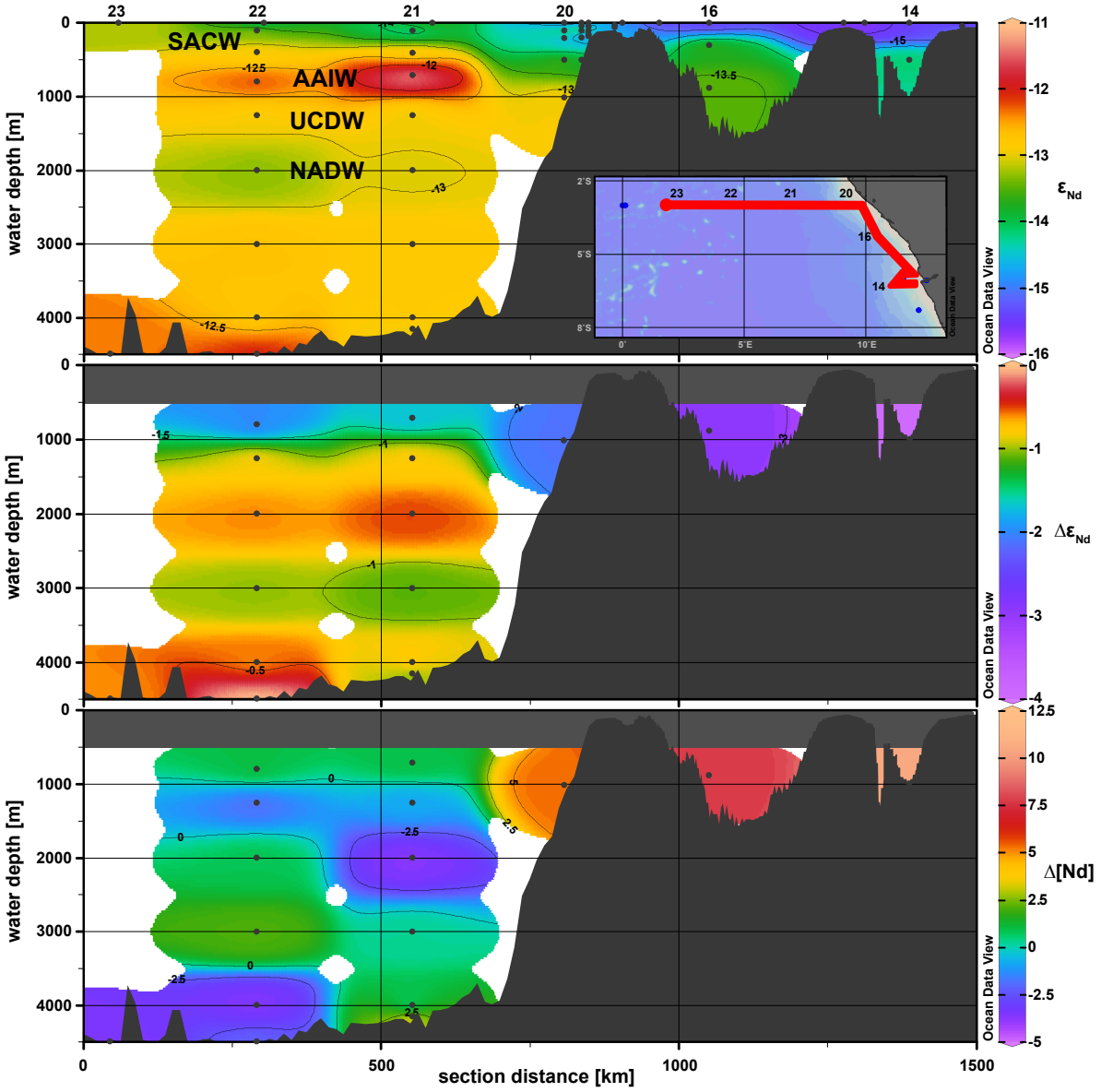

Figure 2.10: Distributions of the Nd isotope compositions and the differences between measured ε_{Nd}/[Nd] values and the corresponding ε_{Nd}/[Nd] values expected from conservative water mass mixing shown in a section including nearshore and offshore stations. The $\Delta\varepsilon_{Nd}$ and Δ[Nd] were calculated only for intermediate, deep and bottom waters (> 500 m depth).

Mixing relationships for intermediate water masses reveal that all stations have less radiogenic ε_{Nd} signatures than expected from conservative mixing ($\Delta\varepsilon_{Nd}$) with $\Delta\varepsilon_{Nd}$ reaching -4 units at station 14. Intermediate waters are also marked by excess Nd concentrations with stations 14 and 16 showing the largest Δ_{Nd} values of 11 pmol/kg and 8 pmol/kg, respectively (Fig. 2.10). Stations 14 and 16 are also characterized by the largest enrichment of other LREEs compared to BATS 2000 m, which combined with the shift observed in ε_{Nd} is indicative for REE release from Congo-derived shelf sediments or from particles supplied by the Congo River plume. Deep waters are 0.5 to 1 ε_{Nd} units less radiogenic and Nd concentrations are up to 2 pmol/kg higher than expected from conservative mixing (Fig. 2.10), also suggesting release of dissolved Nd from Congo River particles to NADW. However, release at these depths is more limited compared to that in the intermediate water column above. Apart from that, a small Nd deficiency is only observed for UCDW and NADW of station 21 (2000 m depth), which may, however, be an artifact of the chosen end-members. Nd isotope compositions of bottom waters are consistent with conservative behavior, whereas Nd concentrations indicate Nd release of only up to 4 pmol/kg from seafloor sediments at station 21 (Fig. 2.10). A similar release has also been observed before in the central Angola Basin (Rahlf et al., 2020) and in the Gulf of Guinea, where REEs are released from suboxic surface sediments (Bayon et al., 2011). These sediments likely are not formed by deposition of Congo-derived detrital material only and their dissolution therefore does not cause a detectable change towards less radiogenic seawater compositions. Bottom waters of stations 22 and 23 have a negative Δ[Nd] indicating REE removal, possibly caused by resuspended sediments.

5. Summary and conclusions

We investigated the distribution of REEs and Hf along with Nd and Hf isotope compositions of filtered seawater samples collected at the Congo River mouth, and in full water depth profiles along the coast of Congo and Gabon and along a connected latitudinal offshore section at 3°S . We found highest REE and Hf concentrations in the river water and in estuarine surface waters near the river mouth. The concentrations of Nd and Hf, which likely mainly originate from preformed riverine Fe-hydroxides,

vary seasonally between ~2000 and ~4000 pmol/kg for Nd and between ~33 and ~54 pmol/kg for Hf. Nd and Hf isotope compositions only show a small seasonal variability between -15.6 and -16.4 and between 0.4 and -1.4, respectively. Despite that no samples are available at salinities between 0 and 23 a pronounced decrease in REE concentrations and HREE enrichment relative to LREE indicates rapid scavenging and removal of LREEs (at least ~60% in the case of Nd) and MREEs by coagulation processes, forming typical seawater REE patterns likely close to the discharge area. At higher salinities above 23 riverine REEs in surface waters are then mixed conservatively for up to 1000 km northwest of the river mouth within the Benguela Current and the South Equatorial Current. Surface water Hf concentrations and Nd and Hf isotope compositions appear to behave conservatively during mixing between river water and ambient seawater based on our high-salinity data. However, particle-seawater interactions may occur in the in the low salinity zone and result in Nd release from or exchange with Congo-derived particulate phases. This is indicated by elevated Congo-shelf-zone REE and Hf fluxes, which suggests dissolution of Congo-derived particulate phases if we assume that strong estuarine removal of REEs and Hf occurred in the low salinity zone. In contrast, the Nd and Hf isotopic compositions do not provide evidence for any release from suspended riverine particles due to identical dissolved and particulate isotope compositions of the Congo River. The Congo-shelf-zone flux even exceeds that of the Amazon River by almost a factor of 2 based on the data available for the Amazon River plume, suggesting that the Congo River is more important for the global Nd budget than previously assumed. The offshore export of Congo-derived Nd across the 3 °S section amounts to 150 Mg/year, which corresponds to ~40 % of the Congo-shelf-zone flux and indicates that the Congo plume significantly influences large areas of the open South Atlantic Ocean.

Subsurface waters between 50 and 100 m depth are also marked by riverine REE removal, whereas below 1000 m depth, Nd concentrations are only slightly elevated compared to the values expected from conservative mixing due to release from Congo River particles in the northeastern and northern Angola Basin. REE concentrations of bottom waters of the offshore section indicate limited REE release from seafloor sediments similar to observations from the central Angola Basin and the Guinea Basin further north. Overall, Nd and Hf isotope compositions (having passed the estuarine filter) can be reliably used as conservative tracers for surface water mass advection and

mixing of the Congo River plume. These isotope systems and the REE/Hf concentrations also show that the Congo is a major source of trace elements to the South Atlantic Ocean and affects the distribution of elements in the entire water column of the deep northeastern Angola Basin by vertical exchange processes and limited release from particles.

Acknowledgments

We thank the captain and crew of RV Meteor for their help and support during cruise M121. We also thank Jutta Heinze, Ana Kolevica, Bettina Domeier, Marcus Gutjahr and Christopher Siebert for laboratory support. We are deeply indebted to Bomba Sangolay (Instituto Nacional de Investigação Pesqueira, Luanda, Angola) and his colleagues for the Congo River water sampling.

CHAPTER III

Release of Rare Earth Elements and unradiogenic Nd isotope signatures from the West African coast to surface waters of the Angola Basin

To be submitted as: *Peer Rahlf, Ed Hathorne, Martin Frank Release of Rare Earth Elements and unradiogenic Nd isotope signatures from the West African coast to surface waters of the Angola Basin*

Abstract

Boundary exchange with continental margin sediments has been proposed to be the dominant mechanism controlling the oceanic budget of dissolved rare earth elements (dREEs) but systematic data on the involved processes are scarce. Here we present the first dREE concentration and neodymium (Nd) isotope (ε_{Nd}) distributions of the full water column along the coast of Namibia and Angola between 7°S and 29°S. Surface waters of the Angolan coast near the Angola Benguela Front (ABF) have ε_{Nd} signatures of up to -21 and elevated REE concentrations (~ 35 pmol/kg for Nd), which are most likely controlled by dissolution of Fe-Mn oxide coatings of coastal sediment particles in the prevailing oxygen minimum zone. Decreasing REE concentrations in intermediate and deep waters suggest removal via scavenging due to high vertical particle fluxes. ε_{Nd} signatures of near -15 in intermediate and deep waters do not reflect mixtures of AAIW and NADW signatures but indicate release of unradiogenic Nd from sinking particles.

In contrast, surface waters off the Namibian coast have more radiogenic Nd isotope compositions and lower REE concentrations, suggesting terrestrial input from the Namib and Kalahari deserts or the Orange River. Alternatively, strong coastal currents related to the Benguela upwelling, likely in combination with the interaction of internal waves enhance the resuspension of shelf sediments, which are partially decomposed in the oxygen minimum zone between 100 and 200 m water depth. This

process is consistent with ε_{Nd} signatures of shelf sediments off the Namibian coast similar to those of the surface waters above.

Mixing calculations based on REEs reveal that the unradiogenic Nd isotope signature of surface waters of the open western Angola Basin is not solely controlled by unradiogenic waters from the Agulhas Current (AC) but also by the unradiogenic coastal waters near the ABF, which are transported westward by the prevailing winds and as part of eddies.

1. Introduction

The transfer of terrestrial material into seawater at the land ocean interface largely controls the chemical composition of the oceans. The sources of material supplied to the oceans are diverse and include the atmosphere, rivers, sediments, submarine groundwater discharge and mid-ocean ridges/volcanic arcs (Jeandel, 2016). The bidirectional exchange (dissolution and scavenging, adsorption and desorption, remineralization, etc.) of elements between particulate matter and seawater at the land ocean interface has been termed boundary exchange (Lacan and Jeandel, 2005, Jeandel et al., 2007, Jeandel, 2016). Rare earth elements (REEs) and neodymium (Nd) isotope compositions are key parameters to investigate the origin of continental inputs, their transport processes as well as the interactions between seawater and sediment particles and pore waters at land ocean interfaces and in the open ocean (Haley et al., 2003, Grasse al., 2012, Grenier et al., 2013, Garcia-Solsona et al., 2014, Abbott et a., 2015).

REEs released from fresh lithogenic continental inputs into surface waters have shale-like PAAS-normalized REE patterns (Elderfield, 1990). Upon contact with seawater, heavy REEs (HREEs) preferentially form complexes with aqueous ligands than light REEs (LREEs), which in contrast are preferentially adsorbed on particle surfaces and removed from the water column (Sholkovitz et al., 1994), resulting in LREE-depleted PAAS-normalized dissolved REE patterns and a pronounced negative Ce anomaly as a consequence of the higher particle reactivity of Ce (Elderfield and Greaves, 1982). A recent study proposed that this REE fractionation already occurs in the rivers because

colloidal and truly dissolved riverine pools have different REE patterns (Pourret and Tuduri, 2017).

The radiogenic isotope composition of the REE Nd in seawater has been widely used as a long-distance tracer of water mass advection and mixing, enabled by its ocean residence time of 300-1000 years (Jeandel et al., 1995, Tachikawa et al., 1999, Tachikawa et al., 2003, Siddall et al., 2008, Arsouze et al., 2009, Rempfer et al., 2011). The radiogenic Nd isotope ratio ($^{143}Nd/^{144}Nd$) is expressed as $\varepsilon_{Nd} = [(^{143}Nd/^{144}Nd)_{sample}/(^{143}Nd/^{144}Nd)_{CHUR} -1] \times 10^4$ with CHUR = 0.512638 (Jacobsen and Wasserburg, 1980).

Here we present the distribution of dissolved REEs as well as of dissolved Nd isotopic compositions and concentrations in seawater along the coast of Angola and Namibia from 7°S to 29°S. We investigated 44 water samples from 19 full water column profiles collected during GEOTRACES cruise GA08 (Fig. 3.1). We discuss the potential sources of unradiogenic Nd isotopic signatures of the coastal surface waters and demonstrate that these waters strongly affect the composition of surface waters of the entire Angola Basin via westward advection.

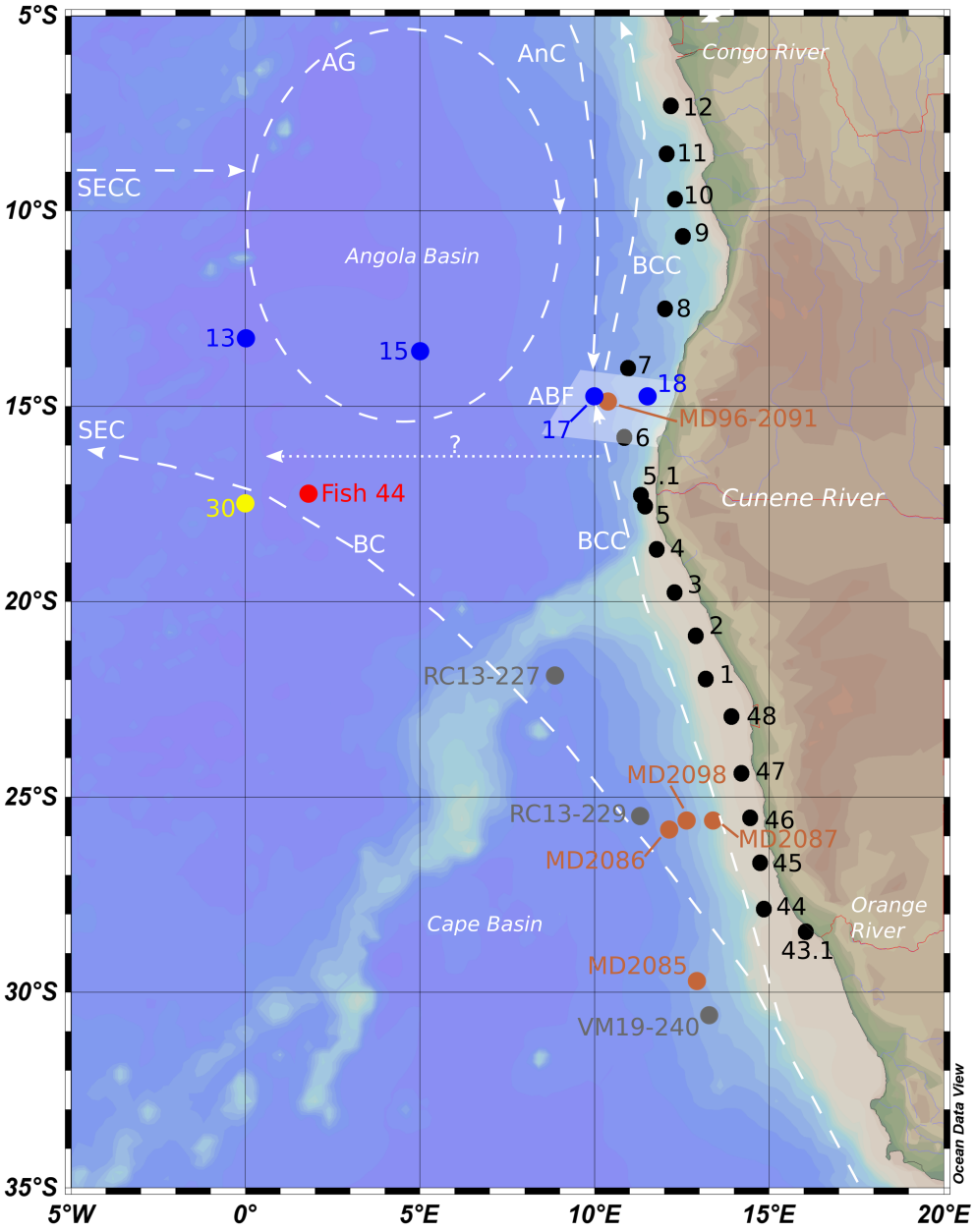

Figure 3.1: Map showing water sample locations from this study (black dots), from Rahlf et al., 2020 (yellow dot), from Zheng et al., 2016 (blue dots), Rickli et al., 2010 (red dot) and sediment core locations from Bayon et al., 2004 (brown dots) and from Franzese et al., 2006 (grey dots). White dashed arrows indicate surface currents: BC = Benguela Current, BCC = Benguela Coastal Current, SEC = South Equatorial Current, ABF = Angola Benguela Front, ABF = Angola Benguela Front, SECC = South Equatorial Counter Current, AG = Angola Gyre, AnC = Angola Current.

1.1. Hydrography

The Benguela Current (BC) is the dominant surface current of the southeastern Atlantic Ocean, which originates from the Agulhas Current and is introduced via the Agulhas Leakage (Stramma and England, 1999). The BC then feeds into the South Equatorial Current, which flows in northwesterly direction across the entire South

Atlantic. Near the Brazilian coast it changes direction and then continues to flow eastwards across the South Atlantic as the South Equatorial Counter Current that feeds into the cyclonic Angola Gyre (AG) (Stramma and England, 1999). At ~34°S the Benguela Coastal Current (BCC) branches off from the BC and flows north along the West African coast between 34°S and 15°S (Fig. 3.1). This region is influenced by intense and seasonally variable upwelling driven by southeasterly winds and is associated with high bioproductivity and high biogenic particle fluxes (Calvert et al., 1971, Lutjeharms and Meeuwis, 1987, (Meeuwis and Lutjeharms, 1990, Wefer and Fischer, 1993). The strongest upwelling occurs near 26°S in the Luderitz upwelling cell (Shannon et al., 1985). Further north at 15 °S, the cold BCC in Fig. 3.1 meets the warm southward flowing Angola Current (AnC) at the seasonally variable Angola-Benguela Front (ABF). The convergence zone is located between 14 and 16 °S (Meeuwis and Lutjeharms, 1990) but was also found at 19 °S (Mohrholz et al., 2001) and is also associated with upwelling of cool subsurface waters and with the formation of large eddies in surface and deep waters (Meeuwis and Lutjeharms, 1990).

The mixed layer (upper 50 m) of the northernmost stations (station 6-12) is dominated by well oxygenated (oxygen ~4 ml/l) Tropical Surface Water (TSW), characterized by warm temperatures near 27°C, and by Subtropical Underwater (STUW), characterized by temperatures near 20°C and high salinities of up to 36 (station 7, 8) (Fig. 3.2, 3). TSW and STUW of the northern stations are underlain by South Atlantic Central Water (SACW) between 50 and 500 m water depth (Fig. 3.2) (Sverdrup et al., 1942, Stramma and England, 1999), which partly originates from Indian Central Water (ICW) and is advected into the Atlantic Ocean by the Agulhas Current (Stramma and Schott, 1999). In contrast to the northern stations, SACW of the southern stations 5-43.1 reaches surface waters and is not overlain by TSW and STUW. These surface waters are colder (15-18 °C), less saline (~35 psu) and more oxygenated (~6 ml/l) than surface waters in the northern part of the section (Fig. 3.2, 3). Intermediate waters are characterized by low salinities between 34.3 and 34.6 and potential temperatures between 4 and 6 °C, which are typical for nutrient-rich Antarctic Intermediate Water (AAIW) (Fig. 3.2) (Whitworth and Nowlin, 1987). In the South East Atlantic Ocean (SEAO), AAIW originates from the Indian Ocean and is advected as part of the Agulhas Current leakage (Roman and Lutjeharms, 2010, Stramma and England, 1999). Northward

propagation of AAIW occurs between 500 and 1200 m water depth (Talley, 1996). Below AAIW, Upper Circumpolar Deep Water (UCDW) prevails at salinities between 34.8 and 34.6 and at potential temperatures between 3 and 4°C (Fig. 3.2). The oxygen-poor and nutrient-rich UCDW also originates from the ACC, propagates northwards and loses its characteristics through mixing by the time it reaches the equator (Stramma and Schott, 1999). In the Angola Basin, deep and bottom waters below AAIW are dominated by North Atlantic Deep Water (NADW), characterized by higher salinities between 34.8 and 35 and potential temperatures between 2 and 3 °C (Fig. 2). NADW is advected into the SEAO via a branch of the Deep Western Boundary Current that forms near the equator (Rhein et al., 1995) and enters the Angola Basin across the Romanche Fracture Zone.

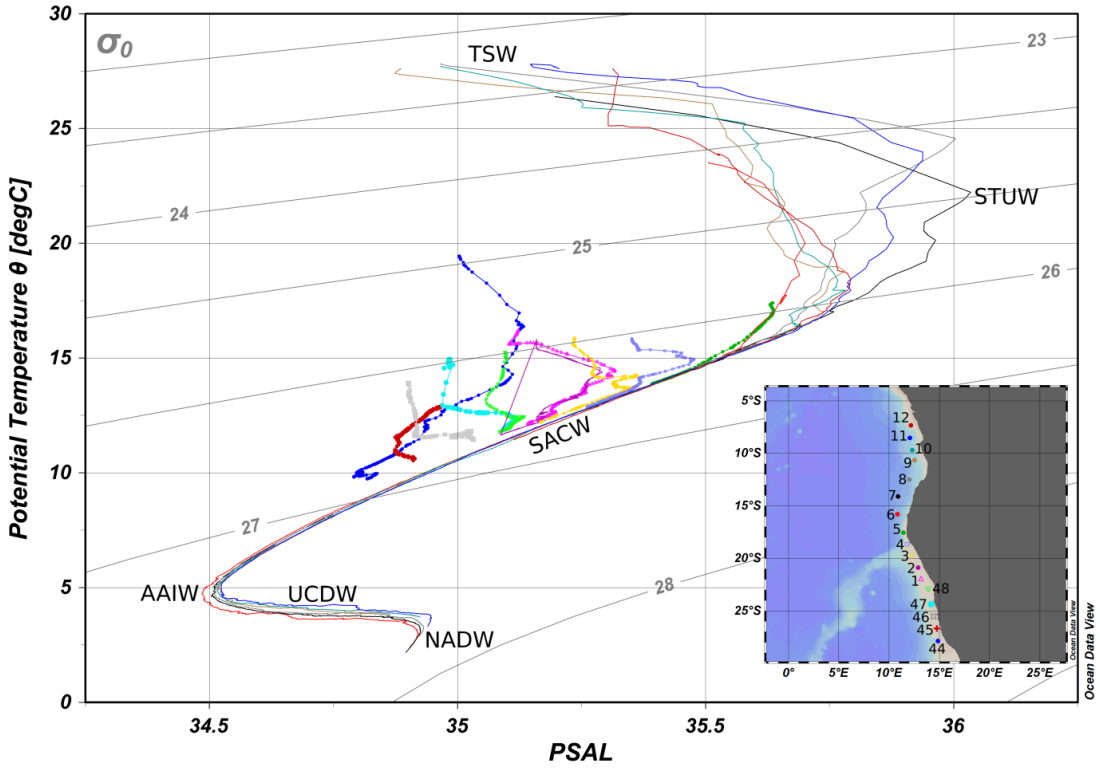

Figure 3.2: T-S plot of the main water masses present in the study area. TSW = Tropical Surface Water, STUW = Sub Tropical Under Water, SACW = South Atlantic Central Water, AAIW = Antarctic Intermediate Water, UCDW = Upper Circumpolar Deep Water, NADW = North Atlantic Deep Water. TSW is only present in the northern stations (stations 6-12), whereas surface waters of the southern stations (stations 5-44) are occupied by SACW.

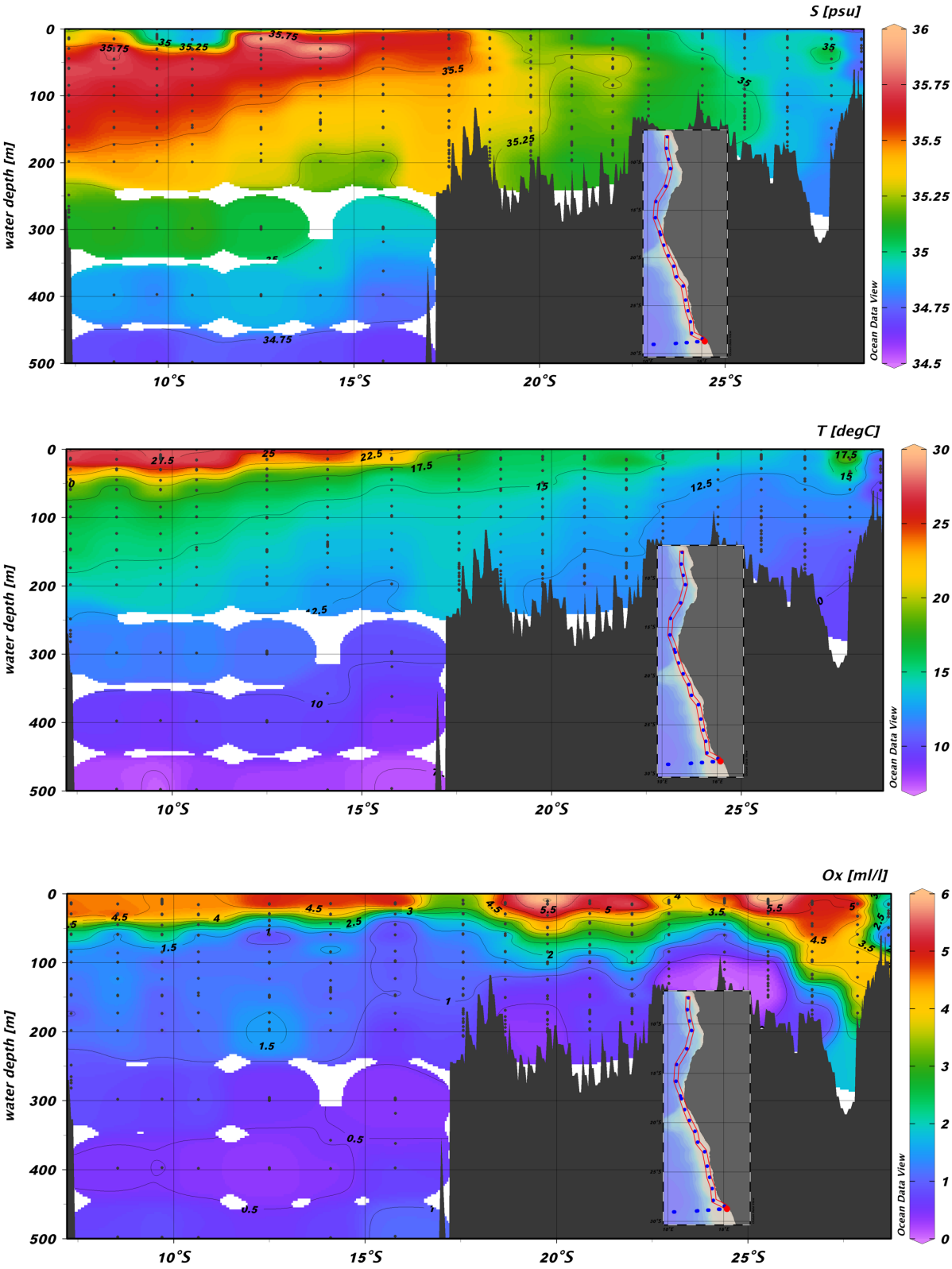

Figure 3.3: N-S sections of salinity, temperature and oxygen along the cruise track. Surface and subsurface waters of the northern part of the section are charachterized by high salinities and temperatures, whereas surface and subsurface waters of the southern part are less saline and colder due to the supply of upwelled water. Subsurface waters show low oxygen concentrations, in particular above the shelf off the Namibian coast.

2. Methods

44 water samples were taken along the coast of Angola and Namibia from 7 °S to 28 °S during GEOTRACES cruise GA08 (RV Meteor cruise M121) in November/December 2015 (Fig. 3.1). Samples from the full water column were collected with 10 L Niskin bottles attached to a stainless steel CTD rosette, while surface water samples were recovered with a towed stainless steel fish. The samples were then treated in the onboard laboratory strictly following recommended GEOTRACES protocols (van de Flierdt et al., 2012). Each 20 L sample was filtered through a nitro-cellulose acetate filter (0.45 µm pore diameter) into an acid-cleaned LDPE-cubitainer with a peristaltic pump within 2 hours after sample collection, and subsequently acidified with ~20 ml concentrated, distilled HCl. For Nd concentration measurements, 2 L aliquots from each filtered sample were collected in acid-cleaned 2-liter PE-bottles. To each large volume sample 400 µl $FeCl_3$ solution (~200 mg Fe/ml) were added and the sample was left to equilibrate for 24 hours. Ammonia solution (25 %, Merck Suprapur®) was then added to raise the pH from about 2 to 7.5-8.0. After 48 hours, the trace elements co-precipitated with the FeOOH settled to the bottom of the cubitainers and the supernatant was syphoned off.

The precipitates were transported to the home laboratory at GEOMAR in 2 L bottles and were centrifuged and rinsed three times with deionized water (MilliQ, 18.2 MΩcm) in 50 ml centrifuge tubes to remove major seawater ions. After dissolution in 6 M HCl/0.5 M HF and transfer into Teflon vials the samples were evaporated to dryness. To remove organic compounds, the samples were treated with aqua regia at 120 °C for 24 h. Most of the Fe was subsequently removed via liquid–liquid extraction with pre-cleaned di-ethyl ether (Stichel at al., 2012b). The rare earth elements (REEs) were chromatographically separated from matrix elements using cation exchange resin AG 50W-X8 (1.4 ml, 200-400 µm) and following a modified protocol of Münker et al. (2001). Neodymium was then separated from the other REEs for isotope measurements using Eichrom®LN-Spec resin (2 ml, 50-100 µm) following a modified protocol of Pin and Zalduegui (1997). To remove residual traces of the resin and organic compounds, the Nd cuts were treated with 100 µl quartz distilled HNO_3 and 100 µl H_2O_2 (30 wt.%, Merck Suprapur®).

For the determination of Nd concentrations, 1 L aliquots were spiked with a pre-weighed ^{150}Nd spike and then purified with the same cation column chemistry that was used for the Nd isotope separation. Nd concentrations were then determined via isotope dilution on a Neptune Plus MC-ICPMS.

The $^{143}Nd/^{144}Nd$ ratios of the samples were measured on a Neptune Plus MC-ICPMS. Isobaric interferences between ^{144}Sm and ^{144}Nd were corrected by measuring the abundance of the interference-free isotope ^{147}Sm and by calculating the potential ^{144}Sm contribution on mass 144 from the natural abundance of Sm. The $^{143}Nd/^{144}Nd$ ratios of all samples were double-corrected for instrumental mass bias with $^{146}Nd/^{144}Nd$ = 0.7219 and $^{142}Nd/^{144}Nd$ = 1.141876 following the approach of Vance and Thirlwall (2002) and then normalized to the accepted JNdi-1-standard value of 0.512115 (Tanaka et al., 2000).

The external reproducibility of the Nd isotope measurements was estimated by repeated measurements of in-house Nd standard solutions, which gave values between 0.15 and 0.28 ε_{Nd} units (2SD). The external reproducibility for Nd concentration measurements was 2 % (2SD, n = 4 sample replicates).

3. Results

3.1. Neodymium isotope compositions and concentrations

The ε_{Nd} and Nd concentration signatures of the surface waters show a wide range varying between -8.38 and -20.45 and between 10.74 and 20.31 pmol/kg, respectively (supplementary Table A6, Fig. 3.4, 5, 6). The most radiogenic ε_{Nd} value of -8.38 is found at the southernmost station 43.1 corresponding to a concentration of 22 pmol/kg. Further north between 28 and 17 °S, ε_{Nd} values shift to less radiogenic values reaching -20.45 at station 5.1, which is accompanied by an increase in Nd concentrations to 36 pmol/kg. Between 17 °S and 7 °S, Nd concentrations vary between 31 and 39 pmol/kg, whereas ε_{Nd} values become gradually more radiogenic and reach -15 at station 12. Intermediate, deep and bottom water ε_{Nd} signatures are more uniform and only range from -14 to -16, while Nd concentrations are on average 20 pmol/kg and increase towards the seafloor to about 25 pmol/kg (Fig. 3.4, 6). Nd concentration patterns of

the water column profiles of stations 6 and 7 (~15 °S) are similar to measurements at station 18 of Zheng et al. (2016).

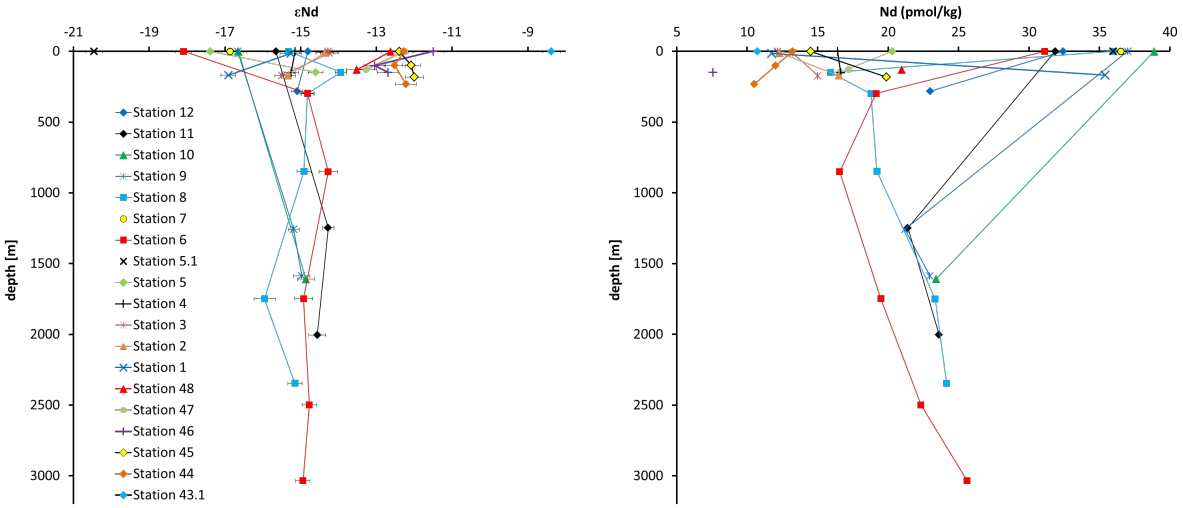

Fig. 3.4: Nd isotope compositions and Nd -concentrations of all stations.

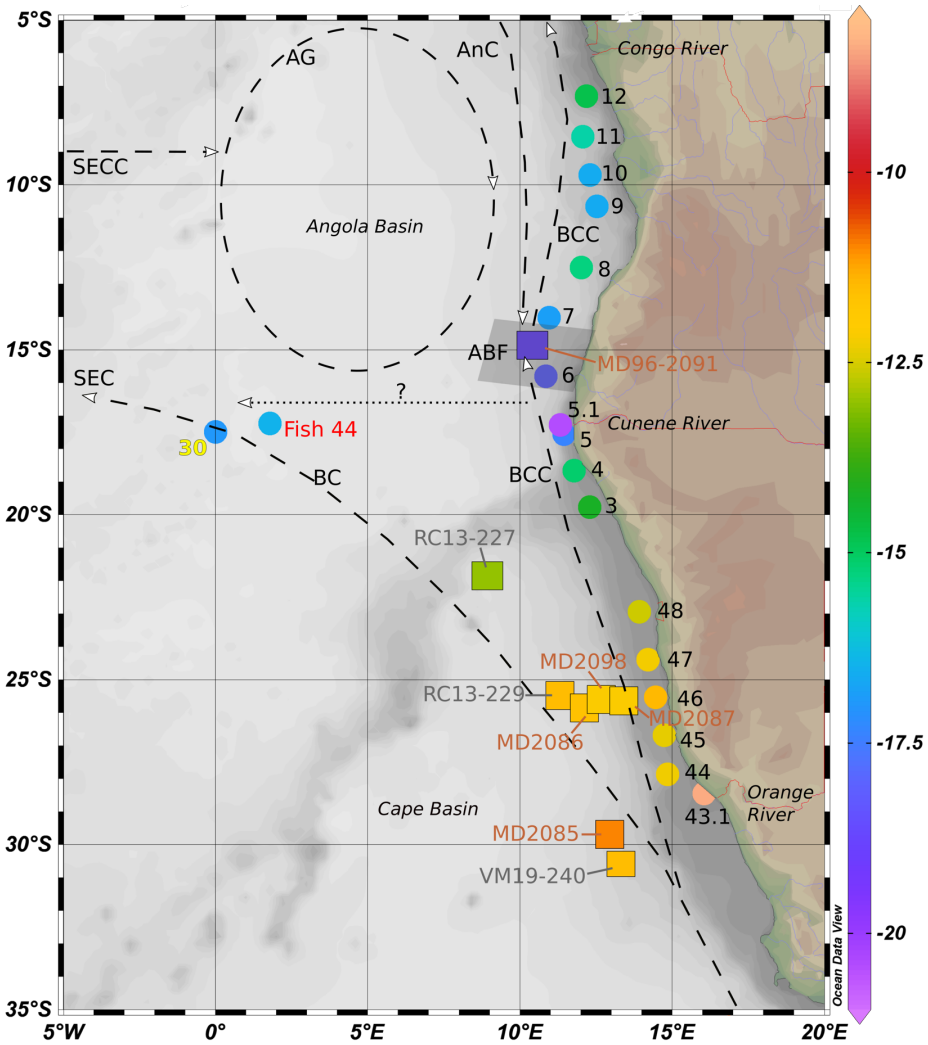

Fig. 3.5: Comparison of dissolved Nd isotope compositions of surface waters (circles) and surface sediments (squares) off the Angolan and Namibian coast.

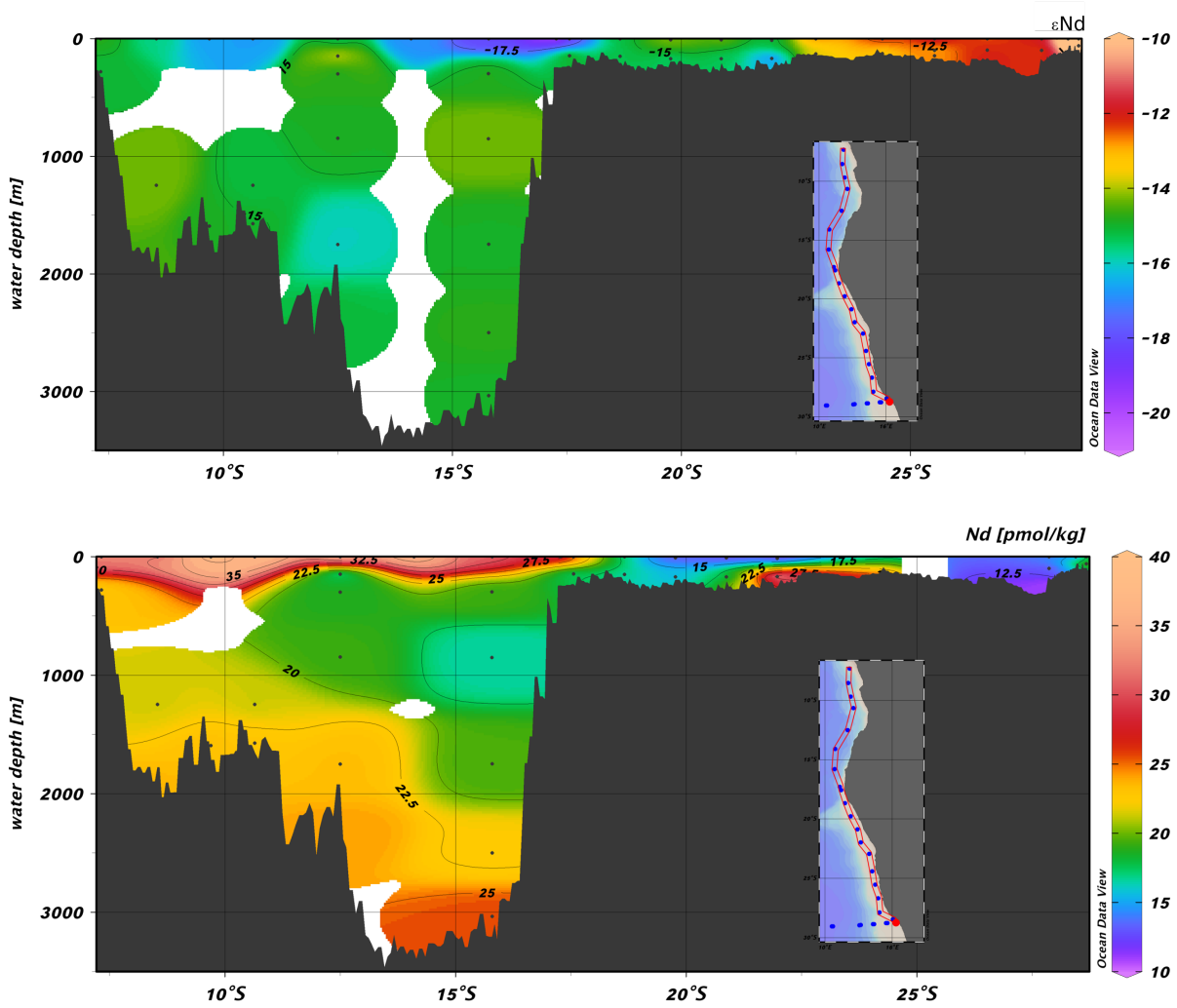

Fig. 3.6: Sections of Nd isotope signatures and Nd concentrations along the cruise track.

3.2. REE patterns

Near surface water REE concentration profiles are highly variable (supplementary Table A7, Fig. 3.7). While surface water Nd concentrations of the southern stations (stations 43.1-5) are only between 10 and 20 pmol/kg, the northern stations (stations 5.1-12) reach 30 to 40 pmol/kg (Fig. 3.7). Compared to surface water concentrations, subsurface water concentrations at 200 m water depth of the northern stations decrease, while subsurface water concentrations of the southern stations increase, in particular those of station 1 (Fig. 3.7). REE concentrations of intermediate, deep and bottom waters are more uniform at values around 22 pmol/kg in the case of Nd.

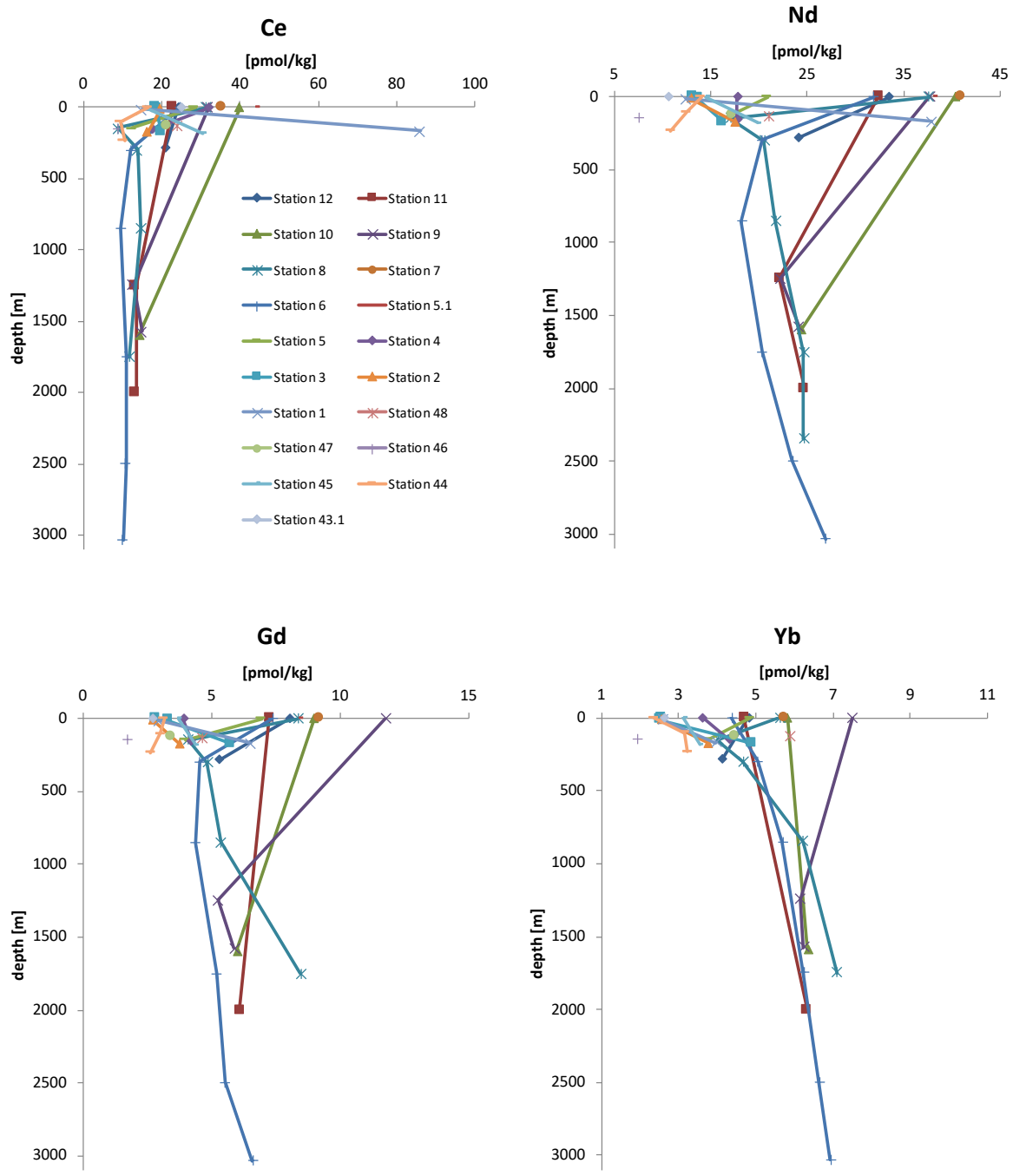

Figure 3.7: Concentrations of the REEs Ce, Nd, Gd and Yb of all stations.

PAAS-normalized (Post-Archean Average Shale; Taylor and McLennan, 1985) REE patterns of surface, subsurface, intermediate and deep waters and of BATS 15 m and BATS 2000 m from the Bermuda Atlantic Time Series (van de Flierdt et al., 2012) are applied to evaluate the processes and sources controlling REE distributions (Fig. 3.8). Surface waters of the northern stations (stations 12-5.1) show markedly elevated LREEs, whereas surface waters of the southern stations (stations 5-43.1) have depleted

HREEs, compared with BATS 15 m (Fig. 3.8a). Subsurface water patterns are flatter than that of BATS 15 m, in particular at station 1 (Fig. 3.8b). Intermediate and deep-water patterns closely follow the pattern of BATS 2000 m ((Fig. 3.8c, d).

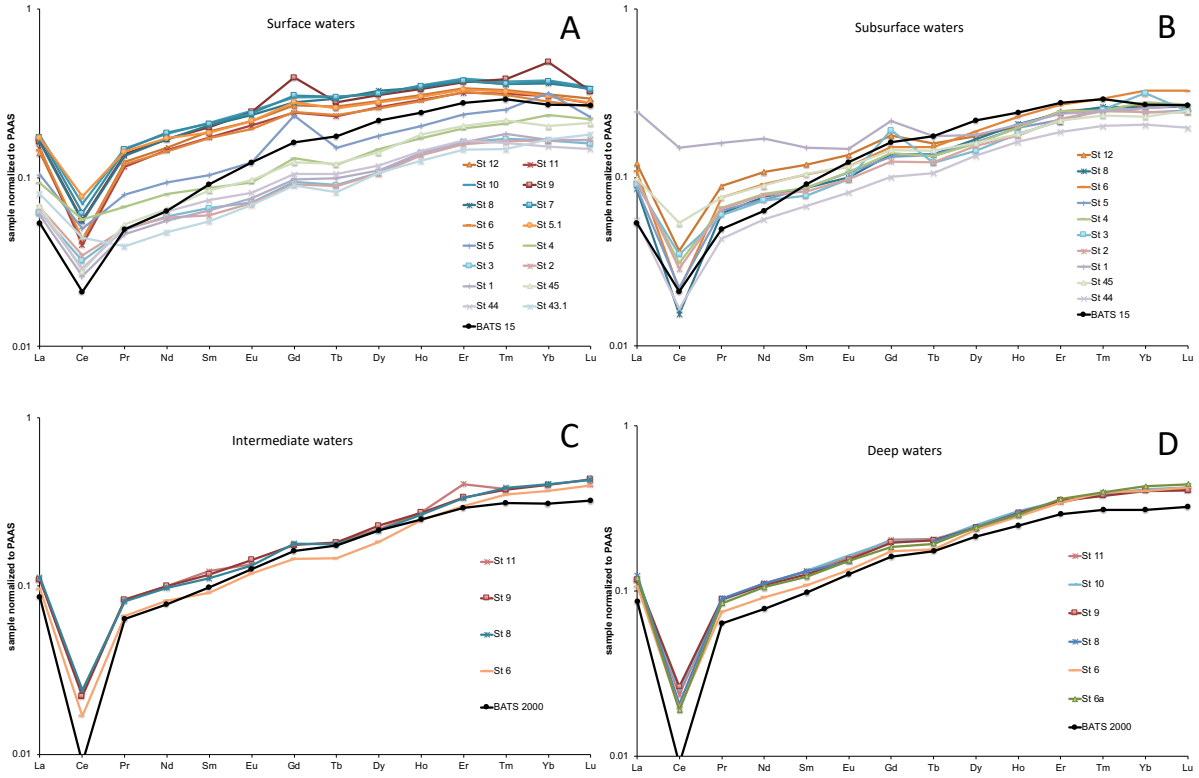

Fig. 3.8: PAAS-normalized REE patterns of all stations.

HREE/LREE ratios (HREE/LREE = $([Tm]_N+[Yb]_N+[Lu]_N)/([La]_N+[Pr]_N+[Nd]_N)$, whereby subscript N refers to PAAS-normalized concentrations) ranging between 1.8 and 3.4 are much lower than BATS 15 m (HREE/LREE = 4.98) (Fig. 3.9a). The lowest HREE/LREE ratio is found at station 5.1, whereas the highest ratio is found at station 45. HREE/LREE ratios of subsurface waters increase with water depth, except for stations 1 and 45. MREE/MREE* ratios (MREE/MREE* = $([Gd]_N+[Dy]_N)/([Yb]_N+[Nd]_N)$) of surface waters are between 0.9 and 1.2 and decrease with increasing water depth (Fig. 3.9b). The highest MREE enrichments are found at stations 5.1, 6 and 12. Ce anomalies of the surface waters (Ce/Ce* = $[Ce_N]/[([La]_N+[Pr]_N)/2]$) range between 0.3 and 0.73 (Fig. 3.9c). The strongest anomaly is found at station 11, whereas the weakest anomaly is found at station 43.1. Ce anomalies of subsurface waters increase strongly, except for stations 1 and 45.

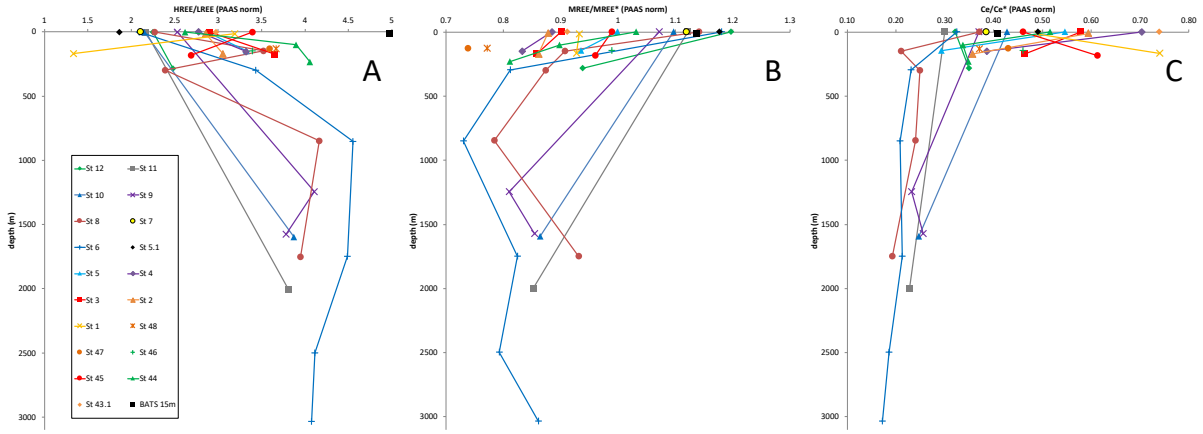

Fig. 3.9: PAAS-normalized HREE/LREE, MREE/MREE* and Ce/Ce* depth profiles of all stations.

4. Discussion

4.1. Distribution of REE concentrations and Nd isotope compositions along the coast of Angola

4.1.1. River inputs

Unradiogenic ε_{Nd} signatures of up to -21 accompanied by high REE concentrations (Nd concentrations reach up to 40 pmol/kg) as well as low HREE/LREE ratios in surface waters of the Angolan coast reflect terrestrial inputs, which are potentially originated by the Congo River entering the Atlantic further north at 6 °S. The Congo River has the second largest water and sediment discharge in the world after the Amazon River (Coynel et al., 2005, Savoye et al., 2009). Distributions of sea surface temperature, salinity, chlorophyll, and mean sea level anomaly fields as well as Nd isotope and concentration data indicate that the main axis of its plume is subject to seasonal variability but generally extends between 400 und 1000 km in northwesterly direction as forced by wind driven currents and the Benguela Coastal Current (Denamiel et al., 2013, Hopkins et al., 2013, Rahlf et al., submitted). Unradiogenic Nd isotope signatures of Fe-Mn oxide fractions from near surface sediments (ε_{Nd} ~ -22) far south of the Congo River mouth at 14 °S (MD96-2091) and near our station 5.1 (ε_{Nd} ~ -21) (Fig. 3.5) have previously been ascribed to a Congo Fan origin based on the sediments displaying similar REE patterns (Bayon et al., 2009). However, Nd isotope signatures of Congo Fan sediments and of the river water are clearly more radiogenic (ε_{Nd} ~ -16) (Bayon et

al., 2009, Rahlf et al., submitted) than the sediments at station MD96-2091 rendering this interpretation questionable. In addition, the dissolved REE patterns of the unradiogenic surface waters of stations 10, 8, 7, and 5.1, which are located south of the Congo River outflow, have a stronger LREE enrichment than the pattern of station 12 located immediately south of the Congo mouth (Fig. 3.10). This documents that the Congo river cannot be the main source of the highly unradiogenic signatures, but another more local source of terrigenous input must be responsible for the unradiogenic surface waters and sediments along the coast of Angola.

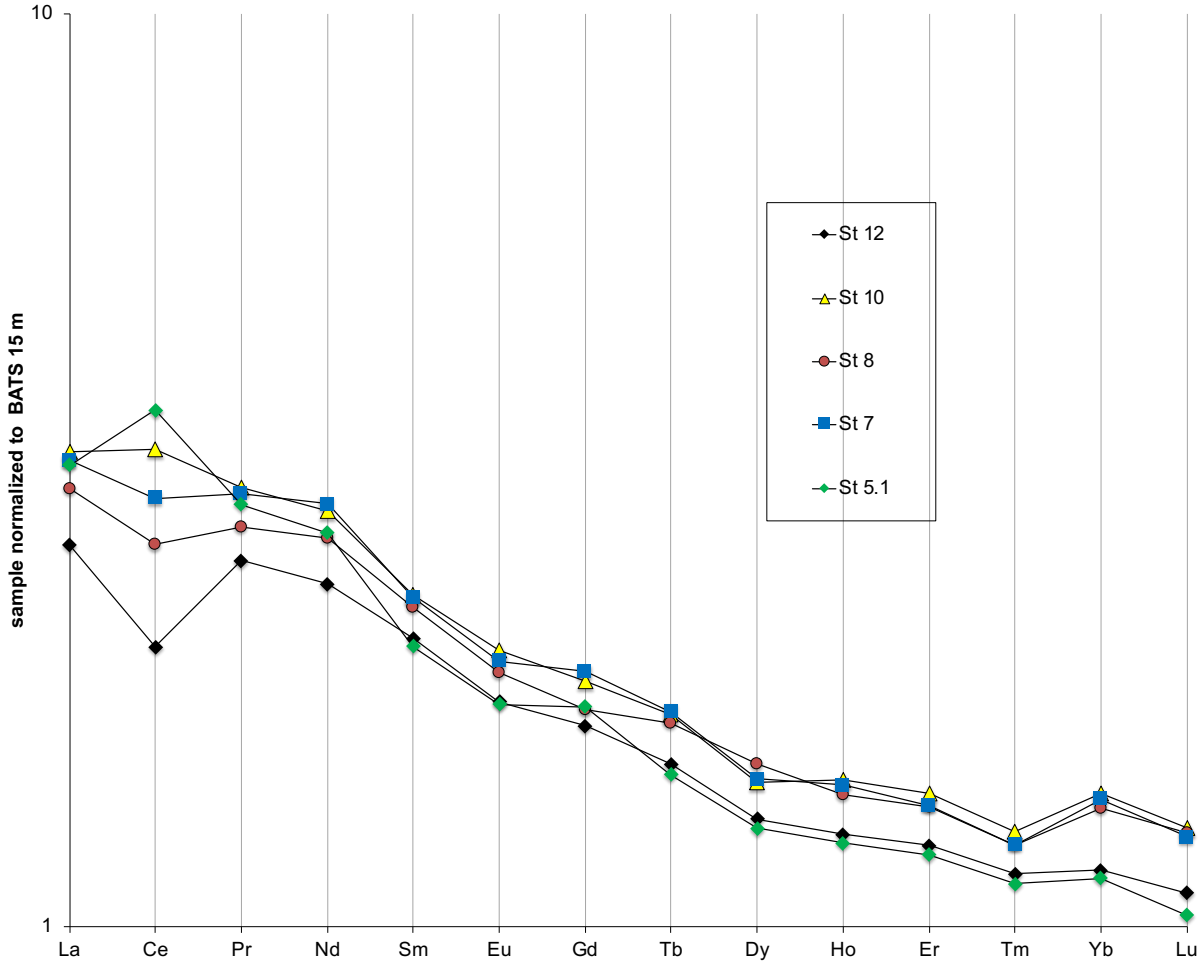

Fig. 3.10: REE patterns of selected surface water stations normalized to BATS 15 (van de Flierdt et al., 2012).

Bayon et al. (2009) suggested that the unradiogenic isotope signatures of the sediments at station MD96-2091 reflect a contribution from the nearby Kunene River entering the Angola Basin at 17 °S. Partial dissolution of this material may thus also contribute to the dissolved surface water isotope signatures along the coast. However, the Kunene

River discharge of 25 $m^3 s^{-1}$ (de Moor et al., 2000) is very low, compared to that of the Congo River (42,800 $m^3 s^{-1}$ Savoye et al., 2009) and no major salinity decrease reflecting any major freshwater inputs is detectable at 17°S (Fig. 3.3). In addition, the Nd isotope compositions of rocks drained by the Kunene River basin are too radiogenic (ε_{Nd} -7.9 to +6.4, Drüppel et al., 2007, Geißner et al., 2011) to explain the unradiogenic surface water signatures. However, at 10 °S the unradiogenic surface signature is accompanied by a salinity decrease (Fig. 3.3), which can be attributed to the discharge of the Rio Longa.

4.1.2. Dissolution of Fe-Mn-oxide coatings of particles

Fe-Mn-oxide coatings of particles are major contributors of dissolved REEs to the ocean and are delivered by dust, river inputs and decomposition of sediments. However, the ε_{Nd} signatures of dust from the nearby Namib and Kalahari range between -3 and -12 (Grousset, et al., 1992, Bayon et al., 2004) and are thus too radiogenic to explain the observed Nd isotope compositions. In addition, the amount of dust supplied from these deserts to the eastern South Atlantic is low compared to the inputs from the Sahara to the Central and North Atlantic (Mahowald et al., 2005), which clearly dominate the surface water Nd isotope compositions between the equator and 20°N (Rickli et al., 2010).

The most plausible source of unradiogenic Nd isotope compositions and high REE concentrations in surface waters is the reduction of Fe-Mn-oxides of coastal sediments in the oxygen minimum zone off the Angolan coast. This is supported by other studies that detected elevated REE concentrations off the coast of Angola at ~15°S, which were accompanied by high trace metal concentrations such as of Co, Fe and Mn (Noble et al., 2012, Zheng et al., 2016). Decreasing REE concentrations in intermediate and deep waters of the Angolan coast suggest removal via scavenging due to high vertical particle fluxes (Fig. 3.7). A similar behavior of REEs has been observed off the coast of Panama (Grasse et al., 2017). At the same time, ε_{Nd} signatures near -15 in intermediate and deep waters off the Angolan coast do not reflect AAIW and NADW compositions, which are the prevailing deep water masses of the Angola Basin (Rahlf et al., 2020) and indicate release of unradiogenic Nd from sinking particles. Highly unradiogenic

surface sediments of core MD96-2091 at ~15°S (Bayon et al., 2004) (Fig. 3.5) are consistent with the release of REE from particles.

4.2. Distribution of REE concentrations and Nd isotope compositions along the coast of Namibia

Southeasterly trade winds in the Benguela region result in strong upwelling of cold and nutrient rich waters, which correspond to the SACW. The strongest upwelling occurs in the Luderitz upwelling cell at about 26 °S (Shannon, 1985, Lutjeharms and Valentine, 1987, Meeuwis and Lutjeharms, 1990), which is characterized by water temperatures of about 10 °C (Fig. 3.3). The Benguela region is characterized by high productivity and sinking particulate matter (Lutjeharms and Meeuwis, 1987, Wefer and Fischer, 1993) accompanied by an oxygen minimum zone between 100 and 200 m water depth, in which oxygen concentrations drop below 1 ml/l (Fig. 3.3).

In contrast to the surface waters of the Angolan coast, surface waters of the Namibian coast have more radiogenic Nd isotope compositions (ε_{Nd} ~ -12), lower REE concentrations (~ 12 pmol/kg for Nd) (Fig 4, 5, 6) and higher HREE/LREE ratios (Fig 9). However, these surface waters are still less radiogenic than and have higher Nd concentrations than pure South Atlantic Central Water (8.5 pmol/kg, ε_{Nd} of -10) (Jeandel et al., 1993). The elevated Nd concentrations and isotope compositions may be delivered by Fe-Mn-oxide coatings of dust particles from the nearby Namib and Kalahari deserts (Grousset, et al., 1992, Bayon et al., 2004), which are decomposed in the oxygen minimum zone. In addition, the Orange River located at ~29 °S (Fig. 3.5) may also be a potential source for Fe-Mn-oxides or organic matter carrying additional Nd. However, the Orange River discharge is low and the plume direction is dominantly southward (Shillington et al., 1990).

Recent studies found that the continental slope brakes internal waves, which cause strongly elevated near-bottom turbulence that can erode surface sediments (e.g. Cacchione et al., 2012, Pomar et al., 2012, Lamb, 2014, Erdem et al., 2016). The resulting resuspension of shelf sediments into the coastal upwelling system may transport particles into the oxygen minimum zone, where they release their Nd isotope

compositions and concentrations. In addition, pore water REE fluxes from the oxygen depleted shelf sediments into the bottom waters may also be enhanced (Abbott et al., 2015). This mechanism may also be responsible for the similar ε_{Nd} signatures of surface shelf and slope sediments in the Cape Basin between 25 and 31 °S (Bayon et al., 2004, Franzese et al., 2006) and those of the surface waters above the shelf region (Fig. 3.5).

4.3. Surface water mixing

To investigate surface water mixing processes of the coast of Angola and the influence of the advection of unradiogenic coastal surface waters in the open western Angola Basin, we calculated mixing relationships between station 43.1, 5.1 and station 30 from the study of Rahlf et al. (2020). (Fig. 3.11). The relationships indicate a continuous change from more radiogenic ε_{Nd} values (-8.4) in the south to less radiogenic values ε_{Nd} (-17.4) at the ABF with increasing salinity. This linear relationship that deviates from the hypothetical mixing line between stations 43.1 and 5.1, however, likely mainly reflects the continuous change of the Nd isotope composition of the adjacent continental rocks and their sediments off the Namibian coast rather than surface water mass mixing.

The isotopic composition of surface waters from offshore station 30 is influenced by an unradiogenic ε_{Nd} signature advected by the Agulhas Current (Rahlf et al., 2020). Salinities and ε_{Nd} signatures of station 5.1 (Sal = 35.38, ε_{Nd} = -20.5) and station S1 (Sal = 35.5, ε_{Nd} = -19) (Stichel et al., 2012a) are similar and there are no Nd isotope data available that plot on the mixing line between station 30 and 5.1 (Fig. 3.11). Thus, based on Nd isotope compositions alone, the unradiogenic Nd isotope signal of station 5.1 does not mix with the unradiogenic Nd isotope composition of the western Angola Basin at station 30.

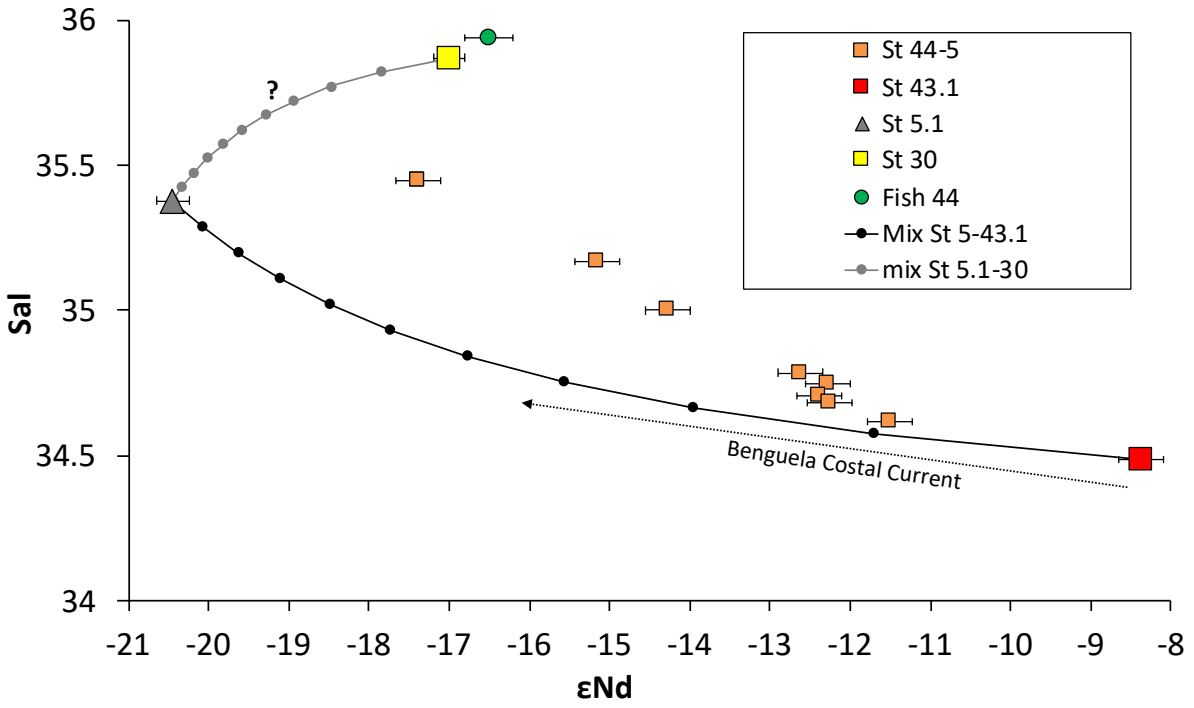

Fig. 3.11: Potential mixing relationships between surface waters of stations 43.1, 5.1 and station 30 from the study of Rahlf et al. (2020).

However, surface water REE patterns normalized to BATS 15 m (van de Flierdt et al., 2012), along a section perpendicular to the coast formed by stations 5.1 and 30 (Rahlf et al., 2020), as well as those of stations 13, 15, 17 and 18 (Zheng et al, 2016) show LREE enriched patterns with a positive Ce anomaly near the coast (stations 5.1, 18, 17) and become flatter with slightly negative Ce anomalies offshore (stations 15, 13, 30) (Fig. 3.12a). The coastal patterns are typical for the reduction of Fe-Mn oxides (Bayon et al., 2004, Freslon et al., 2014), while the patterns offshore reflect the lateral transport of dissolved REEs originating from the coast. This is supported by a mixing line of Nd (pmol/kg) vs. HREE/LREE (PAAS norm), for which stations 5.1 and 30 represent the endmember compositions (Fig. 3.12b). Stations 18-13 plot on or near the mixing line reflecting nearly conservative mixing of coastal surface waters with surface waters of the western Angola Basin. These coastal surface waters are likely transported westward by a combination of wind stress and surface water eddies along the ABF (Shannon et al., 1987, Meeuwis and Lutjeharm, 1990).

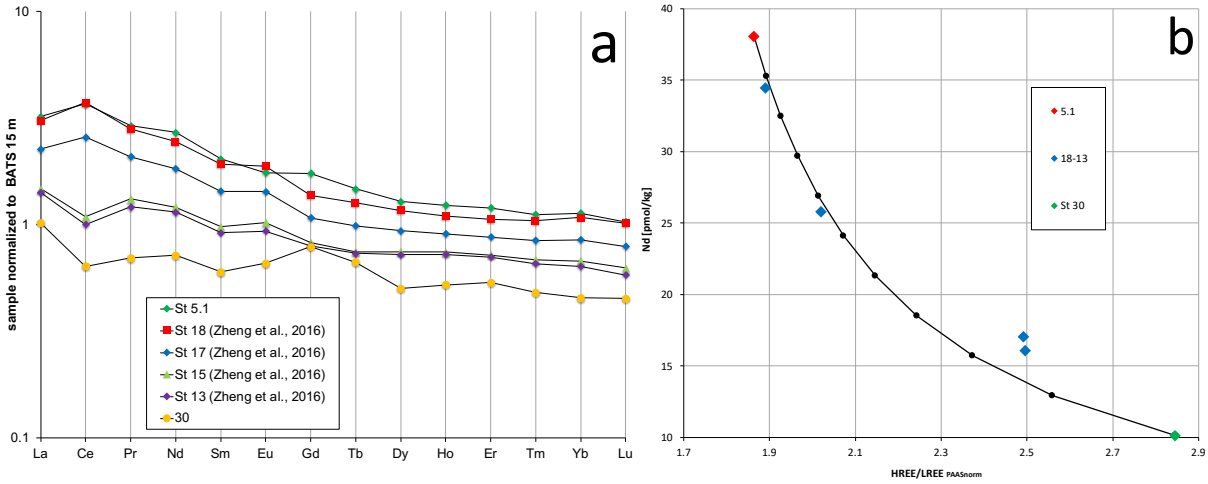

Fig. 3.12: a) Comparison of BATS 15 normalized REE patterns of station 5.1 and stations from the CoFeMg section (Zheng et al, 2016), b) mixing relationship between the coastal station 5.1 and station 30 (Rahlf et al. 2020) of the western Angola Basin.

5. Conclusions

Dissolved REEs and Nd isotope compositions of filtered seawater samples collected along the coast of Angola and Namibia between 7°S and 29°S reveal unradiogenic surface water ε_{Nd} signatures as low as -21 accompanied by elevated REE concentrations off the Angolan coast. Nd concentrations of surface waters reach 40 pmol/kg between 10 and 18 °S. The source is most likely the reduction of Fe-Mn-oxides of coastal sediments in the oxygen minimum zone off the Angolan coast. Decreasing REE concentrations in intermediate and deep waters below suggest removal via scavenging due to high vertical particle fluxes. ε_{Nd} signatures near -15 in intermediate and deep waters do not reflect AAIW and NADW compositions and indicate release of unradiogenic Nd from sinking particles.

In contrast, surface waters off the Namibian coast are influenced by the Benguela upwelling and have more radiogenic Nd isotope compositions and lower REE concentrations, suggesting terrestrial input from the Namib and Kalahari deserts or the Orange River. Alternatively, strong coastal currents related to the upwelling, likely in combination with the interaction of internal waves enhance the resuspension of shelf sediments, which are partially decomposed in the oxygen minimum zone between 100 and 200 m water depth. This process can explain similar ε_{Nd} signatures of shelf sediments off the Namibian coast and those of the surface waters above.

Mixing calculations based on REEs reveal that the Nd isotope composition of surface waters of the western Angola Basin are influenced by unradiogenic inputs originating from the west African coast. These waters are probably transported westward by a combination of wind stress and surface waters eddies, forming at the ABF.

Acknowledgments

We thank Jutta Heinze, Ana Kolevica and Christopher Siebert for their support in the laboratory. We also thank the crew and captain of RV Meteor for their support during cruise M121.

4. SUMMARY, CONCLUSIONS AND OUTLOOK

4.1. Summary and Conclusions

Chapter I presents and discusses the first full water column Nd isotope and concentration data across the western Angola Basin and along the northern Cape Basin sampled during GEOTRACES cruise GA08. Compared to the well ventilated southwestern Atlantic basin overall less radiogenic εNd signatures reaching −17 in the uppermost 200 m of the restricted Angola Basin are found as a consequence of the admixture of an unradiogenic coastal plume, originating from the dissolution of Fe-Mn coatings of particles in an oxygen minimum zone. Highly unradiogenic Nd isotope signatures of -17.6 in the upper water column of the northern Cape Basin, in contrast, originate from advection of shallow waters originating from the Mozambique Channel via the Agulhas and Benguela currents into the southeastern Atlantic Ocean. The Nd isotope compositions of the deep water masses in both basins primarily reflect conservative water mass mixing. However, Nd isotope signatures in the central Angola Basin are significantly overprinted by terrestrial inputs originating from the coast. Bottom waters accumulate unradiogenic Nd released from sinking particles. At

the deep eastern margin of the Cape Basin Nd is removed from ambient seawater without significantly altering the Nd isotope compositions as a consequence of resuspension of shelf and slope sediments. Bottom waters of the Cape Basin show excess Nd concentrations, originating from resuspended bottom sediments and/or dissolution of dust. However, the isotopic composition of the bottom waters are not changed significantly due to similar εNd values of particles and bottom waters, but non-conservative Nd isotopic effects may have been significant under past glacial boundary conditions when bottom waters were more radiogenic.

Chapter II presents the first detailed study about element fluxes and transport mechanisms across and beyond the Congo River plume and their impacts on the marine distribution and cycling of major and trace elements by investigation of combined dissolved Nd and Hf isotopes and rare earth element (REE) concentrations. The Congo River freshwater carries extraordinarily high Nd and Hf concentrations of up to 4000 pmol/kg and 54 pmol/kg, and is characterized by ε_{Nd} and ε_{Hf} values that range between -15.6 and -16.4 and between 0.35 and -1.4, respectively. At salinities between 0 and 23 a pronounced decrease in REE concentrations and HREE enrichment relative to LREE indicate rapid scavenging and removal of LREEs and MREEs by coagulation processes, forming typical seawater REE patterns. Above salinities of 23 Nd and Hf concentrations and isotopic signatures are mixed conservatively for up to 1000 km northwest of the river mouth within the Benguela Current and the South Equatorial Current. However, particle-seawater interactions likely occur in the low salinity zone and result in Nd release from or exchange with Congo-derived particulate phases. This is indicated by elevated Congo-shelf-zone REE and Hf fluxes calculated based on radium isotope compositions. In contrast, the Nd and Hf isotopic compositions do not provide evidence for any release from suspended riverine particles due to identical dissolved and particulate isotope compositions of the Congo River. Subsurface waters between 50 and 100 m depth are marked by riverine REE removal, whereas intermediate and deep waters below the plume and in the open northern Angola Basin are strongly affected by inputs from the Congo River. REE concentrations of bottom waters of the offshore section indicate limited REE release from seafloor sediments similar to observations from the central Angola Basin and the Guinea Basin further north.

Chapter III presents the first study of dissolved REE concentrations and neodymium isotope distributions of the full water column along the coast of Namibia and Angola between 7 and 29°S. Surface waters of the Angolan coast near the Angola Benguela Front (ABF) are characterized by unradiogenic ε_{Nd} signatures of up to -21 and elevated REE concentrations (~ 35 pmol/kg for Nd), which are most likely controlled by dissolution of Fe-Mn oxide coatings of coastal sediment particles in the prevailing oxygen minimum zone. Decreasing REE concentrations in intermediate and deep waters suggest removal via scavenging due to high vertical particle fluxes, while ε_{Nd} signatures of about -15 indicate release of unradiogenic Nd. In contrast, surface waters off the Namibian coast are more radiogenic (ε_{Nd} ~ -12) and have lower REE concentrations (~ 12 pmol/kg for Nd), suggesting minor terrestrial input from the Namib and Kalahari or the Orange River. Waters off the Namibian coast are strongly influenced by upwelling and resuspension of particles by coastal currents related to upwelling or by internal waves from shelf sediments into the oxygen minimum zone, which then release their isotope signature into the surface waters. This is supported by similar ε_{Nd} signatures of shelf sediments and surface waters. Mixing calculations based on REEs reveal that the unradiogenic Nd isotope signature of surface waters of the open western Angola Basin is not solely controlled by unradiogenic waters from the Agulhas Current (AC) but also by the unradiogenic coastal waters near the ABF, which are transported westward by the prevailing winds and as part of eddies.

Overall, Nd isotopes are a reliable quasi-conservative tracer of present and past deep water mass mixing in the southern and northern Angola Basin and in the Cape Basin and can also be used together with Hf isotope compositions as conservative tracers for surface water mass advection and mixing of the Congo River plume at salinities above 23. These isotope systems and the REE/Hf concentrations also show that the Congo is a major source of trace elements to the South Atlantic Ocean and affects the distribution of elements in the entire water column of the deep northeastern Angola Basin by lateral freshwater advection, vertical exchange processes, and limited release from particles. The Congo-shelf-zone flux exceeds that of the Amazon River almost by a factor of 2 suggesting that the Congo River is more important for the global Nd budget than previously assumed. The offshore export of Congo-derived Nd along the 3 °S transect amounts to 150 Mg/year, which corresponds to ~40 % of the Congo-shelf-

zone flux and indicates that the Congo plume influences large areas of the open South Atlantic Ocean but only accounts for a small part of the missing global Nd flux of 5,500-11,000 Mg/year. Release of non-conservative Nd from the Angolan coast change the isotope composition of surface and bottom waters of the Angola Basin, as well as the entire water column of the central Angola Basin. Surface water Nd isotope compositions of the Cape Basin are affected by admixture of waters of the Agulhas Current. The Nd isotope compositions of the Cape basin deep and bottom waters are only weakly modified by non-conservative Nd addition today, which may have been more significant in the past such as during glacial maxima when the waters were more radiogenic. The Benguela upwelling area is an important area of high dissolved fluxes of Nd where the isotope composition and REE concentration of the entire water column of the Namibian coast affected.

4.2. Outlook

To fully understand the contributions to dissolved REE concentrations and isotope compositions to the southeastern Atlantic Ocean it is necessary to determine and calculate fluxes from all potential sources contributing to the total budget. These sources include freshwater discharge from all rivers along the coasts of Angola and Namibia and release from particulate phases such as aeolian dust as well as release from sedimentary sources of the river fans, shelves, slopes, continental margins and the deep Angola and Cape basins. These fluxes can be quantified via Ra isotopes in analogy to the Congo River shelf and offshore fluxes in chapter II and should be subject of future investigations. Fluxes such as from the Congo River should also be determined for all seasons during periods of low, mid and high discharge.

Further on, boundary exchange processes such as seawater-particle interactions near the land-ocean interfaces have to be investigated in more detail in order to better resolve the processes of particle dissolution, adsorbtion, and reversible scavenging along the coastal areas, especially in the Benguela upwelling zone. For this purpose, particulate phases such as Fe-Mn coatings of shelf sediments, sinking particles in the

water column and colloids in river estuaries need to be analyzed for their radiogenic isotope compositions and REE concentrations.

The investigation of Hf isotope compositions and concentrations should be completed for the remaining seawater profiles, in particular along the coastal sections to trace continental weathering inputs. Samples from the low salinity zone of the Congo River should also be collected to investigate estuarine removal and release of Hf and REEs.

Overall, this thesis demonstrates that Nd and Hf isotope compositions are not only suitable traces of deep water mass circulation in the open ocean, where current speeds are high, but also suitable for oceanic basins with a more sluggish circulation such as the Angola Basin. Additionally, Nd and Hf isotopes are suitable tracers of river plumes that they were found to mix conservatively with surface waters at salinities above 23. This has implications on the application of these tracers in other oceanic areas near continental margins. However, isotope signatures and REE concentrations of water masses close to continental margins which are significantly influenced by terrestrial inputs from dust, rivers or interactions with shelf and slope sediments and thus do not display conservative mixing can instead be used as provenance tracers. A potential area to investigate the application of Nd and Hf isotopes as water mass and provenance tracer is the Mozambique Channel between southeast Africa and Madagascar. There it is of particular interest to investigate a) how the radiogenic isotope signature of the Northeast Madagascar Current that feeds into the southward flowing Agulhas Current is changed by the sedimentary river inputs, dust inputs and resuspension of sediments by eddies and b) if the isotope signature of the Agulhas Current is further altered by potential continental inputs from the South African coast. Additionally, Nd and Hf isotopes can be applied to trace the plumes of the major rivers such as the Zambezi and Limpopo and how REEs are distributed into the Mozambique Channel. Another region that is barely investigated for water mass circulation with radiogenic isotopes is the Southern Indian Ocean. There it is of particular interest, to trace the advection and mixing of major water masses as well as to investigate the influence of continental inputs such as dust from the Australian continent on the isotope composition and trace element distribution of the South Indian Ocean, especially of its surface waters.

DANKSAGUNG

Mein erster und größter Dank gilt meinem Betreuer Martin Frank. Deine Bürotür ist immer offen und genauso bist du immer offen für Fragen und Nöte. Du nimmst dir Zeit für Deine Doktoranden und versuchst ihnen durch Anregungen und Tipps weiterzuhelfen. Ich hätte mir keinen besseren Betreuer wünschen können. Mach weiter so!

Liebe Jutta, ohne Deine Hilfe hätte ich nie so viele Proben sammeln können und ohne Dich hätte die Zeit als Doktorand nicht so viel Spaß gemacht. Du bist immer da, wenn man Dich braucht und wenn man dringend einen Keks oder einen Kaffee benötigt. Du bist unersetzlich im Labor und hast alles im Blick.

Lieber Ed, auch ohne Dich hätte ich meine vielen Daten nicht bekommen. Du bist Ansprechpartner, wenn es um die seaFAST geht und auch Deine Tür ist immer offen, wenn man Hilfe braucht.

Lieber Chris, ich danke Dir ganz herzlich für die Einweisung an der NU und dass Du dich immer um sie gekümmert hast, wenn es technische Probleme gab. Ohne Dich hätte ich nie so viel über das Gerät gelernt und hätte es nicht so beherrschen können.

Lieber Marcus, vielen Dank für Deine Geduld und Zeit, die Du für mich an der Neptune aufgebracht hast! Die super Qualität der Ergebnisse ist Dir geschuldet, denn Du hast das nötige Händchen und den Ehrgeiz das Optimum aus der Maschine herauszuholen.

Lieber Georgi, ich danke Dir von ganzem Herzen für die vielen Gespräche und Diskussionen der Daten die wir hatten.

Ich danke außerdem allen, Die mich unterstützt haben und mit denen ich meine Zeit als Doktorand genossen habe: Moritz, Kirsten, Sarina, Lara, Stefan, David, Lisa, Katrina, Jaqui, Sebastian S., Sebastian, F., Steffen, Sasha, Kristin, Janett, Veit, Daniel, Zeynep.

Ich danke meiner Familie, dass Sie mich in meiner Zeit begleitet und unterstützt hat. Vielen Dank Elke und Hartwig, Manuela und Hans-Ludwig, Frauke und Sebastian!

Lieber Tim, ich danke dir für Deine unendliche Geduld, Dein Lächeln und Deine unfassbare Entspanntheit! Du hast mir die Zeit versüßt und mich oft an die wichtigen und essentiellen Dinge im Leben erinnert!

Liebe Meike, ich danke Dir von ganzem Herzen für Deine Unterstützung und Deine Geduld! Ohne Dich wäre ich nicht dahin gekommen, wo ich jetzt bin. Du bist immer da und auf Dich kann ich mich immer verlassen!

REFERENCES

Abbott, A. N., Haley, B. A., McManus, J., & Reimers, C. E., 2015. The sedimentary flux of dissolved rare earth elements to the ocean. Geochimica et Cosmochimica Acta, 154, 186–200. https://doi.org/10.1016/j.gca.2015.01.010.

Albarède, F., Simonetti, A., Vervoort, J. D., Blichert-Toft, J., & Abouchami, W., 1998. A Hf-Nd isotopic correlation in ferromanganese nodules. Geophysical Research Letters, 25(20), 3895–3898. https://doi.org/10.1029/1998GL900008.

Allègre, C. J., Dupré, B., Négrel, P., & Gaillardet, J., 1996. Sr-Nd-Pb isotope systematics in Amazon and Congo River systems: Constraints about erosion processes. Chemical Geology 131, 93–112.

Alley, R.B., 2007. Wally was right: Predictive ability of the North Atlantic "conveyor belt" hypothesis for abrupt climate change. Annual Reviews of Earth and Planetary Sciences, 35, 241-272.

Amakawa, H., Yu, T.-L., Tazoe, H., Obata, H., Gamo, T., Sano, Y., Shen, C.-C., Suzuki, K., 2019. Neodymium concentration and isotopic composition distributions in the southwestern Indian Ocean and the Indian sector of the Southern Ocean. Chemical Geology. doi:10.1016/j.chemgeo.2019.01.007.

Arsouze, T., Dutay, J.-C., Lacan, F., Jeandel, C., 2009. Reconstructing the Nd oceanic cycle using a coupled dynamical – biogeochemical model, Biogeosciences, 6, 2829–2846, https://doi.org/10.5194/bg-6-2829-2009.

Bau, M. and Koschinsky, A., 2006. Hafnium and neodymium isotopes in seawater and in ferromanganese crusts: The "element perspective". Earth and Planetary Science Letters 241, 952–961.

Bayon, G., Birot, D., Ruffine, L., Caprais, J. C., Ponzevera, E., Bollinger, C., Donval, J.-P., Charlou, J.-L., Voisset, M., Grimaud, S., 2011. Evidence for intense REE scavenging at cold seeps from the Niger Delta margin. Earth and Planetary Science Letters 312, 443-452.

Bayon, G., Burton, K. W., Soulet, G., Vigier, N., Dennielou, B., Etoubleau, J., Nesbitt, R. W., 2009. Hf and Nd isotopes in marine sediments: Constraints on global silicate weathering. Earth Planet. Sci. Lett., 277(3–4), 318–326. http://doi.org/10.1016/j.epsl.2008.10.028.

Bayon, G., German, C. R., Burton, K. W., Nesbitt, R. W., and Rogers, N., 2004. Sedimentary Fe – Mn oxyhydroxides as paleoceanographic archives and the role of aeolian flux in regulating oceanic dissolved REE, Earth Planet. Sci. Lett. 224, 477–492. http://doi.org/10.1016/j.epsl.2004.05.033.

Bayon, G., Toucanne, S., Skonieczny, C., André, L., Bermell, S., Cheron, S., Dennielou, B., Etoubleau, J., Freslon, N., Gauchery, T., Germain, Y., Jorry, S., Ménot, G., Monin, L., Ponzevera, E., Rouget, M. L., Tachikawa, K., Barrat, J. A., 2015. Rare earth elements and neodymium isotopes in world river sediments revisited. Geochimica et Cosmochimica Acta 170, 17-38.

Bayon, G., Vigier, N., Burton, K.W., Brenot ,A., Carignan, J., Etoubleau, J. and Chu, N.C., 2006. The control of weathering processes on riverine and seawater hafnium isotope ratios. Geology 34, 433–436.

Beal, L. M., & Elipot, S., 2016. Broadening not strengthening of the Agulhas Current since the early 1990s. Nature, 540(7634), 570–573. doi:10.1038/nature19853.

Böhm, E., Lippold, J., Gutjahr, M., Frank, M., Blaser, P., Antz, B., Fohlmeister, J., Frank, N., Andersen, M., and Deininger, M., 2015. Strong and deep Atlantic Meridional Overturning Circulation during the last glacial cycle. Nature 517, 73-76.

Bouvier, A., Vervoort, J. D., & Patchett, P. J., 2008. The Lu-Hf and Sm-Nd isotopic composition of CHUR: Constraints from unequilibrated chondrites and implications for the bulk composition of terrestrial planets. Earth and Planetary Science Letters 273, 48-57.

Boyle, E., Edmond, J. and Sholkovitz. R., 1977. Mechanisms of iron removal in estuaries. Geochimica et Cosmochimica Acta 41, 1313-1324.

Broecker, W. S., & Takahashi, T., 1981. Hydrography of the central Atlantic—IV. Intermediate waters of antarctic origin. Deep Sea Research Part A. Oceanographic Research Papers, 28(3), 177–193. doi:10.1016/0198-0149(81)90061-3.

Broecker, WS, Peteet, DM, Rind, D. 1985. Does the ocean-atmosphere system havemore than one stable mode of operation? Nature315:21–26.

Byrne, R.H. and Sholkovitz, E.R., 1996. Chapter 158 Marine chemistry and geochemistry of the lanthanides. 23, 497-593. http://dx.doi.org/10.1016/s0168-1273(96)23009-0.

Cacchione, D.A., Pratson, L.F., Ogston, A.S., 2002. The shaping of continental slopes by internal tides. Science 296, 724. http://dx.doi.org/10.1126/science.1069803.

Calvert, S. E., & Price, N. B., 1971. Upwelling and nutrient regeneration in the Benguela Current, October, 1968. Deep-Sea Research and Oceanographic Abstracts, 18(5), 505–523. https://doi.org/10.1016/0011-7471(71)90074-X.

Chao, Y., Farrara, J. D., Schumann, G., Andreadis, K. M., & Moller, D., 2015. Sea surface salinity variability in response to the Congo River discharge. Continental Shelf Research 99, 35-45.

Chester, R., Elderfield, H., Griffin, J. J., Johnson, L. R., and Padgham, R. C., 1972. Eolian dust along the eastern margins of the Atlantic Ocean. Marine Geology, 13(2), 91–105. http://doi.org/10.1016/0025-3227(72)90048-5.

Chu, N. C., Taylor, R. N., Chavagnac, V., Nesbitt, R. W., Boella, R. M., Milton, J. A., German, C. R., Bayon, G. and Burton, K., 2002. Hf isotope ratio analysis using multi-collector inductively coupled plasma mass spectrometry: an evaluation of isobaric interference corrections. Journal of Analytical Atomic Spectrometry 17, 1567–1574.

Connary, S. D. and Ewing, M., 1974. Penetration of Antarctic Bottom Water from the Cape Basin into the Angola Basin. Journal of Geophysical Research. 79. 463-469.

Coynel, A., Seyler, P., Etcheber, H., Meybeck, M., & Orange, D., 2005. Spatial and seasonal dynamics of total suspended sediment and organic carbon species in the Congo River. Global Biogeochemical Cycles, 19(4), 1–17. https://doi.org/10.1029/2004GB002335.

Curry, W., and Oppo, D., 2005. Glacial water mass geometry and the distribution of delta C-13 of Sigma CO_2 in the western Atlantic Ocean. Paleoceanography 20, PA1017, 10.1029/2004PA001021.

D'Addezio, J. M., & Subrahmanyam, B., 2016. Sea surface salinity variability in the Agulhas Current region inferred from SMOS and Aquarius. Remote Sensing of Environment, 180, 440–452. https://doi.org/10.1016/j.rse.2016.02.006.

Dausmann, V., Frank., M., Gutjahr, M., and Rickli, J., 2017. Glacial reduction of AMOC strength and long term transition in weathering inputs into the Southern Ocean since the Mid Miocene: Evidence from radiogenic Nd and Hf isotopes. Paleoceanography 32, 265-283.

David, K., Frank, M., O'Nions, R.K., Belshaw, N.S., Arden, J.W., 2001. The Hf isotope composition of global seawater and the evolution of Hf isotopes in the deep Pacific Ocean from Fe-Mn crusts. Chemical Geology 178, 23-42.

de Moor, F.C., Barber-James, H.M., Harrison, A.D. & Lugo-Ortiz, C.R., 2000. The macroinvertebrates of the Cunene River from the Ruacana Falls to the river mouth and assessment of the conservation status of the river, African. Journal of Aquatic Science, 25:1, 105-122, DOI: 10.2989/160859100780177857.

Denamiel, C., Budgell, W. P., & Toumi, R., 2013. The congo river plume: Impact of the forcing on the far-field and near-field dynamics. Journal of Geophysical Research: Oceans, 118(2), 964–989. https://doi.org/10.1002/jgrc.20062.

Drüppel, K., Littmann, S., Romer, R. L., & Okrusch, M., 2007. Petrology and isotope geochemistry of the Mesoproterozoic anorthosite and related rocks of the Kunene Intrusive Complex, NW Namibia. Precambrian Research, 156(1–2), 1–31. https://doi.org/10.1016/j.precamres.2007.02.005.

Dupré, B., Gaillardet, J., Rousseau, D., Allègre, J.,1996. Major and trace elements of river-borne material: The Congo Basin. Geochimica et Cosmochimica Acta 60, 1301–1321.

Durgadoo, J.V., Rühs, S., Biastoch, A., Böning, C.W.B., 2017. Indian Ocean sources of Agulhas leakage. J. Geophys. Res., Oceans122, 3481-3499. https://doi .org /10 .1002 /2016JC012676.

Eisma, D., & Kalf, J., 1984. Dispersal of Zaire river suspended matter in the estuary and the Angola Basin. Netherlands Journal of Sea Research, 17(2-4), 385–411. doi:10.1016/0077-7579(84)90057-7.

Elderfield, H. and Greaves, M.J., 1982. The rare earth elements in seawater. Nature 296, 214-219. http://dx.doi.org/10.1038/296214a0.

Elderfield, H., Upstill-Goddard, R., & Sholkovitz, E. R., 1990. The rare earth elements in rivers, estuaries, and coastal seas and their significance to the composition of ocean waters. Geochimica et Cosmochimica Acta, 54(4), 971–991. https://doi.org/10.1016/0016-7037(90)90432-K.

Erdem, Z., Schönfeld, J., Glock, N., Dengler, M., Mosch, T., Sommer, S., Elger, J., Eisenhauer, A., 2016. Peruvian sediments as recorders of an evolving hiatus for the last 22 thousand years. Quaternary Science Reviews, 137, 1–14. doi:10.1016/j.quascirev.2016.01.029.

Filippova, A., M. Frank, M. Kienast, J. Rickli, E. Hathorne, I. M. Yashayaev, and P. Pahnke, 2017. Water mass circulation and weathering inputs in the Labrador Sea based on coupled Hf–Nd isotope compositions and rare earth element distributions, Geochim. Cosmochim. Acta, 199, 164–184, doi:10.1016/j.gca.2016.11.024.

Firdaus, M.L., Norisuye, K., Nakagawa, Y., Nakatsuka, S., Sohrin, Y., 2008. Dissolved and labile particulate Zr, Hf, Nb, Ta, Mo and W in the western North Pacific Ocean. Journal of Oceanography 64, 247-257.

Frank, M., 2002. Radiogenic isotopes: Tracers of past ocean circulation and erosional input. Reviews of Geophysics, 40(1), 1001. http://doi.org/10.1029/2000RG000094.

Franzese, A. M., Hemming, S. R., Goldstein, S. L., & Anderson, R. F., 2006. Reduced Agulhas Leakage during the Last Glacial Maximum inferred from an integrated provenance and flux study. Earth and Planetary Science Letters, 250(1–2), 72–88. https://doi.org/10.1016/j.epsl.2006.07.002.

Freslon, N., Bayon, G., Toucanne, S., Bermell, S., Bollinger, C., Chéron, S., Eatoubleau, J., Germain, Y., Khripounoff, A., Ponzevera, E., Rouget, M. L., 2014. Rare earth elements and neodymium isotopes in sedimentary organic matter. Geochim. Cosmochim. Acta. https://doi.org/10.1016/j.gca.2014.05.016.

Garcia-Solsona, E., Jeandel, C., Labatut, M., Lacan, F., Vance, D. and Chavagnac, V., Pradoux, C., 2014. Rare earth elements and Nd isotopes tracing water mass mixing and particle–seawater interactions in the SE Atlantic. Geochim. Cosmochim. Acta 125, 351–372.

Gleißner, P., Drüppel, K., & Romer, R. L., 2011. The role of crustal contamination in massif-type anorthosites, new evidence from Sr-Nd-Pb isotopic composition of the Kunene Intrusive Complex, NW Namibia. Precambrian Research, 185(1–2), 18–36. https://doi.org/10.1016/j.precamres.2010.11.004.

Godfrey, L. V., M. P. Field, and R. M. Sherrell, 2008. Estuarine distributions of Zr, Hf, and Ag in the Hudson River and the implications for their continental and anthropogenic sources to seawater, Geochem. Geophys. Geosyst., 9, Q12007, doi:10.1029/2008GC002123.

Godfrey, L.V., Zimmermann, B., Lee, D.C., King, R.L., Vervoort, J.D., Sherrell, R.M., Halliday, A.N., 2009. Hafnium and neodymium isotope variations in NE Atlantic seawater. Geochemistry Geophysics Geosystems 10.

Goldstein, S. J. and Jacobsen, S. B., 1987. The Nd and Sr isotopic systematics of river-water dissolved material: Implications for the sources of Nd and Sr in seawater. Chemical Geology 66, 245–272.

Goldstein, S. L., and Hemming, S. R., 2003. Long-lived Isotopic Tracers in Oceanography, Paleoceanography, and Ice-sheet Dynamics. Treatise on Geochemistry: Second Edition, 8, 453–483. http://doi.org/10.1016/B978-0-08-095975-7.00617-3.

Goldstein, S. L., O'Nions, R. K., Hamilton, P. J., O'Nions, R. K., and Hamilton, P. J., 1984. A Sm-Nd isotopic study of atmospheric dusts and particulates from major river systems. Earth Planet. Sci. Lett., 70, 221–236. http://doi.org/10.1016/0012-821X(84)90007-4.

Goldstein, S., J. and Jacobsen, S., B., 1988. Nd and Sr isotope systematics of river water suspended material - Implications for crustal evolution. Earth and Planetary Science Letters 87, 249-265.

Goslin, J., & Sibuet, J. C., 1975. Geophysical study of the easternmost Walvis Ridge, South Atlantic: Deep structure. Bulletin of the Geological Society of America, 86(12), 1713–1724. https://doi.org/10.1130/0016-7606(1975)86<1713:GSOTEW>2.0.CO;2.

Grasse, P., Bosse, L., Hathorne, E. C., Böning, P., Pahnke, K., & Frank, M., 2017. Short-term variability of dissolved rare earth elements and neodymium isotopes in the entire water column of the Panama Basin. Earth and Planetary Science Letters, 475, 242–253. https://doi.org/10.1016/j.epsl.2017.07.022.

Grasse, P., Stichel, T., Stumpf, R., Stramma, L. and Frank, M., 2012. The distribution of neodymium isotopes and concentrations in the Eastern Equatorial Pacific: water mass advection versus particle exchange. Earth Planet. Sci. Lett. 353–354, 198–207.

Grenier, M., Jeandel, C., Lacan, F., Vance, D., Venchiarutti, C., Cros, A., Cravatte, S., 2013. From the subtropics to the central equatorial Pacific Ocean: neodymium isotopic composition and rare earth element concentration variations. J. Geo-phys. Res.118, 592–618. http://dx.doi.org/10.1029/2012JC008239.

Grousset, F. E., Biscaye, P. E., Zindler, A., Prospero, J., and Chester, R., 1988. Neodymium Isotopes As Tracers in Marine-Sediments and Aerosols - North-Atlantic. Earth Planet. Sci. Lett., 87(4), 367–378. http://doi.org/10.1016/0012-821x(88)90001-5.

Grousset, F. E., Rognon, P., Coudé-Gaussen, G., & Pédemay, P., 1992. Origins of peri-Saharan dust deposits traced by their Nd and Sr isotopic composition. Palaeogeography, Palaeoclimatology, Palaeoecology, 93(3–4), 203–212. https://doi.org/10.1016/0031-0182(92)90097-O.

Haley, B.A., Klinkhammer, G.P., 2003. Complete separation of rare earth elements from small volume seawater samples by automated ion chromatography: method development and application to benthic flux. Mar. Chem. 82 (3–4), 197–220.

Hathorne, E. C., Haley, B., Stichel, T., Grasse, P., Zieringer, M., & Frank, M., 2012. Online preconcentration ICP-MS analysis of rare earth elements in seawater. Geochemistry, Geophysics, Geosystems 13, Q01020, doi.org/10.1029/2011GC003907.

Hofmann, A.W.,1988. Chemical differentiation of the Earth: the relationship between mantle, continental crust, and oceanic crust. Earth and Planetary Science Letters 90, 297-314. http://dx.doi.org/10.1016/0012-821x(88)90132-x.

Hopkins, J., Lucas, M., Dufau, C., Sutton, M., Stum, J., Lauret, O., & Channelliere, C., 2013. Detection and variability of the Congo River plume from satellite derived sea surface temperature, salinity, ocean colour and sea level. Remote Sensing of Environment, 139, 365–385. https://doi.org/10.1016/j.rse.2013.08.015.

Jacobsen, S.B. and Wasserburg, G.J., 1980. Sm-Nd Isotopic Evolution of Chondrites. EarthPlan. Sci. Lett. 50, 139-155. http://dx.doi.org/10.1016/0012-821x(80)90125-9.

Jeandel, C., 1993. Concentration and Isotopic Composition of Nd in the South-Atlantic Ocean. Earth Planet. Sci. Lett., 117(3–4), 581–591. http://doi.org/10.1016/0012-821x(93)90104-h.

Jeandel, C., 2016. Overview of the mechanisms that could explain the "Boundary Exchange" at the land-ocean contact. Philosophical Transactions of the Royal Society A: Mathematical, Physical and Engineering Sciences, 374(2081). https://doi.org/10.1098/rsta.2015.0287.

Jeandel, C., Arsouze, T., Lacan, F., Téchiné, P. and Dutay, J.-C., 2007. Isotopic Nd compositions and concentrations of the lithogenic inputs into the ocean: a compilation, with an emphasis on the margins. Chem. Geol. 239, 156–164.

Jeandel, C., Bishop, J. K., & Zindler, A., 1995. Exchange of neodymium and its isotopes between seawater and small and large particles in the Sargasso Sea. Geochimica et Cosmochimica Acta, 59(3), 535–547. https://doi.org/10.1016/0016-7037(94)00367-U.

Jonkers, L., Zahn, R., Thomas, A., Henderson, G.M, Abouchami, W., François, R., Masque, P., Hall, I.R., Bickert, T., 2015. Deep circulation changes in the central South Atlantic during the past 145 kyrs reflected in a combined $^{231}Pa/^{230}Th$, neodymium isotope and benthic δC13 record. Earth Planet. Sci. Lett., 419, 14–21. https://doi.org/10.1016/j.epsl.2015.03.004.

Karyampudi, V. M., Palm, S. P., Reagen, J. A., Fang, H., Grant, W. B., Hoff, R. M., Melfi, S. H., 1999. Validation of the Saharan Dust Plume Conceptual Model Using Lidar, Meteosat, and ECMWF Data. Bulletin of the American Meteorological Society, 80(6), 1045–1075. doi:10.1175/1520-0477(1999)080<1045:vots.

Klevenz, V., Vance, D., Schmidt, D. N., & Mezger, K., 2008. Neodymium isotopes in benthic foraminifera: Core-top systematics and a down-core record from the Neogene south Atlantic. Earth Planet. Sci. Lett., 265(3–4), 571–587. https://doi.org/10.1016/j.epsl.2007.10.053.

Kraft, S., Frank, M., Hathorne, E. C., & Weldeab, S., 2013. Assessment of seawater Nd isotope signatures extracted from foraminiferal shells and authigenic phases of Gulf of Guinea sediments. Geochimica et Cosmochimica Acta 121, 414-435.

Kuhlbrodt, T., Griesel, A., Montoya, M., Levermann, A., Hofmann, M., & Rahmstorf, S., 2007. On the driving processes of the Atlantic meridional overturning circulation. Reviews of Geophysics, 45(2). doi:10.1029/2004rg000166.

Lacan, F. and Jeandel, C., 2001. Tracing Papua New Guinea imprint on the central EquatorialPacific Ocean using neodymium isotopic compositions and Rare Earth Elementpatterns. Earth Planet. Sci. Lett. 186, 497-512. http://dx.doi.org/10.1016/S0012-821x(01)00263-1.

Lacan, F., and Jeandel, C., 2005b. Neodymium isotopes as a new tool for quantifying exchange fluxes at the continent-ocean interface. Earth Planet. Sci. Lett., 232(3–4), 245–257.

Lacan, F., Jeandel, C., 2005a. Acquisition of the neodymium isotopic composition of the North Atlantic Deep Water. Geochem Geophys Geosyst. 61. https://doi.org/10.1029/2005GC000956.

Lamb, K., 2014. Internal wave breaking and dissipation mechanisms on the continental slope/shelf. Annu. Rev. Fluid Mech. 231e254. http://dx.doi.org/10.1146/annurev-fluid-011212-140701.

Lambelet, M., van de Flierdt, T., Crocket, K., Rehkämper, M., Kreissig, K., Coles, B., Steinfeldt, R., 2016. Neodymium isotopic composition and concentration in the western North Atlantic Ocean: Results from the GEOTRACES GA02 section. Geochim. Cosmochim. Acta, 177, 1–29. http://doi.org/10.1016/j.gca.2015.12.019.

Laraque, A., Bricquet, J. P., Pandi, A., & Olivry, J. C., 2009. A review of material transport by the Congo River and its tributaries. Hydrological Processes, 23(22), 3216–3224. https://doi.org/10.1002/hyp.7395.

Laukert, G., Frank, M., Bauch, D., Hathorne, E. C., Gutjahr, M., Janout, M., & Hölemann, J., 2017. Transport and transformation of riverine neodymium isotope and rare earth element signatures in high latitude estuaries: A case study from the Laptev Sea. Earth and Planetary Science Letters 477, 205–217.

Loveday, B. R., Durgadoo, J. V., Reason, C. J. C., Biastoch, A., and Penven, P., 2014. Decoupling of the Agulhas Leakage from the Agulhas Current. Journal of Physical Oceanography, 44(7), 1776–1797. http://doi.org/10.1175/JPO-D-13-093.1.

Lutjeharms, J. R. E. & Meeuwis, J. M., 1987. The extent and variability of South-East Atlantic upwelling, South African Journal of Marine Science, 5:1, 51-62.

Lutjeharms, J. R. E. & Valentine, H. R., 1987. Water types and volumetric considerations of the South-East Atlantic upwelling regime, South African Journal of Marine Science, 5:1, 63-71, DOI: 10.2989/025776187784522487.

Mahowald, N. M., Baker A. R., Bergametti G., Brooks N., Duce R.A., Jickells T. D., Kubilay N., Prospero J. M. and Tegen I., 2005. Atmospheric global dust cycle and iron inputs to the ocean. Glob. Biogeochem. Cyc. 19, GB4025. doi:10.1029/2004GB002402.

McLennan, S.M., 2001. Relationships between the trace element composition of sedimentary rocks and upper continental crust. Geochemistry Geophysics Geosystems 2, http://dx.doi.org/10.1029/2000GC000109.

Meeuwis, J. M., and Lutjeharms, J. R. E., 1990. Surface thermal characteristics of the Angola-Benguela front. South African Journal of Marine Science, 9(1), 261–279. http://doi.org/10.2989/025776190784378772.

Meissner, R., 2005. Interest groups and the proposed Epupa Dam: Towards a theory of water politics. Politeia. 24.

Menzel Barraqueta, J.L., Klar, J.K., Gledhill, M., Schlosser, C., Shelley, R., Planquette, H.F., Wenzel, B., Sarthou, G., & Achterberg, E.P., 2019. Atmospheric deposition fluxes over the Atlantic Ocean: a GEOTRACES case study. Biogeosciences 16, 1525–1542.

Merschel, G., Bau, M., & Dantas, E.L., 2017a. Contrasting impact of organic and inorganic nanoparticles and colloids on the behavior of particle-reactive elements in tropical estuaries: an experimental study. Geochim. Cosmochim. Acta 197, 1–13.

Merschel, G., Bau, M., Schmidt, K., Münker, C., & Dantas, E.L., 2017b. Hafnium and neodymium isotopes and REY distribution in the truly dissolved, nanoparticulate/colloidal and suspended loads of rivers in the Amazon Basin, Brazil. Geochimica et Cosmochimica Acta 213, 383–399.

Metcalf, W. G., Heezen, B. C., & Stalcup, M. C., 1964. The sill depth of the mid-atlantic ridge in the equatorial region. Deep-Sea Research and Oceanographic Abstracts, 11(1), 1–10. https://doi.org/10.1016/0011-7471(64)91078-2.

Middleton, N. J., and Goudie, A. S., 2001. Saharan dust: sources and trajectories. Transactions of the Institute of British Geographers, 26(2), 165–181. doi:10.1111/1475-5661.00013.

Mohrholz, V., Schmidt, M. und Lutjeharms, J. R. E., 2001. The hydrography and dynamics of the Angola-Benguela Frontal Zone and environment in April 1999. South African Journal of Science 97, 199-208.

Moreno, T., Querol, X., Castillo, S., Alastuey, A., Cuevas, E., Herrmann, L., Gibbons, W., 2006. Geochemical variations in aeolian mineral particles from the Sahara-Sahel Dust Corridor. Chemosphere, 65(2), 261–270. http://doi.org/10.1016/j.chemosphere.2006.02.052.

Münker, C., Weyer, S., Scherer, E., Mezger, K., 2001. Separation of high field strength elements (Nb, Ta, Zr, Hf) and Lu from rock samples for MC-ICPMS measurements. Geochem. Geophys. Geosyst. 2. https://doi .org /10 .1029 /2001GC000183.

Naafs, B. D. A., & Pancost, R. D., 2014. Environmental conditions in the South Atlantic (Angola Basin) during the Early Cretaceous. Organic Geochemistry, 76, 184–193. https://doi.org/10.1016/j.orggeochem.2014.08.005.

Naveira Garabato, A.C., Heywood, K.J., Stevens, D.P., 2002. Modification and pathways of Southern Ocean deep waters in the Scotia Sea. Deep-Sea Research I 49, 681–705.

Noble, A. E., Lamborg, C. H., Ohnemus, D. C., Lam, P. J., Goepfert, T. J., Measures, C. I., Saito, M. A., 2012. Basin-scale inputs of cobalt, iron, and manganese from the Benguela-Angola front to the South Atlantic Ocean. Limnology and Oceanography, 57(4), 989–1010. http://doi.org/10.4319/lo.2012.57.4.0989.

Nowell, G. M., Kempton, P. D., Noble, S. R., Fitton, J. G., Saunders, A. D., Mahoney, J. J., & Taylor, R. N., 1998. High precision Hf isotope measurements of MORB and OIB by thermal ionisation mass spectrometry: insights into the depleted mantle. Chemical Geology 149, 211-233.

Nozaki, Y. and Alibo, D.S., 2003. Dissolved rare earth elements in the Southern Ocean,southwest of Australia: Unique patterns compared to the South Atlantic data. Geochemical Journal 37, 47-62. http://dx.doi.org/10.2343/geochemj.37.47.

Orsi, A., Johnson, G.C., Bullister, J.L., 1999. Circulation, mixing, and production of Antarctic Bottom Water. Progress In Oceanography. 43. 55-109. doi:10.1016/S0079-6611(99)00004-X.

Osborne, A. H., Haley, B. A., Hathorne, E. C., Plancherel, Y., & Frank, M., 2015. Rare earth element distribution in Caribbean seawater: Continental inputs versus lateral transport of distinct REE compositions in subsurface water masses. Marine Chemistry 177, 172-183.

Peron-Pinvidic, G., Manatschal, G., & Osmundsen, P. T., 2013. Structural comparison of archetypal Atlantic rifted margins: A review of observations and concepts. Marine and Petroleum Geology, 43, 21–47. https://doi.org/10.1016/j.marpetgeo.2013.02.002.

Peterson, R., Stramma, L., 1991. Upper-level circulation in the South Atlantic Ocean. Progress In Oceanography 26, 1-73.

Piepgras, D. and Wasserburg G., 1987. Rare earth element transport in the western North Atlantic inferred from Nd isotopic observations. Geochim. Cosmochim. Acta 51, 1257–1271.

Pin, C., Zalduegui, J.F.S., 1997. Sequential separation of light rare-earth elements, thorium and uranium by miniaturized extraction chromatography: application to isotopic analyses of silicate rocks. Anal. Chim. Acta 339, 79–89.

Piotrowski, A. M., Goldstein, S. L., Hemming, S. R., & Fairbanks, R. G., 2004. Intensification and variability of ocean thermohaline circulation through the last deglaciation. Earth and Planetary Science Letters, 225(1–2), 205–220. https://doi.org/10.1016/j.epsl.2004.06.002.

Piotrowski, A. M., Lee, D. C., Christensen, J. N., Burton, K. W., Halliday, A. N., Hein, J. R., & Günther, D., 2000. Changes in erosion and ocean circulation recorded in the Hf isotopic compositions of North Atlantic and Indian Ocean ferromanganese crusts. Earth and Planetary Science Letters 181, 315–325.

Piotrowski, A.M., Goldstein, S.L., Hemming, S.R., Fairbanks, R.G., 2005. Temporal relationships of carbon cycling and ocean circulation at glacial boundaries. Science 307, 1933–1938.

Pokrovsky, O.S., Shirokova, L.S., Viers, J., Gordeev, V.V., Shevchenko, V.P., Chupakov, A.V., Vorobieva, T.Y., Candaudap, F., Causserand, C., Lanzanova, A. and Zouiten, C., 2014. Fate of colloids during estuarine mixing in the Arctic. Ocean Science 10, 107-125.

Pomar, L., Morsilli, M., Hallock, P., Bádenas, B., 2012. Internal waves, an under-explored source of turbulence events in the sedimentary record. Earth Sci.Rev. 111, 56e81.http://dx.doi.org/10.1016/j.earscirev.2011.12.005.

Pourret, O., & Tuduri, J., 2017. Continental shelves as potential resource of rare earth elements. Scientific Reports 7, 5857, https://doi.org/10.1038/s41598-017-06380-z.

Rahlf, P., Hathorne, E., Laukert, G., Gutjahr, M., Weldeab, S., & Frank, M., 2020. Tracing water mass mixing and continental inputs in the southeastern Atlantic Ocean with dissolved neodymium isotopes. Earth and Planetary Science Letters, 530, 115944. https://doi.org/10.1016/j.epsl.2019.115944.

Rahlf, P., Laukert, G., Hathorne, E., Vieira, L.H., Frank, M., 2020. Dissolved neodymium and hafnium isotopes and rare earth elements in the Congo River Plume: Tracing and quantifying continental inputs into the southeast Atlantic. Submitted to Geochim. Cosmochim. Acta.

Rahmstorf, S., 2002. Ocean circulation and climate during the past 120,000 years. Nature 419, 207–214. https://doi.org/10.1038/nature01090.

Rempfer, J., Stocker, T. F., Joos, F., Dutay, J. C., and Siddall, M., 2011. Modelling Nd-isotopes with a coarse resolution ocean circulation model: Sensitivities to model parameters and source/sink distributions. Geochim. Cosmochim. Acta, 75(20), 5927–5950. http://doi.org/10.1016/j.gca.2011.07.044.

Rhein, M., L. Stramma, and Send, U., 1995. The Atlantic Deep Western Boundary Current: Water masses and transports near the equator, J. Geophys. Res., 100, 2441-2457.

Rickli, J., 2009. The hafnium and neodymium isotopic composition of seawater and rivers. Doctoral thesis, Swiss Federal Institute Of Technology Zurich. https://doi.org/10.3929/ethz-a-005772464.

Rickli, J., Frank, M., and Halliday, A. N., 2009. The hafnium-neodymium isotopic composition of Atlantic seawater. Earth Planet. Sci. Lett., 280(1–4), 118–127. http://doi.org/10.1016/j.epsl.2009.01.026.

Rickli, J., Frank, M., Baker, A. R., Aciego, S., de Souza, G., Georg, R. B., and Halliday, A. N., 2010. Hafnium and neodymium isotopes in surface waters of the eastern Atlantic Ocean: Implications for sources and inputs of trace metals to the ocean. Geochim. Cosmochim. Acta, 74(2), 540–557. http://doi.org/10.1016/j.gca.2009.10.006.

Roman, R. and Lutjeharms, J. R. E., 2010. Antarctic intermediate water at the Agulhas Current retroflection region. Journal of Marine Systems, 81(4), 273–285. doi:10.1016/j.jmarsys.2010.01.003.

Rousseau, T. C. C., Sonke, J. E., Chmeleff, J., Van Beek, P., Souhaut, M., Boaventura, G., Seyler, P., Jeandel, C., 2015. Rapid neodymium release to marine waters from lithogenic sediments in the Amazon estuary. Nature Communications 6, 7592, https://doi.org/10.1038/ncomms8592.

Sætre, R., & Da Silva, A. J., 1984. The circulation of the Mozambique channel. Deep-Sea Res., Vol. 31, No. 5, 485-508. https://doi.org/10.1016/0198-0149(84)90098-0.

Sahoo, Y. V., Nakai, S., & Ali, A., 2006. Modified ion exchange separation for tungsten isotopic measurements from kimberlite samples using multi-collector inductively coupled plasma mass spectrometry. Analyst 131, 434-439.

Savoye, B., Babonneau, N., Dennielou, B., & Bez, M., 2009. Geological overview of the Angola-Congo margin, the Congo deep-sea fan and its submarine valleys. Deep-Sea Research Part II: Topical Studies in Oceanography 56, 2169-2182.

Schlitzer, R., 2019. Ocean Data View. http://odv.awi.de.

Shannon, L. V., & Chapman, P., 1991. Evidence of Antarctic bottom water in the Angola Basin at 32°S. Deep Sea Research Part A, Oceanographic Research Papers, 38(10), 1299–1304. https://doi.org/10.1016/0198-0149(91)90028-E.

Shannon, L. V., 1985. The Benguela ecosystem. 1. Evolution of the Benguela, physical features and processes, in: Barnes M (Ed.), Oceanography and Marine Biology: An Annual Review, 23. Aberdeen University Press, Aberdeen, 105-182 pp.

Shannon, L. V., Agenbag, J. J., & Buys, M. E. L., 1987. Large- and mesoscale features of the Angola-Benguela front. South African Journal of Marine Science, 5(1), 11–34. https://doi.org/10.2989/025776187784522261.

Shillington, F. A. G., Brundrit, B., Lutjeharms, J. R. E., Boyd, A. J., Agenbag, J. J. & Shannon, L. V., 1990. The coastal current circulation during the Orange River flood 1988. Transactions of the Royal Society of South Africa, 47:3, 307-330, DOI:10.1080/00359199009520245.

Sholkovitz, E. R., 1976. Fluctuation of dissolved organic and inorganic matter during the mixing of river water and seawater. Geochimica et Cosmochimica Acta 40, 831-845.

Sholkovitz, E. R., 1995. The aquatic chemistry of rare earth elements in rivers and estuaries. Aquatic Geochemistry 1, 1-34.

Sholkovitz, E. R., Landing, W. M. and Lewis, B. L., 1994. Ocean particle chemistry: the fractionation of rare earth elements between suspended particles and seawater. Geochim. Cosmochim. Acta 58, 1567–1579.

Sholkovitz, E., & Szymczak, R., 2000. The estuarine chemistry of rare earth elements: Comparison of the Amazon, Fly, Sepik and the Gulf of Papua systems. Earth and Planetary Science Letters 179, 299-309.

Sholkovitz, E.R., 1993. The geochemistry of rare earth elements in the Amazon River estuary. Geochimica et Cosmochimica Acta 57, 2181-2190. http://dx.doi.org/10.1016/0016-7037(93)90559-f.

Siddall, M., Khatiwala, S., van de Flierdt, T., Jones, K., Goldstein, S. L., Hemming, S., & Anderson, R. F., 2008. Towards explaining the Nd paradox using reversible scavenging in an ocean general circulation model. Earth Planet. Sci. Lett.,274(3–4), 448–461. https://doi.org/10.1016/j.epsl.2008.07.044.

Stichel, T., 2010. Tracing water masses and continental weathering by neodymium and hafnium isotopes in the Atlantic sector of the Southern Ocean. Doctoral Thesis, Christian-Albrechts-Universität (CAU), 129pp.

Stichel, T., Frank, M., Rickli, J., and Haley, B. A., 2012b. The hafnium and neodymium isotope composition of seawater in the Atlantic sector of the Southern Ocean. Earth Planet. Sci. Lett., 317–318, 282–294. http://doi.org/10.1016/j.epsl.2011.11.025.

Stichel, T., Frank, M., Rickli, J., Hathorne, E. C., Haley, B. A., Jeandel, C., and Pradoux, C., 2012a. Sources and input mechanisms of hafnium and neodymium in surface waters of the Atlantic sector of the Southern Ocean. Geochim. Cosmochim. Acta, 94, 22–37. http://doi.org/10.1016/j.gca.2012.07.005.

Stramma L. and England M., 1999. On the water masses and mean circulation of the South Atlantic Ocean. J. Geophys. Res. 104, 20863–20883

Stramma, L. and Lutjeharms, J. R. E., 1997. The flow field of the subtropical gyre of the South Indian Ocean. J. Geophys. Res., 102, 5513–5530.

Stramma, L. and Schott, F., 1999. The mean flow field of the tropical Atlantic Ocean. Deep Sea Research Part II, Vol46, 279–303.

Stramma, L., & Peterson, R. G., 1989. Geostrophic Transport in the Benguela Current Region. Journal of Physical Oceanography, 19(10), 1440–1448. doi:10.1175/1520-0485(1989)019<1440:gtitbc>.

Suga, T., Talley, D., 1995. Antarctic Intermediate Water circulation in the tropical and subtropical South Atlantic. Journal of Geophysical Reasearch 100, 13441-13453.

Sverdrup, H.U., Johnson, M.W. and Fleming, R.H., 1942. The oceans. Prentice-Hall, New Jersey, 520-521.

Tachikawa, K., Athias, V., and Jeandel, C., 2003. Neodymium budget in the modern ocean and paleo-oceanographic implications. Journal of Geophysical Research, 108(C8), 3254. http://doi.org/10.1029/1999JC000285.

Tachikawa, K., Jeandel, C. and Dupré, B., 1997. Distribution of rare earth elements and neodymium isotopes in settling particulatematerial of the tropical Atlantic Ocean (EUMELIsite). Deep Sea Res., Part I, 44, 1769–1792, 1997.

Tachikawa, K., Jeandel, C. and Roy-Barman, M.,1999. A new approach to the Nd residence time in the ocean: the role of atmospheric inputs. Earth and Planetary Science Letters 170, 433-446. http://dx.doi.org/10.1016/s0012-821x(99)00127-2.

Talley, L.D., 1996. Antarctic Intermediate Water in the South Atlantic, in The South Atlantic: Present and Past Circulation, edited by G. Wefer et al., pp. 219-238, Springer-Verlag, New York.

Tanaka, T., Togashi, S., Kamioka, H., Amakawa, H., Kagami, H., Hamamoto, T., Yuhara, M., Orihashi, Y., Yoneda, S., Shimizu, H., Kunimaru, T., Takahashi, K., Yanagi, T., Nakano, T., Fujimaki, H., Shinjo, R., Asahara, Y., Tanimizu, M. and Dragusanu, C., 2000. JNdi-1: a neodymium isotopic reference in consistency with LaJolla neodymium. Chemical Geology 168, 279-281. http://dx.doi.org/10.1016/S0009-2541(00)00198-4.

Taylor, S.R., McLennan, S.M., 1985. The Continental Crust: Its Composition and Evolution. Blackwell Scientific, Boston, Mass.

Tepe, N., & Bau, M., 2016. Behavior of rare earth elements and yttrium during simulation of arctic estuarine mixing between glacial-fed river waters and seawater and the impact of inorganic (nano-)particles. Chemical Geology 438, 134–145.

Tomczak, M. and Godfrey, J.S., 1994. Reagional Oceanography: An introduction. 221 pp., Elsevier, New York.

Ullgren, J. E., van Aken, H. M., Ridderinkhof, H., and de Ruijter, W. P. M., 2012. The hydrography of the Mozambique Channel from six years of continuous temperature, salinity, and velocity observations. Deep-Sea Research Part I: Oceanographic Research Papers, 69, 36–50. http://doi.org/10.1016/j.dsr.2012.07.003.

van Bennekom A.J. and Berger G.W., 1984. Hydrography and Silica Budget of the Angola Basin. Netherlands Journal of Sea Research 17, 149–200.

van de Flierdt T., Pahnke K., Amakawa H., Andersson P., Basak C., Coles B., Colin C., Crocket K., Frank M., Frank N., Goldstein S. L., Goswami V., Haley B. A., Hathorne E. C., Hemming S. R., Henderson G. M., Jeandel C., Jones K., Kreissig K., Lacan F., Lambelet M., Martin E. E., Newkirk D. R., Obata H., Pena L., Piotrowski A. M., Pradoux C., Scher H. D., Schöberg H., Singh S. K., Stichel T., Tazoe H., Vance D., Yang, J., 2012. GEOTRACES intercalibration of neodymium isotopes and rare earth element concentrations in seawater and suspended particles. Part 1: reproducibility of results for the international intercomparison. Limnol. Oceanogr. Methods, 10, 234–251.

van de Flierdt, T., Goldstein, S. L., Hemming, S. R., Roy, M., Frank, M., & Halliday, A. N., 2007. Global neodymium-hafnium isotope systematics - revisited. Earth and Planetary Science Letters, 259(3–4), 432–441. https://doi.org/10.1016/j.epsl.2007.05.003.

van de Flierdt, T., Griffiths, A. M., Lambelet, M., Little, S. H., Stichel, T., & Wilson, D. J., 2016. Neodymium in the oceans: a global database, a regional comparison and implications for palaeoceanographic research. Philosophical Transactions of the Royal Society A: Mathematical, Physical and Engineering Sciences, 374(2081), 20150293. http://doi.org/10.1098/rsta.2015.0293.

van de Flierdt, T., Hemming, S.R., Goldstein, S.L., Abouchami, W., 2006. Radiogenic isotope fingerprint of Wilkes Land–Adélie Coast Bottom Water in the circum-Antarctic Ocean. Geophysical Research Letters 33, 1-5.

van der Lubbe, H. J. L., Frank, M., Tjallingii, R. and Schneider, R. R., 2016. Neodymium isotope constraints on provenance, dispersal, and climatedriven supply of Zambezi sediments along the Mozambique Margin during the past _45,000 years. Geochem. Geophys. Geosyst., 17, 181–198, doi:10.1002/2015GC006080.

Vance, D., Thirlwall, M., 2002. An assessment of mass discrimination in MC-ICPMS using Nd isotopes. Chemical Geology, 185, 227-240. https://doi.org/10.1016/S0009-2541(01)00402-8.

Vangriesheim, A., Khripounoff, A., & Crassous, P., 2009. Turbidity events observed in situ along the Congo submarine channel. Deep-Sea Research Part II: Topical Studies in Oceanography 56, 2208-2222.

Vervoort, J.D., Patchett, P.J., Blichert-Toft, J., Albarède, F., 1999. Relationships between Lu-Hf and Sm-Nd isotopic systems in the global sedimentary system. Earth and Planetary Science Letters 168, 79-99.

Vieira, L.H., Krisch, S., Hopwood, M.J., Beck, A.J., Scholten, J., Liebetrau, V. & Achterberg, E.P., 2020. Unprecedented Fe delivery from the Congo River margin to the South Atlantic Gyre. Nature Communications 11, 556. https://doi.org/10.1038/s41467-019-14255-2.

Wefer, G., & Fischer, G., 1993. Seasonal patterns of vertical particle flux in equatorial and coastal upwelling areas of the eastern Atlantic. Deep-Sea Research Part I, 40(8), 1613–1645. https://doi.org/10.1016/0967-0637(93)90019-Y.

Wei, R., Abouchami, W., Zahn, R., Masqué, P., 2016. Deep circulation changes in the South Atlantic since the Last Glacial Maximum from Nd isotope and multi-proxy records. Earth Planet. Sci. Lett., 434, 18-29, https://doi.org/10.1016/j.epsl.2015.11.001.

Weldeab, S., Stuut, J.-B.W., Schneider, R. R. and Siebel, W., 2013. Holocene climate variability in the winter rainfall zone of South Africa. Clim. Past, 9, 2347–2364, 2013. doi:10.5194/cp-9-2347-2013.

Whitworth, T. and Nowlin, W.D., 1987. Water masses and currents of the southern ocean at the Greenwich Meridian. Journal of Geophysical Research 92: doi: 10.1029/JC092iC06p06462. issn: 0148-0227.

Zheng, X. Y., Plancherel, Y., Saito, M. A., Scott, P. M., & Henderson, G. M., 2016. Rare earth elements (REEs) in the tropical South Atlantic and quantitative deconvolution of their non-conservative behavior. Geochim. Cosmochim. Acta, 177, 217–237. http://doi.org/10.1016/j.gca.2016.01.018.

Zieringer, M., Frank, M., Stumpf, R., Hathorne, E.C., 2019. The distribution of neodymium isotopes and concentrations in the eastern tropical North Atlantic. Chem. Geol. 511, 265-278. https://doi.org /10.1016 /j.chemgeo.2018.11.024.

Zimmermann, B., Porcelli, D., Frank, M., Andersson, P. S., Baskaran, M., Lee, D. C., & Halliday, A. N., 2009. Hafnium isotopes in Arctic Ocean water. Geochimica et Cosmochimica Acta 73, 3218-3233.

DATA TABLES

Table A1: Results from Nd-isotope and -concentration measurements, temperatures and salinities.

Station	Latitude	Longitude	depth [m]	Pot. T [degC]	S [psu]	εNd	2SD [εNd]	Nd [pmol/kg]
24	-3.000	0.121	0	26.65	35.64	-12.73	0.19	24.5
24	-2.999	-0.007	99	15.63	35.65	-13.50	0.19	13.4
24	-2.999	-0.007	397	9.27	34.84	-12.62	0.19	17.0
24	-2.999	-0.007	759	4.96	34.50	-12.37	0.19	16.7
24	-2.999	-0.007	1247	4.25	34.82	-12.68	0.19	16.9
24	-2.999	-0.007	1999	3.32	34.95	-12.83	0.19	17.5
24	-2.999	-0.007	2996	2.41	34.90	-12.80	0.19	20.9
24	-2.999	-0.007	4001	2.01	34.88	-12.26	0.19	24.7
24	-2.999	-0.005	4364	1.85	34.86	-11.73	0.19	24.6
24	-2.999	-0.005	4417	1.83	34.86	-11.83	0.19	26.0
24	-2.999	-0.005	4445	1.82	34.86	-11.98	0.19	26.6
25	-5.499	0.000	0	26.29	35.79	-12.58	0.19	18.8
26	-7.098	0.000	0	24.11	35.87	-14.53	0.19	16.5
26	-7.214	0.001	148	13.77	35.38	-13.23	0.19	14.7
26	-7.214	0.001	397	9.20	34.84	-13.53	0.19	19.4
26	-7.200	0.000	797	4.87	34.51	-12.95	0.19	16.9
26	-7.200	0.000	1246	4.11	34.75	-12.97	0.19	22.3
26	-7.200	0.000	1748	3.66	34.93	-12.94	0.19	17.5
26	-7.200	0.000	2996	2.38	34.90	-12.97	0.19	21.4
26	-7.200	0.000	3998	2.00	34.88	-12.68	0.19	25.5
26	-7.200	0.000	4897	1.91	34.87	-12.55	0.19	27.2
27	-8.845	0.000	0	23.97	36.03	-15.45	0.19	17.6
27.1	-10.813	0.000	0	23.40	36.12	-14.99	0.08	18.3
28	-12.930	0.000	0	22.86	36.25	-14.28	0.21	36.1
28	-13.022	0.001	148	12.83	35.28	-14.33	0.21	16.2
28	-13.022	0.002	347	9.36	34.85	-13.39	0.21	16.1
28	-13.022	0.001	802	4.75	34.49	-13.21	0.21	18.5
28	-13.015	0.000	1248	3.82	34.74	-13.67	0.21	16.9
28	-13.015	0.000	1746	3.47	34.91	-14.39	0.08	19.3
28	-13.015	0.000	2998	2.34	34.89	-13.48	0.21	21.9
28	-13.015	0.000	3998	2.01	34.88	-13.03	0.21	24.8
28	-13.015	0.000	4996	1.92	34.87	-12.81	0.08	29.7
28	-13.015	0.000	5416	1.91	34.87	-12.56	0.21	29.5
29	-15.052	0.000	0	27.68	36.15	-16.24	0.08	14.9
29	-15.070	0.001	5771	1.92	34.871	-12.57	0.21	28.8
30	-17.486	0.000	0	21.29	35.87	-17.01	0.21	11.9
30	-17.516	-0.002	148	15.74	35.58	-15.98	0.21	15.2
30	-17.516	-0.002	348	9.35	34.76	-12.86	0.21	13.7
30	-17.516	-0.002	800	4.39	34.47	-12.48	0.21	14.3
30	-17.515	0.000	1249	3.62	34.70	-12.85	0.21	15.3
30	-17.515	0.000	1995	3.08	34.91	-13.26	0.08	17.6
30	-17.515	0.000	2998	2.33	34.89	-13.32	0.21	21.5
30	-17.515	0.000	4497	1.98	34.88	-12.80	0.08	28.5
30	-17.515	0.000	5327	1.95	34.87	-12.80	0.08	29.2
31	-19.716	0.000	0	21.33	35.76	-16.31	0.21	9.6
32	-22.294	0.000	0	21.85	35.88	-15.76	0.21	10.6
32	-22.294	0.000	149	17.16	35.70	-14.96	0.21	-
32	-22.294	0.000	496	7.67	34.58	-11.95	0.21	12.8
32	-22.294	0.000	800	4.38	34.43	-11.47	0.08	11.8
32	-22.293	0.000	1249	3.56	34.66	-11.88	0.21	15.8
32	-22.293	0.000	1998	2.96	34.89	-12.16	0.21	16.7
32	-22.293	0.000	2999	2.21	34.87	-12.00	0.21	20.4
32	-22.293	0.000	4498	1.99	34.88	-12.70	0.08	29.2
32	-22.293	0.000	5078	1.97	34.88	-12.89	0.08	29.8
33	-24.533	0.000	0	22.17	35.97	-15.78	0.21	9.8
34	-26.996	0.000	0	22.21	35.92	-15.76	0.21	11.4
34	-27.091	-0.001	796	4.53	34.35	-9.99	0.21	12.2
34	-27.092	-0.001	1997	2.66	34.83	-11.39	0.08	16.9
34	-27.092	0.000	4497	1.99	34.88	-12.58	0.08	27.9

Table A1 (continued): Results from Nd-isotope and -concentration measurements, temperatures and salinities.

Station	Latitude	Longitude	depth [m]	Pot. T [degC]	S [psu]	εNd	2SD [εNd]	Nd [pmol/kg]
35	-29.478	0.000	0	21.97	35.89	-14.63	0.31	10.6
35	-29.578	0.001	149	16.71	35.66	-13.82	0.31	10.9
35	-29.579	0.000	399	11.11	34.93	-11.50	0.21	11.5
35	-29.578	0.001	802	5.01	34.36	-10.39	0.08	11.6
35	-29.579	0.000	1248	3.25	34.55	-10.31	0.21	13.9
35	-29.579	0.000	1999	2.57	34.81	-10.99	0.08	16.3
35	-29.579	0.000	2998	2.11	34.86	-11.74	0.08	21.6
35	-29.579	0.000	3997	1.95	34.87	-12.12	0.08	26.1
35	-29.579	0.000	4232	1.94	34.87	-12.21	0.08	25.7
36	-29.376	2.604	0	21.56	35.56	-15.81	0.16	10.8
36	-29.376	2.741	797	4.80	34.36	-10.08	0.16	12.0
36	-29.376	2.741	1997	2.68	34.81	-10.97	0.46	15.9
36	-29.376	2.741	3195	2.06	34.85	-11.25	0.43	21.0
36	-29.376	2.741	3471	1.92	34.84	-11.60	0.43	22.8
37	-29.236	5.397	0	21.29	35.34	-15.06	0.46	11.7
37	-29.230	5.537	147	14.68	35.32	-13.70	0.16	10.8
37	-29.230	5.537	798	4.16	34.33	-9.26	0.16	11.9
37	-29.229	5.536	1247	3.22	34.63	-10.63	0.46	13.8
37	-29.229	5.536	1995	2.77	34.84	-11.91	0.46	16.6
37	-29.229	5.536	2997	2.15	34.85	-11.48	0.43	20.1
37	-29.229	5.536	4854	0.76	34.73	-9.54	0.43	36.3
37	-29.229	5.536	4983	0.75	34.73	-9.62	0.43	37.5
38	-29.133	7.904	0	21.75	35.44	-16.01	0.16	11.9
38	-29.127	8.054	4496	0.82	34.74	-9.60	0.43	33.6
39	-29.036	10.601	0	21.15	35.30	-16.22	0.46	13.1
39	-29.032	10.705	145	12.36	35.00	-13.94	0.46	13.1
39	-29.032	10.705	647	4.45	34.34	-9.79	0.46	11.8
39	-29.031	10.707	1247	2.94	34.65	-10.23	0.46	14.0
39	-29.031	10.707	1999	2.77	34.86	-11.76	0.43	16.7
39	-29.031	10.707	2997	2.13	34.85	-11.78	0.43	20.5
39	-29.031	10.707	4590	0.79	34.73	-10.51	0.43	27.1
39	-29.032	10.707	4719	0.78	34.73	-10.12	0.43	37.4
40	-28.932	13.060	0	20.75	35.22	-17.64	0.43	17.7
40	-28.925	13.178	648	4.92	34.35	-10.34	0.16	11.7
40	-28.925	13.178	996	3.48	34.48	-10.23	0.16	12.8
40	-28.925	13.178	2497	2.48	34.87	-11.86	0.43	18.2
40	-28.925	13.178	2603	2.38	34.87	-12.31	0.46	17.5
41	-28.847	14.273	0	20.46	34.80	-13.32	0.16	11.4
41	-28.839	14.380	95	12.71	35.06	-13.51	0.46	12.6
41	-28.839	14.380	196	10.39	34.83	-11.67	0.16	10.6
41	-28.839	14.380	347	8.83	34.71	-12.08	0.16	11.0
41	-28.839	14.380	456	6.48	34.49	-11.29	0.16	10.8
42	-28.760	15.435	0	19.31	34.71	-11.70	0.46	12.4
42	-28.749	15.558	98	10.47	34.83	-11.71	0.16	10.8
42	-28.749	15.558	178	9.26	34.71	-10.23	0.16	7.5
43	-28.675	16.266	0	13.13	34.69	-8.89	0.43	21.7
43	-28.676	16.268	60	9.59	34.75	-8.25	0.43	21.9

Table A2: Nd isotopic compositions and concentrations of water samples from the Mozambique Channel, collected during cruise M75-3 in 2008.

Station	Latitude	Longitude	depth [m]	T [degC]	S [psu]	εNd	2SD [εNd]	Nd [pmol/kg]
GIK16152	-25.246	33.534	0	29.9	34.3	-22.4	0.18	97.16
			2.5	29.9	34.3	-22.4	0.18	94.66
			5	29.9	34.4	-22.3	0.18	91.87
			15	27.4	35.2	-21.8	0.18	54.06
			20	27.3	35.34	-22.1	0.18	62.97
GIK16156	-18.936	36.403	0	-	32.38	-15.5	0.18	50.59
GIK16157	-18.726	36.549	0	-	31.86	-14.7	0.19	63.89

Table A3: Nd and Hf isotope compositions and concentrations along with hydrographic parameters. Nd concentrations marked with * were measured with a SeaFAST system.

Station	Latitude	Longitude	depth [m]	T [degC]	S [psu]	εNd	2SD	Nd [pmol/kg]	εHf	2SD	Hf [pmol/kg]
12	-7.28	12.17	0	27.72	35.15	-14.18	0.22	32.44	-	-	-
12.1 (22.07.17)	-6.07	12.49	0	-	0	-16.39	0.25	1979.64	-1.40	0.81	32.85
12.2 (08.10.17)	-6.07	12.49	0	-	0	-16.06	0.25	3927.90	0.35	0.74	53.92
12.3 (04.05.17)	-6.07	12.49	0	-	0	-15.55	0.25	2835.62	-1.09	0.78	37.66
13	-6.20	11.99	0	26.30	28.55	-15.80	0.26	204.68	-0.28	0.59	6.61
13	-6.20	11.99	39	22.21	36.45	-14.84	0.20	31.11	0.41	2.76	0.48
13.1	-6.22	11.51	0	27.40	35.81	-	-	35.19	-	-	0.78
14	-6.24	11.23	0	27.65	35.90	-15.41	0.23	33.09	-	-	0.41
14	-6.23	11.16	498	7.93	35.31	-14.15	0.16	23.86	-	-	0.52
14	-6.23	11.16	989	4.56	35.17	-14.24	0.15	24.77	-0.26	1.36	0.62
15	-6.00	11.49	0	27.04	31.54	-15.88	0.26	128.97	-0.27	0.78	4.13
15	-6.00	11.49	197	13.89	36.01	-15.21	0.15	32.15	-	-	1.23
15	-6.00	11.49	346	9.55	35.61	-14.92	0.18	31.10	-0.25	1.55	1.33
15.1	-5.97	11.54	0	27.03	23.45	-15.57	0.26	451.73	0.30	0.61	12.90
15.2	-5.75	11.89	0	26.64	24.37	-15.53	0.26	436.04	0.04	0.63	11.90
15.3	-5.78	11.65	0	27.05	24.34	-15.69	0.26	411.74	0.31	0.62	12.81
16	-4.27	10.48	0	25.33	33.28	-15.41	0.26	92.25	-1.20	0.65	3.16
16	-4.27	10.48	298	10.10	35.47	-13.64	0.17	27.35	-1.94	1.25	0.29
16	-4.27	10.48	881	4.64	35.28	-13.47	0.15	21.71	1.42	1.16	1.08
16.1	-3.60	10.14	0	26.67	33.18	-15.50	0.26	82.09	-0.30	0.67	2.21
17	-3.10	9.88	0	26.76	33.55	-15.49	0.42	61.13*	-	-	-
17	-3.00	9.83	29	23.71	36.11	-14.12	0.25	24.24*	-	-	-
17	-3.00	9.83	52	18.70	36.65	-15.05	0.25	14.45*	-	-	-
18	-3.00	9.48	0	27.04	34.11	-15.11	0.42	61.49*	-	-	-
18	-3.00	9.43	44	20.89	36.19	-14.28	0.63	22.06*	-	-	-
18	-3.00	9.43	99	17.23	36.64	-14.73	0.63	15.15*	-	-	-
18	-3.00	9.43	149	15.53	36.34	-15.69	0.31	12.78*	-	-	-
18	-3.00	9.43	174	15.27	36.22	-14.87	0.25	16.59*	-	-	-
19	-3.00	9.39	0	26.87	33.82	-15.33	0.42	63.06*	-	-	-
19	-3.00	9.33	44	21.01	36.33	-12.83	0.63	20.62*	-	-	-
19	-3.00	9.33	98	17.36	36.54	-13.27	0.25	14.32*	-	-	-
19	-3.00	9.33	198	14.34	35.95	-14.48	0.25	15.79*	-	-	-
19	-3.00	9.33	494	8.12	35.26	-13.81	0.25	19.05*	-	-	-

Table A3 (continued): Nd and Hf isotope compositions and concentrations along with hydrographic parameters. Nd concentrations marked with * were measured with a SeaFAST system.

Station	Latitude	Longitude	depth [m]	T [degC]	S [psu]	εNd	2SD	Nd [pmol/kg]	εHf	2SD	Hf [pmol/kg]
20	-3.00	9.08	0	26.80	33.77	-15.42	0.42	55.59*	-	-	-
20	-3.00	9.07	98	17.03	36.38	-13.68	0.25	13.23*	-	-	-
20	-3.00	9.07	200	14.52	36.04	-14.52	0.63	17.55*	-	-	-
20	-3.00	9.07	495	7.66	35.25	-13.45	0.47	17.82*	-	-	-
20	-3.00	9.07	1011	4.55	35.41	-12.89	0.47	19.61*	-	-	-
21	-3.00	7.08	0	27.47	35.00	-13.77	0.42	32.08*	-	-	-
21	-3.00	6.78	100	16.57	35.75	-14.19	0.25	12.39*	-	-	-
21	-3.00	6.78	401	8.93	34.81	-12.81	0.25	16.65*	-	-	-
21	-3.00	6.78	707	5.04	34.48	-11.36	0.25	13.81*	-	-	-
21	-3.00	6.78	1249	4.43	34.83	-12.97	0.25	15.48*	-	-	-
21	-3.00	6.78	1996	3.55	34.95	-13.02	0.23	14.09*	-	-	-
21	-3.00	6.78	2997	2.65	34.90	-12.80	0.25	19.25*	-	-	-
21	-3.00	6.78	3998	2.32	34.87	-12.73	0.25	24.99*	-	-	-
21	-3.00	6.78	4146	2.33	34.87	-13.05	0.42	29.62*	-	-	-
22	-3.00	4.53	0	27.54	34.60	-14.09	0.25	34.65*	-	-	-
22	-3.00	4.42	100	15.44	35.62	-13.18	0.18	12.59*	-	-	-
22	-3.00	4.42	397	8.69	34.78	-12.88	0.19	16.93*	-	-	-
22	-3.00	4.42	796	4.82	34.50	-12.21	0.19	14.61*	-	-	-
22	-3.00	4.42	1247	4.37	34.82	-12.93	0.18	14.26*	-	-	-
22	-3.00	4.42	1997	3.52	34.95	-13.29	0.19	18.51*	-	-	-
22	-3.00	4.42	2997	2.64	34.90	-12.69	0.25	21.05*	-	-	-
22	-3.00	4.42	3997	2.33	34.88	-12.76	0.42	21.29*	-	-	-
22	-3.00	4.42	4485	2.31	34.87	-11.98	0.25	23.14*	-	-	-
23	-3.00	2.33	0	26.23	35.81	-13.18	0.25	13.81*	-	-	-
23	-3.00	2.21	4485	2.24	34.86	-12.34	0.25	22.34*	-	-	-
24	-3.00	0.12	0	26.65	35.64	-12.73	0.19	24.47	0.34	2.03	0.24
24	-3.00	-0.01	99	15.64	35.65	-13.50	0.19	13.39	-0.32	2.03	0.31
24	-3.00	-0.01	397	9.32	34.84	-12.62	0.19	17.00	-0.15	0.75	0.65
24	-3.00	-0.01	759	5.02	34.50	-12.37	0.19	16.72	2.68	0.75	0.56
24	-3.00	-0.01	1247	4.36	34.82	-12.68	0.19	16.93	0.55	0.75	0.53
24	-3.00	-0.01	1999	3.48	34.95	-12.83	0.19	17.47	1.57	0.75	0.89
24	-3.00	-0.01	2996	2.66	34.90	-12.80	0.19	20.89	2.78	0.75	1.05
24	-3.00	-0.01	4001	2.37	34.88	-12.26	0.19	24.71	0.92	0.75	1.05
24	-3.00	-0.01	4364	2.25	34.86	-11.73	0.19	24.61	-0.72	0.75	0.16
24	-3.00	-0.01	4417	2.23	34.86	-11.83	0.19	26.00	1.77	0.75	0.79
24	-3.00	-0.01	4445	2.23	34.86	-11.98	0.19	26.63	1.47	0.75	0.77

Table A4: REE concentrations in pmol/kg measured with a SeaFAST system.

Station	Depth (m)	La	Ce	Pr	Nd	Sm	Eu	Gd	Tb	Dy	Ho	Er	Tm	Yb	Lu
BATS 15m 2SD (%)		24.8	18.4	18.3	4.9	10.1	9.6	18.9	15.2	6.3	12.7	9.4	23.3	16.7	14.7
12.1	0	1485.06	3238.10	401.30	1552.53	292.22	60.67	292.89	38.61	195.19	37.90	113.63	14.78	90.06	12.87
13.1	0	54.68	71.52	8.06	32.08	6.29	1.34	7.28	1.01	6.54	1.49	5.06	0.70	4.23	0.66
14	989	34.54	29.23	6.90	29.34	5.24	1.14	6.13	0.94	5.78	1.38	5.38	0.79	5.43	0.93
15.3	0	329	623.97	84.05	360.50	74.60	16.08	73.73	10.73	60.33	13.05	40.65	5.65	36.73	5.82
16	881	26.15	16.39	4.69	20.54	3.87	0.83	7.18	0.62	4.88	1.23	4.71	0.75	6.47	0.86
16.1	0	77.48	83.43	16.41	72.43	14.82	3.33	16.13	2.57	15.93	3.62	11.78	1.73	10.94	1.73
17	0	85.32	67.13	12.55	61.13	13.62	3.59	22.94	3.09	16.03	3.78	13.83	1.88	11.32	1.96
17	29	31.93	27.24	5.16	24.24	4.13	1.15	7.40	1.02	5.27	1.33	4.58	0.56	3.44	0.57
17	52	17.44	19.14	3.21	14.54	2.67	0.74	5.02	0.61	3.37	0.93	3.45	0.43	2.83	0.46
18	0	88.83	87.17	13.72	61.95	12.59	3.15	19.54	2.82	15.86	3.77	12.44	1.57	10.06	1.80
18	44	32.71	27.46	4.21	22.22	3.70	1.03	6.33	0.93	5.10	1.25	4.42	0.54	3.16	0.50
18	99	19.38	11.16	3.21	15.26	2.63	0.59	4.48	0.62	3.70	0.99	3.50	0.48	2.68	0.48
18	149	21.80	10.71	2.34	12.87	2.38	0.68	4.35	0.64	3.65	0.98	3.23	0.44	2.73	0.49
18	174	26.32	16.23	3.32	16.72	3.06	0.72	4.57	0.64	3.98	1.08	3.50	0.45	2.62	0.48
19	0	86.47	84.41	13.11	63.53	12.26	3.11	18.63	2.71	16.41	3.51	11.88	1.52	9.37	1.52
19	44	25.96	27.35	5.04	20.78	3.92	1.09	6.86	0.94	5.04	1.36	4.67	0.59	3.29	0.59
19	98	18.69	14.35	3.37	14.43	2.75	0.68	5.09	0.74	4.53	1.18	4.00	0.56	3.07	0.42
19	197	28.28	10.89	3.31	15.91	2.50	0.62	4.42	0.60	3.53	0.93	2.73	0.47	2.94	0.52
19	494	34.98	10.20	4.41	19.19	3.06	0.82	6.43	0.81	5.25	1.34	5.12	0.68	4.06	0.75
20	0	78.95	55.19	11.78	56.00	10.42	2.89	17.75	2.54	13.54	3.20	10.97	1.40	8.59	1.45
20	97	20.25	13.45	2.92	13.33	2.22	0.62	4.32	0.56	3.57	0.94	3.53	0.47	2.67	0.47
20	200	30.44	14.91	4.01	17.68	3.43	0.93	6.49	0.91	4.76	1.29	4.38	0.60	3.44	0.56
20	495	27.86	8.72	3.21	17.96	3.05	0.82	5.53	0.73	4.41	1.19	4.55	0.62	4.02	0.72
20	1011	32.71	9.76	3.92	19.75	3.21	0.91	5.53	0.80	4.67	1.44	5.01	0.76	3.69	0.89

Table A4 (continued): REE concentrations in pmol/kg measured with a SeaFAST system.

21	0	41.59	38.01	7.49	32.32	6.83	1.62	10.01	1.43	7.93	1.78	5.89	0.76	4.23	0.71
21	100	16.15	10.11	2.25	12.48	2.39	0.71	4.48	0.63	3.61	0.99	3.47	0.48	2.77	0.51
21	401	28.35	6.78	3.66	16.77	2.84	0.62	5.35	0.76	4.52	1.25	4.59	0.46	3.89	0.71
21	707	24.63	4.22	2.26	13.92	2.47	0.69	4.53	0.65	4.23	1.23	4.45	0.68	4.15	0.72
21	1249	20.86	6.55	3.14	15.60	3.09	0.91	5.99	0.87	5.43	1.24	4.57	0.67	4.87	0.92
21	1996	21.29	8.07	2.98	14.20	3.60	1.00	6.62	0.97	5.89	1.70	6.19	0.82	5.12	0.83
21	2997	27.04	6.40	3.27	19.39	3.47	1.01	6.90	0.94	5.90	1.67	6.01	0.83	5.48	0.81
21	3998	31.03	6.52	5.37	25.17	4.02	1.14	7.97	1.08	6.22	1.67	5.95	0.75	5.40	0.98
21	4146	46.54	7.60	6.29	29.83	5.04	1.33	8.56	1.24	6.68	1.44	6.80	0.91	6.01	1.07
22	0	34.89	25.61	7.31	34.91	7.02	1.83	11.84	1.61	8.56	2.05	7.07	0.91	5.34	0.84
22	100	20.13	9.41	2.78	12.68	2.05	0.62	3.66	0.57	3.43	0.98	3.23	0.50	2.74	0.49
22	397	24.63	6.63	3.74	17.06	2.63	0.75	4.96	0.68	3.96	1.15	4.06	0.57	3.48	0.67
22	796	28.42	6.39	3.61	14.72	2.62	0.75	4.64	0.70	4.29	1.26	4.61	0.69	4.53	0.70
22	1247	16.96	5.58	2.44	14.36	2.80	0.80	5.81	0.65	4.89	1.20	5.24	0.78	4.82	0.92
22	1997	22.64	12.31	3.33	18.65	3.33	0.97	6.63	0.87	5.35	1.52	5.44	0.82	4.79	0.90
22	2996	33.62	6.67	4.21	21.21	3.89	1.13	7.13	1.01	6.15	1.75	6.63	0.86	5.75	1.04
22	3997	45.71	6.52	4.07	21.44	3.85	1.04	7.47	0.99	5.49	1.62	5.47	0.80	5.35	0.97
22	4485	33.97	6.16	5.37	23.31	3.93	1.07	7.77	1.04	6.77	1.69	6.46	0.89	5.88	0.95
23	0	24.63	15.69	3.39	13.92	2.55	0.66	5.05	0.66	3.35	0.90	2.95	0.33	1.72	0.25
23	4485	34.65	8.07	3.95	22.51	3.57	0.97	7.49	1.03	6.07	1.68	6.00	0.83	4.97	0.96

Table A5: Nd and Hf fluxes of the Congo River, the Congo-shelf-zone and the offshore 3 °S transect.

	Congo River	Congo-Shelf-zone	Off-shelf 3°S transect
Nd-Flux (mol/year)	$3.8 \pm 1.3 \times 10^6$	$2.6 \pm 1.0 \times 10^6$	$1.0 \pm 0.3 \times 10^6$
Nd-Flux (Mg/year)	547 ± 183	387 ± 151	150 ± 50
Hf-Flux (mol/year)	$5.4 \pm 1.4 \times 10^4$	$7.6 \pm 3.1 \times 10^4$	$8.5 \pm 3.6 \times 10^4$
Hf-Flux (Mg/year)	10 ± 3	14 ± 5	15 ± 7

Table A6: Results from Nd-isotope and -concentration measurements, temperatures, salinities and oxygen.

Station	water depth [m]	Latitude	Longitude	T [degC]	S [psu]	Ox [ml/l]	εNd	2SD [εNd]	Nd [pmol/kg]
12	0	-7.283	12.173	27.7	35.15	-	-14.81	0.22	32.44
12	282	-7.325	12.180	11.5	35.11	0.83	-15.09	0.15	23.01
11	0	-8.537	12.063	28.0	35.00	-	-15.65	0.22	31.86
11	1247	-8.537	12.063	4.2	34.79	3.89	-14.27	0.15	21.41
11	2004	-8.537	12.063	3.5	34.93	4.98	-14.56	0.22	23.62
10	0	-9.696	12.294	27.9	34.80	-	-16.64	0.22	38.90
10	1594	-9.696	12.294	3.8	34.92	4.74	-14.86	0.22	23.41
9	0	-10.647	12.526	27.8	34.72	-	-16.66	0.15	37.02
9	1248	-10.647	12.526	4.0	34.79	3.88	-15.18	0.15	21.19
9	1573	-10.647	12.526	3.9	34.91	4.66	-14.97	0.22	22.98
8	0	-12.499	12.016	28.8	34.80	-	-15.32	0.22	35.95
8	148	-12.499	12.015	14.2	35.42	1.32	-13.94	0.15	15.92
8	299	-12.499	12.015	11.3	35.06	0.52	-14.82	0.15	18.79
8	847	-12.499	12.016	4.7	34.51	2.59	-14.91	0.19	19.20
8	1749	-12.499	12.016	3.6	34.92	4.79	-15.95	0.28	23.34
8	2346	-12.499	12.016	3.1	34.92	4.93	-15.15	0.19	24.15
7	0	-14.024	10.958	26.4	35.12	-	-16.87	0.19	36.54
6	0	-15.794	10.849	23.8	35.32	-	-18.09	0.22	31.12
6	297	-15.785	10.847	10.2	34.95	0.42	-14.82	0.19	19.16
6	851	-15.785	10.847	4.6	34.48	2.76	-14.27	0.24	16.56
6	1748	-15.794	10.849	3.5	34.89	4.7	-14.92	0.24	19.49
6	2498	-15.794	10.849	2.9	34.91	4.94	-14.77	0.19	22.33
6	3034	-15.794	10.849	2.6	34.90	4.86	-14.94	0.19	25.61
5.1	0	-17.271	11.326	24.0	35.38	-	-20.45	0.22	36.00
5	0	-17.557	11.440	17.5	35.45	-	-17.39	0.15	20.31
5	147	-17.557	11.440	14.2	35.42		-14.60	0.19	16.58
4	0	-18.659	11.782	16.1	35.17	-	-15.15	0.15	16.40
4	150	-18.661	11.781	13.3	35.30	1.13	-15.25	0.19	16.64
3	0	-19.765	12.290	16.4	35.00	-	-14.27	0.24	12.16
3	11	-19.764	12.288	15.9	35.23	6.09	-14.24	0.24	13.21
3	172	-19.765	12.289	12.9	35.24	0.42	-15.49	0.19	15.02
2	11	-20.869	12.892	15.4	35.15	5	-14.36	0.24	12.31
2	171	-20.870	12.892	12.2	35.15	0.8	-15.33	0.19	16.52

Table A6 (continued): Results from Nd-isotope and -concentration measurements, temperatures, salinities and oxygen.

1	15	-21.974	13.183	15.8	35.10	5.67	-15.26	0.28	11.73
1	168	-21.974	13.183	12.4	35.16	0.53	-16.91	0.19	35.40
48	0	-22.938	13.922	15.5	34.79	-	-12.62	0.24	-
48	130	-22.938	13.922	11.9	35.09	0.03	-13.52	0.28	20.97
47	0	-24.388	14.200	15.2	34.68	-	-12.25	0.24	-
47	127	-24.386	14.200	11.9	35.09	0.03	-13.28	0.28	17.20
46	0	-25.529	14.456	14.8	34.62	-	-11.50	0.28	-
46	100	-25.529	14.456	11.5	35.01	0.06	-13.05	0.28	-
46	147	-25.529	14.456	11.4	35.02	0.04	-12.69	0.28	7.56
45	0	-26.678	14.743	13.7	34.71	-	-12.39	0.24	14.50
45	98	-26.678	14.743	11.8	34.88	4.4	-12.08	0.24	-
45	182	-26.678	14.743	10.6	34.90	0.67	-12.00	0.24	19.89
44	0	-27.864	14.849	19.7	34.75	-	-12.28	0.24	13.23
44	100	-27.864	14.849	11.8	34.92	4.16	-12.52	0.28	12.01
44	231	-27.864	14.849	9.8	34.81	1.85	-12.22	0.28	10.50
43.1	0	-28.442	16.046	15.1	34.49	-	-8.38	0.28	10.74

Table A7: REE concentrations in pmol/kg measured with a SeaFAST system.

Station	depth	La	Ce	Pr	Nd	Sm	Eu	Gd	Tb	Dy	Ho	Er	Tm	Yb	Lu	Ce/Ce*
BATS 15m 2SD (%)		8.9	13.7	11.3	12.7	8.2	9.7	9.9	9.0	13.7	12.3	7.1	11.9	7.9	11.2	-
12	0	38.51	24.29	7.86	33.48	6.65	1.57	8.02	1.19	7.74	1.88	5.89	0.80	4.80	0.73	-0.53
12	282	33.30	21.06	5.63	24.03	4.21	0.98	5.30	0.72	4.78	1.23	4.29	0.62	4.13	0.66	-0.50
11	0	41.00	22.82	7.38	32.35	6.11	1.47	7.26	1.04	7.11	1.77	5.53	0.76	4.69	0.69	-0.57
11	1247	30.16	13.38	5.26	22.16	4.31	0.97	12.33	0.82	5.93	1.68	6.99	0.90	9.77	1.00	-0.66
11	2004	32.33	13.45	5.63	24.71	4.64	1.14	6.10	0.93	6.52	1.83	5.94	0.93	6.32	1.03	-0.69
10	0	48.66	39.99	9.45	40.29	7.42	1.79	8.97	1.35	8.50	2.16	6.71	0.89	5.82	0.86	-0.41
10	1594	31.83	14.34	5.55	24.38	4.66	1.19	6.00	0.91	6.78	1.86	6.08	0.91	6.35	1.06	-0.66
9	0	44.93	31.93	8.74	37.62	6.99	1.77	11.74	1.26	8.41	2.05	6.39	0.92	7.49	0.81	-0.47
9	1245	29.84	12.71	5.25	22.24	4.13	1.03	5.24	0.82	6.19	1.66	5.82	0.89	6.14	1.08	-0.68
9	1573	31.93	15.01	5.63	24.14	4.46	1.11	5.88	0.91	6.55	1.81	6.09	0.91	6.23	1.02	-0.64
8	0	44.42	31.52	8.56	37.58	7.19	1.69	8.36	1.32	8.91	2.08	6.50	0.86	5.61	0.85	-0.47
8	148	23.47	8.85	3.87	16.99	3.07	0.72	4.10	0.62	4.57	1.27	4.19	0.63	4.01	0.66	-0.73
8	299	58.33	69.68	5.09	20.55	3.51	0.91	4.84	0.71	4.98	1.46	4.90	0.71	4.67	0.81	-0.15
8	847	30.85	13.78	5.15	21.66	3.91	0.96	5.35	0.80	5.80	1.62	5.76	0.92	6.22	1.07	-0.65
8	1749	33.24	14.67	5.85	24.60	4.62	1.10	8.47	0.89	6.76	1.81	6.62	0.93	7.10	1.08	-0.66
8	2346	33.93	11.75	5.69	24.66	4.62	1.09	56.05	0.90	6.59	1.80	11.28	0.94	15.79	1.09	-0.76
7	0	47.61	35.35	9.31	40.95	7.36	1.74	9.19	1.36	8.57	2.13	6.52	0.86	5.74	0.84	-0.46
6	0	40.00	24.72	7.61	31.86	6.06	1.40	7.36	1.06	6.99	1.74	5.57	0.74	4.37	0.66	-0.53
6	297	29.84	12.21	4.81	20.31	3.68	0.84	4.54	0.68	5.10	1.40	4.68	0.71	5.05	0.82	-0.68
6	851	26.45	9.68	4.21	18.20	3.22	0.86	4.36	0.66	4.98	1.50	5.16	0.84	5.68	0.99	-0.73
6	1748	29.15	11.03	4.73	20.34	3.82	0.97	5.20	0.80	6.37	1.72	5.96	0.95	6.23	1.06	-0.72
6	2498	32.62	10.81	5.33	23.45	4.31	1.10	5.51	0.87	6.55	1.77	6.23	0.95	6.64	1.11	-0.78
6	3034	29.49	10.18	6.30	26.86	5.09	1.19	6.58	1.00	7.36	2.02	6.58	1.01	6.93	1.17	-0.80
5.1	0	47.12	44.16	9.05	38.08	6.51	1.56	8.41	1.16	7.57	1.84	5.76	0.78	4.70	0.69	-0.35

Table A7 (continued): REE concentrations in pmol/kg measured with a SeaFAST system.

Station	depth	La	Ce	Pr	Nd	Sm	Eu	Gd	Tb	Dy	Ho	Er	Tm	Yb	Lu	Ce/Ce*
5	0	28.49	28.61	5.03	20.89	3.66	0.89	6.96	0.68	4.80	1.24	4.10	0.61	4.87	0.57	-0.30
5	147	23.80	12.61	4.05	16.38	3.07	0.77	3.98	0.61	4.41	1.20	3.83	0.61	3.73	0.63	-0.57
4	0	25.48	32.27	4.27	17.72	3.05	0.68	3.90	0.54	4.01	1.04	3.41	0.50	3.61	0.56	-0.20
4	151	26.07	17.81	4.20	17.72	3.07	0.78	4.19	0.60	4.32	1.21	4.28	0.60	4.31	0.68	-0.46
3	0	17.05	18.44	3.11	13.03	2.32	0.51	2.84	0.41	2.91	0.86	2.82	0.41	2.55	0.40	-0.28
3	11	18.11	18.86	3.24	13.66	2.30	0.55	3.29	0.44	3.09	0.88	2.88	0.39	2.53	0.43	-0.29
3	172	24.87	19.98	3.80	16.24	2.75	0.70	5.70	0.55	3.91	1.11	3.74	0.61	4.89	0.62	-0.39
2	11	18.26	19.74	3.15	12.91	2.10	0.51	2.72	0.40	2.87	0.83	2.74	0.39	2.56	0.42	-0.27
2	171	26.53	16.49	4.12	17.46	2.93	0.70	3.73	0.55	4.17	1.08	3.88	0.59	3.77	0.61	-0.50
1	15	16.40	14.89	2.94	12.38	2.25	0.54	2.93	0.45	3.01	0.86	2.82	0.44	2.59	0.42	-0.35
1	168	67.65	86.06	10.12	37.89	5.31	1.07	6.51	0.79	4.87	1.26	4.14	0.59	3.97	0.67	-0.17
48	130	39.44	23.98	5.20	20.97	3.34	0.82	4.62	0.77	5.78	1.65	5.95	0.90	5.89	1.05	-0.48
47	128	30.14	21.41	4.06	17.20	2.76	0.71	3.41	0.60	4.26	1.31	4.57	0.70	4.46	0.80	-0.42
46	147	13.38	8.78	1.79	7.56	1.40	0.33	1.70	0.27	1.86	0.61	1.90	0.31	1.91	0.33	-0.46
45	0	18.68	15.90	3.34	14.50	2.97	0.70	3.70	0.54	3.83	1.10	3.52	0.53	3.12	0.53	-0.38
45	182	26.98	30.60	4.84	19.89	3.70	0.84	4.37	0.65	4.36	1.10	3.78	0.56	3.54	0.62	-0.25
44	0	17.33	16.66	3.15	14.03	2.59	0.59	3.15	0.47	3.20	0.88	2.88	0.39	2.36	0.37	-0.34
44	100	15.25	9.54	2.75	12.52	2.39	0.59	3.02	0.48	3.65	1.00	3.23	0.49	3.17	0.49	-0.53
44	231	17.91	10.47	2.52	10.87	2.02	0.46	2.63	0.40	3.30	0.91	3.23	0.48	3.23	0.54	-0.51
43.1	0	21.95	25.22	2.48	10.57	1.94	0.50	2.69	0.37	2.91	0.77	2.54	0.35	2.61	0.45	-0.20